The Dissertation Committee for Hongyan Yang certifies that this is the approved version of the following dissertation:

Functional Assessment and Development of Treatment Strategies for Brain Tumors: Promoting Neurorestoration and Reducing Harm to Bystander Cells and Neuroplasticity

Committee:

Timothy Schallert, Supervisor

Michael Chopp

Michael Domjan

Theresa Jones

Jonathan Sessler

Functional Assessment and Development of Treatment Strategies for Brain Tumors: Promoting Neurorestoration and Reducing Harm to Bystander Cells and Neuroplasticity

by

Hongyan Yang, MD

Dissertation

Presented to the Faculty of the Graduate School of

The University of Texas at Austin

in Partial Fulfillment

of the Requirements

for the Degree of

Doctor of Philosophy

The University of Texas at Austin

December 2007

Dedication

My exceptional family,

Especially

My husband, Jingwen Hu,

My son, Albert Y. Hu,

And

My parents, Xinnan Wang and Wenkui Yang

For their love and support

Acknowledgements

I am forever grateful to my mentor, Dr. Timothy Schallert, for giving me the precious opportunity to participate in this amazing neuroscience program, and for supporting and providing me with continuous inspiration and guidance. This has truly been one of the greatest experiences of my entire life.

I am greatly indebted to both Dr. Timothy Schallert and Dr. Michael Chopp, for letting me fulfill my dissertation study in Dr. Chopp's laboratory at Henry Ford Hospital, Detroit, MI, allowing me to join my husband in Michigan. I will never forget their kindness, concern, and thoughtfulness.

Dr. Chopp is like my co-supervisor, and half of my dissertation work was finished in his lab. I am genuinely grateful for his unwavering encouragement and generous help.

I deeply appreciate Dr. Theresa Jones for the invaluable input and advice she gave to help me with my research and writing.

I thank my entire dissertation committee for their contributions in improving the quality of my dissertation.

I also truly thank all the members in both Dr. Schallert's and Dr. Chopp's laboratories, especially Marnie Preston, Martin Woodlee, Xuepeng Zhang, Feng Jiang, Cynthia Roberts H.T. and Qing-e Lu for their extraordinary help.

To my family, no words could adequately describe my gratitude for what they have done for me. No matter what happens, they are always there, giving me love, comfort, security, and support unconditionally. Their pride is my source of motivation and their faith is my source of strength.

I especially thank my husband for always being supportive. He helped me solve statistics problems, prepare graphs, and format articles and presentations. My eight-month-old son deserves thanks for bringing me so much fun. I am eternally grateful to my wonderful parents. What I achieve is their achievement too. I hope my beloved grandparents could share my happiness too, and I always feel that they have been watching me from afar, praying for me, and smiling proudly when I have achieved some success.

I could not help being sentimental when thinking about the years and years of hard work, the many people supporting and encouraging me, and the new beginning that I now face. My strongest feeling at the moment is gratitude to all the visible and invisible powers of the universe for helping me realize my dreams.

Functional Assessment and Development of Treatment Strategies for Brain Tumors: Promoting Neurorestoration and Reducing Harm to Bystander Cells and Neuroplasticity

Publication No._____

Hongyan Yang, MD, PhD
The University of Texas at Austin, 2007

Supervisor: Timothy Schallert

Current treatment options for malignant brain tumors not only frequently fail to cure the disease due to local recurrence, but also may severely compromise quality of remaining life even when tumor mass is reduced in large part because they interfere with mechanisms of neuroplasticity and function of bystander tissue. The aims of this dissertation are to: (a) assess neurological impairments associated with rapid focal cortical tissue displacement; (b) evaluate the specific impact of conventional and novel treatments on neurorestoration while controlling tissue compression without the confound of related events linked to tumor physiology; (c) identify the behavioral change pattern

during brain tumor progression and investigate the stealth nature of brain tumors; (d) demonstrate how anti-cancer treatments affect brain function especially when administered in the silent stages of brain tumors; and (e) develop treatment strategies that might improve therapeutic effectiveness and brain function.

We adopted a new focal mass compression model providing rapid displacement of tissue in the underlying sensorimotor cortex, as well as the traditional rat and mouse glioma xenograft models that exhibit prominent tumor growth and invasion, given the varied aims and contexts of our different studies. Various conventional and novel brain tumor treatments were employed in this dissertation, including local and systemic chemotherapy, antiangiogenic agents, photodynamic therapy, and a glutamate antagonist. A neurorestorative therapy with atorvastatin was evaluated in its effects on functional recovery after photodynamic therapy.

Functional outcomes were measured with an array of behavioral tests, which are sensitive to mild focal insults to the sensorimotor cortex and can detect recovery of function. Histopathological assessments consisted of Nissl staining, hematoxylin-and-eosin (H&E) staining, and immunohistochemistry, depending on varied purposes, used in conjunction with a computer imaging analysis system.

In clinical trials, functional outcome is as critical to gauging the success of a treatment as is patient survival time. Both preclinical screening of anti-cancer interventions for the ability to shrink tumors effectively with minimal disturbance of neuroplasticity and developing combination therapy with neurorestorative regimens following neurotoxic cancer treatments should allow for optimal promotion of plastic mechanisms in the remaining normal brain tissue.

Table of Contents

List of Tables xviii

List of Figures xix

Chapter 1: Introduction 1

1.1 Epidemiology, symptoms and treatment of brain tumors 1

1.2 Dilemmas in treating brain tumors 2

1.3 Aims of the dissertation research 6

Chapter 2: Mass-induced Brain Tissue Displacement and Behavioral Impairment 14

2.1 Abstract 14

2.2 Introduction 15

2.3 Materials and methods 16

2.3.1 Subjects 16

2.3.2 Materials 16

2.3.3 Experimental model 17

2.3.4 Behavioral tests 18

2.3.5 Tissue processing and analysis 23

2.3.6 Statistical analysis 25

2.4 Results 26

2.4.1 SMC lesion extent and placement 26

2.4.2 Behavioral deficits of compression are dependent on implant locations 30

2.4.3 Behavioral deficits are dependent on the timing of compression release 31

2.4.4 Behavioral deficits of compression depend on the magnitude of compression 34

2.5 Discussion 36

Chapter 3: Interruption of Functional Recovery by the NMDA Glutamate Antagonist MK-801 after Compression of the Sensorimotor Cortex 41

3.1 Abstract 41

3.2 Introduction 41

3.3 Materials and methods 43

3.3.1 Subjects 43

3.3.2 Experimental model 43

3.3.3 Behavioral tests 44

3.3.4 Tissue processing and analysis 44

3.3.5 Statistical Analysis 45

3.4 Results 45

3.5 Discussion 48

Chapter 4: Local Fluorouracil Chemotherapy Interferes with Neural and Behavioral Recovery after Brain Tumor-like Mass Compression 50

4.1 Abstract 50

4.2 Introduction 51

4.3 Materials and methods 52

4.3.1 Animals 52

4.3.2 Experimental model 52

4.3.2.1 Local delivery of 5FU 53

4.3.2.2 Bead implantation 53

4.3.3 Behavioral testing 53

4.3.4 Histological assessment 54

4.3.5 Statistical analysis 55

4.4 Results 55

4.4.1 Local delivery of 5FU exaggerates brain tissue loss after brain compression 55

4.4.2 Local delivery of 5FU induces elevated necrosis after brain compression 57

4.4.3 5FU microinjection causes extended damage around the needle track 57

4.4.4 Local delivery of 5FU induces elevated apoptosis after brain compression 59

4.4.5 Local delivery of 5FU exacerbates compression-induced functional deficits 61

4.5 Discussion 65

Chapter 5: Sensorimotor Deficits Associated with Brain Tumor Progression and Tumor-induced Brain Plasticity Mechanisms 68

5.1 Abstract 68

5.2 Introduction 69

5.3 Materials and methods 70

5.3.1 Experiment 1 70

5.3.1.1 Animals 70

5.3.1.2 Experimental model 70

5.3.1.3 Behavioral testing 72

5.3.1.4 Histological assessment 72

5.3.1.5 Statistical analysis 74

5.3.2 Experiment 2 75

5.3.2.1 Animals, experimental model, and behavioral testing 75

5.3.2.2 MRI measurement 75

5.3.2.3 Statistical analysis 76

5.4 Results 77

5.4.1 Experiment 1 77

5.4.1.1 Late onset of significant behavioral deficits in 9L glioma-bearing rats 77

5.4.1.2 Tumor volume and placement 80

5.4.1.3 Reactive peri-tumoral brain plastic events 80

5.4.2 Experiment 2 84

5.4.2.1 Significant correlation between magnitude of somatosensory asymmetry and brain tumor volume 84

5.5 Discussion 85

Chapter 6: Functional Outcome after Antiangiogenic Treatment in a Mouse Glioma Model 90

6.1 Abstract 90

6.2 Introduction 90

6.3 Materials and methods 92

6.3.1 Cell culture 92

6.3.2 Experimental model 92

6.3.3 Antiangiogenic treatment regimen 93

6.3.4 Histopathology 93

6.3.4.1 Tissue preparation 93

6.3.4.2 Measurement of tumor volume 94

6.3.4.3 Immunohistochemistry 94

6.3.4.4 Quantification 94

6.3.5 Behavioral testing (rearing) 95

6.3.6 Statistical analysis 95

6.4 Results 96

6.4.1 Delayed onset of significant functional deficits in U87 glioma-bearing mice treated with MF1 and DC101 96

6.4.2 Reduced U87 glioma growth under treatment with MF1 and DC101 97

6.4.3 Increased tumor necrosis and apoptosis and reduced tumor cell proliferation after treatment with MF1 and DC101 98

6.5 Discussion 100

6.5.1 Importance of functional assessment in preclinical research of brain tumor therapy 100

6.5.2 Behavioral changes in mouse models of brain tumors 101

6.5.3 Rationale for using antiangiogenic therapy targeting both VEGFR-1 and -2 to treat gliomas 101

6.5.4 Functional effects of the novel antiangiogenic treatment targeting both VEGFR-1 and -2 on the tumor-bearing brain 103

6.5.5 Suppression of glioma growth by the novel antiangiogenic treatment targeting both VEGFR-1 and -2 104

6.5.6 Summary 105

Chapter 7: Systemic Administration of BCNU Suppresses Glioma Growth and Inhibits the Onset of Glioma-induced Sensorimotor Deficits 106

7.1 Abstract 106

7.2 Introduction 106

7.3 Materials and methods 108

7.3.1 Animals 108

7.3.2 9L gliosarcoma cell culture and 9L cell implantation in Fischer rats 108

7.3.3 BCNU treatment regimen 108

7.3.4 Behavioral testing 108

7.3.5 MRI measurement 108

7.3.6 Statistical analysis 109

7.4 Results 109

7.5 Discussion 111

Chapter 8: Photofrin-mediated Photodynamic Therapy Induces Behavioral Deficits and Attempts at Using a Neurorestorative Agent for Functional Recovery 114

8.1 Abstract 114

8.2 Introduction 114

8.3 Materials and methods 116

8.3.1 Animals 116

8.3.2 Experimental model 116

8.3.3 Behavioral testing 118

8.3.4 Histological assessment 118

8.3.5 Statistical analysis 118

8.4 Results 119

8.5 Discussion 121

Chapter 9: General Discussion and Future Directions 123

Glossary 129

References 131

Copyright Statement 170

Vita 172

List of Tables

Table 2.1: Histological analysis after brain compression. 29

Table 3.1: Percentage of animals in each treatment group showing placing deficits. 47

List of Figures

Figure 1.1: Overview of the dissertation. 8

Figure 2.1: Example picture of a rat in the forelimb-use asymmetry test. 19

Figure 2.2: Example pictures of a rat in the somatosensory asymmetry test. . 20

Figure 2.3: Example picture of a rat in the foot-fault test. 21

Figure 2.4: Example picture of a rat in the tapered ledged beam test. 22

Figure 2.5: Example pictures of a rat in the placing tests. 23

Figure 2.6: Schematic diagram of a cross section from the compressed area. 25

Figure 2.7: Histological images of brain compression. 27

Figure 2.8: Behavioral responses in rats with brain compression in varied locations. 31

Figure 2.9: Behavioral responses in rats with brain compression released at different times. 33

Figure 2.10: Behavioral responses in rats with different magnitudes of brain compression. 35

Figure 3.1: Histological and behavioral examinations after MK801 administration in rats with brain compression. 47

Figure 4.1: Local chemotherapy exaggerates compression-induced tissue loss in the SMC. 56

Figure 4.2: Local chemotherapy induces increase in necrosis following either focal cortical compression or needle damage. 58

Figure 4.3: Local chemotherapy leads to increase in apoptosis following focal cortical compression. 60

Figure 4.4: Local chemotherapy exacerbates compression-induced placing deficits. 62

Figure 4.5: Local chemotherapy exacerbates compression-induced behavioral deficits in both the forelimb-use and the forelimb somatosensory asymmetry tests. 64

Figure 5.1: Behavioral deficits associated with brain tumor progression. 79

Figure 5.2: Significant increase in MAP2 and GFAP expression in the peri-tumoral area. 82

Figure 5.3: Significant increase in vWF and synaptophysin expression in the peri-tumoral area. 83

Figure 5.4: Significant correlation between tumor volume and magnitude of somatosensory asymmetry. 85

Figure 6.1: Retarded onset of significant behavioral deficits in U87 tumor-bearing mice after MF1 and DC101 treatment. 97

Figure 6.2: Reduced U87 tumor growth after MF1 and DC101 treatment. 99

Figure 7.1: Systemic BCNU treatment inhibits the onset of glioma-induced somatosensory deficit..... 110

Figure 7.2: Systemic BCNU treatment inhibits tumor growth..... 111

Figure 8.1: Behavioral response to high-dose PDT and functional outcome after atorvastatin administration to PDT-treated rats..... 120

Figure 8.2: Histological images of PDT-induced brain damage. 120

Chapter 1: Introduction

1.1 EPIDEMIOLOGY, SYMPTOMS AND TREATMENT OF BRAIN TUMORS

The incidence rate of brain tumors is 14 per 100,000 with the five-year survival rate only 25.6% (central brain tumor registry of the United States, CBTRUS, 1995-1999 Data). Approximately 17,000 people develop new cases of primary brain tumors each year in the United States (Landis et al., 1998). About 60% of primary brain tumors are gliomas and the majority of these are clinically aggressive and high grade (Ries et al., 1991). Central nervous system (CNS) neoplasm is the most common type of all childhood solid tumors and the No. 2 leading cause of cancer deaths in children (Wingo et al., 1995). Despite the routine therapy—resection surgery, radiation and chemotherapy, the prognosis is generally grim with 24.6 average life years lost for CNS cancers ［surveillance epidemiology and end results (SEER) ］.

Brain tumors are distinguished from other tumors in that every brain area has an associated function, and the tumors arise in the skull with little room for expansion. Brain tumors carry high rates of mortality and morbidity. Symptoms of brain tumors are produced by the tumor mass primarily, and also by the surrounding edema, the infiltration and destruction of normal brain tissue (Soo et al., 1995). The nonspecific symptoms of brain tumors, due to increased intracerebral pressure (ICP), are headache, nausea and vomiting. The specific signs and symptoms, depending on the tumor location, include seizures, aphasia, visual deficits, hearing loss, one-sided muscle weakness (hemiparesis), and changes in personality, concentration and memory (DeAngelis et al., 2004). In the early stage of many types of brain tumors, the tumor grows so slowly and

the symptoms appear so gradually that they may be ignored for a long period, which results in a delayed diagnosis.

Surgery is generally the first step and the most effective treatment for both malignant and non-malignant brain tumors to reduce tumor size as well as brain pressure. Radiation therapy plays a central role in the management of malignant tumors and chemotherapy is important in prolonging the survival in some but not all types of brain tumors. Although most primary brain tumors rarely metastasize, the regional infiltration into the surrounding normal tissue during tumor progression leads to badly demarcated borders and underlies their great propensity for recurrence (Mikkelsen and Edvardsen, 1996). Malignant gliomas are highly invasive, characterized by high incidence of recurrence and poor prognosis (Burger and Kleihues, 1989; Nicholas et al., 1997; Kleihues et al., 2002). Aggressive brain tumor treatments, such as extensive surgical resection, high dose radiation and local chemotherapy, tend to enhance tumor destruction and delay tumor recurrence. However, this goal is built upon damage to adjacent normal tissue, and thus not easily attained. Therefore, novel therapeutic strategies aimed at improving the efficacy/toxicity ratio are desperately needed. New compounds, that demonstrate selective tumor localization and/or can increase the sensitivity of tumor cells to radiotherapy, chemotherapy, and photodynamic therapy (Sessler and Miller, 2000; Magda et al., 2001; Naumovski et al., 2005; Wei et al., 2005b; Naumovski et al., 2006; Wang et al., 2007b), represent the future of cancer treatment.

1.2 DILEMMAS IN TREATING BRAIN TUMORS

The ultimate goal in tumor therapy is to cure the disease and save life. To fulfill the goal, a combination of treatment modalities is needed, including “killing paradigms”, such as surgery, radiation, chemotherapy, aimed at maximal debulking of tumor burden

and destruction of tumor cells in the circulatory system, as well as "regulatory paradigms", such as anti-invasive and anti-angiogenic treatments, aimed at controlling tumor growth and spread (Mikkelsen, 1998). For brain tumors, the "killing paradigms" can directly damage the surrounding normal brain tissue, due to their toxicity and lack of selectivity. The "regulatory paradigms" may not directly damage normal brain tissue, but they may harm the neuroplastic mechanisms which are important in functional recovery. Inhibition of vascular endothelial growth factor (VEGF) suppresses the growth of gliomas (Kim et al., 1993; Cheng et al., 1996); however, it also impedes revascularization and neural repair after brain injury (Krum and Khaibullina, 2003). Inhibition of basic fibroblast growth factor (FGF-2) impedes glioma growth (Stan et al., 1995); however, it also retards functional recovery from motor cortex injury (Rowntree and Kolb, 1997). Low-dose radiation attenuates neurogenesis and exacerbates ischemia-induced functional deficits (Raber et al., 2004). Many treatments that can shrink brain tumors may not increase survival meaningfully, and even if they increase survival, they may not necessarily improve function, at least not optimally, because of adverse effects on restorative mechanisms. Radiation and chemotherapy are widely blamed for their neurological complications (Vigliani et al., 1999; Plotkin and Wen, 2003; Aarsen et al., 2006). Deterioration in neurological function is accompanied by significant deterioration in global quality of life in patients with high-grade glioma (Osoba et al., 1997). The need for functional improvement and prevention of further neurological decline is well appreciated but difficult to investigate systematically because the functional benefit of treatments that shrink tumors might be offset if treatments compromise processes critical to recovery and maintenance of function.

Current supportive treatment primarily includes anticonvulsants and corticosteroids, focusing on relieving symptoms (DeAngelis et al., 2004). However, no

neurorehabilitative strategy is clinically available to protect from treatment-related toxicity and improve long-term neurological function. Ramipril, an inhibitor of angiotensin-converting enzyme (ACE), ameliorates radiation-induced brain damage in a rat optic neuropathy model (Kim et al., 2004). A thrombin inhibitor was used in a rat glioma model to reduce tumor size with functional benefit (Hua et al., 2005a; Hua et al., 2005b). A preliminary, retrospective investigation in a sample of patients with primary malignant brain tumors showed the effectiveness of postacute brain injury rehabilitation methods, originally developed for traumatic brain injury survivors, in ameliorating neurobehavioral deficits due to the tumor, surgical resection, and subsequent radiation and chemotherapy (Sherer et al., 1997).

To a limited extent, the brain repairs itself after damage. Neurogenesis, angiogenesis, upregulation of growth factors and inhibition of spontaneous apoptosis play important roles in the recovery and restoration after stroke and other brain injuries (Gomez-Pinilla et al., 1992; Cramer and Chopp, 2000; Chao et al., 2002; Keyvani and Schallert, 2002; Mattson et al., 2002; Parent et al., 2002). A brain tumor, acting as a lesion, can trigger reactive neuroplastic responses that make the brain adapt to the tumor insult gradually (Duntsch et al., 2005; Glass et al., 2005; Bexell et al., 2007; Yang et al., 2007b). However, many of the developmental and neuroplastic mechanisms also may be what brain tumors rely on to support growth, differentiation, invasion and metastasis (Eberhart et al., 2001; Singh et al., 2004; Arrieta et al., 2005; Kaur et al., 2005; Rege et al., 2005). Gliomas are angiogenesis-dependent (Plate and Risau, 1995; Kargiotis et al., 2006). VEGF secreted by glioma cells plays a prime role in the induction of tumor angiogenesis (Plate et al., 1992; Plate et al., 1993; Plate et al., 1994). FGF-2 produced by some types of gliomas is related to angiogenesis and tumorigenicity (Stan et al., 1995; Segal et al., 1997; Ke et al., 2000; Auguste et al., 2001). Again, one of the dilemmas

confronting brain tumor management is that treatment regimens targeting tumor promotion pathways may depress neuroplasticity and functional recovery. To summarize, neutralization of endogenous VEGF causes decreases in angiogenic activity and astroglial proliferation, resulting in impediment to neural repair following stab wound brain injury (Krum and Khaibullina, 2003). Blockade of FGF-2 with neutralizing antibodies retards functional recovery from suction lesions of the motor cortex (Rowntree and Kolb, 1997). On the other side, treatments that can protect and benefit injured neuronal tissue may also protect and benefit tumor tissue. Fluid derived from wound injury was shown to accelerate growth of C6 glioma in spheroid culture, suggesting the stimulatory effect of injury on tumor progression (Abramovitch et al., 1999).

However, brain repair and tumor suppression may not always be contradictory and they can possibly be monitored in the same way. Malignant glioma cells attract endogenous precursor cells as a reparative mechanism and the presence of precursor cells is antitumorigenic (Duntsch et al., 2005; Glass et al., 2005; Bexell et al., 2007). Increased neuronal differentiation and synaptogenesis are associated with decreased aggressiveness in retinoblastoma (Johnson et al., 2007). Neurotrophins [Nerve growth factor (NGF), brain-derived neurotrophic factor (BDNF), and Neurotrophin 3 (NT-3)] are essential mediators of proliferation, differentiation, and survival of cells in the normal brain (Ibanez et al., 1995). BDNF is widely established as a major trophic factor in normal and injured brain function (Keyvani and Schallert, 2002; Vaynman et al., 2004; Kim et al., 2005; Kleim et al., 2006). Human origin gliomas generate neurotrophins with BDNF being the most abundantly expressed, and extrinsic neurotrophins failed to stimulate mitosis of the glioma cultures (Hamel et al., 1993). There is evidence that neurotrophin signaling is involved in the process of apoptosis and neuronal differentiation in medulloblastomas (Chou et al., 1997; Eberhart et al., 2001). Whereas in normal blood

vessel Ang-1 expression exceeds Ang-2 expression, the opposite is true in tumor blood vessels (Stratmann et al., 1998; Tse et al., 2003). Block of the stabilizing effect of Ang1 on both preexisting and newly formed blood vessels by Ang2 cooperates with VEGF to induce tumor blood vessel growth (Stratmann et al., 1998; Holash et al., 1999; Zagzag et al., 1999; Audero et al., 2001; Ding et al., 2001; Papetti and Herman, 2002; Tse et al., 2003). Therefore, normalization of the expression pattern of Ang-1, Ang-2 and their endothelial cell receptor Tie2 may normalize the abnormal structure and function of tumor vasculature to make it more efficient for oxygen and anti-cancer drug delivery (Jain, 2005). Interestingly, in addition to reducing vascular permeability and enhancing vascular stabilization and maturation (Suri et al., 1996; Suri et al., 1998), Ang1 can trigger the migration of immature neurons to the site of brain damage and promote functional recovery after stroke (Ohab et al., 2006), thus linking the two processes of neurogenesis and angiogenesis together.

1.3 AIMS OF THE DISSERTATION RESEARCH

The main challenge for modern brain cancer research is to design novel interventions or improve the existing therapy to reduce undesirable neurological side effects while maintaining anti-cancer efficacy, as well as to develop treatments that can provide neuroprotection during cancer therapy or promote neurorestoration afterwards. In clinical trials, functional outcome is a major target, but seems to be neglected in translational brain tumor research. This might be due to the assumption that it should be primary for a treatment to avert a patient's death, or that reduction of tumor size may result in functional improvement in parallel. However, it may also be that there has been a lack of suitable experimental approaches to assess the adverse effects of anti-cancer treatments on functional outcomes. Unfortunately, this void places a serious limitation on

the ability to weigh the risks and benefits of new therapies and to develop strategies to rehabilitate damaged function.

To summarize, limitations of contemporary brain tumor research are that: 1) Preclinically promising anti-cancer treatments can cause worsening of neurological symptoms in clinical trials; 2) Functional measurements are rarely used in preclinical cancer research; 3) Injury and neuroplastic mechanisms induced by brain tumor progression are not clear; 4) There is a distinct lack of research on developing treatments that can provide neuroprotection during cancer therapy or promote neurorestoration afterwards.

Fig. 1.1 shows the overview of the whole dissertation. My dissertation research was aimed at developing animal models to facilitate preclinical screening for anti-cancer drugs with minimum neurotoxicity and reduced harm to neuroplasticity and to assist the investigation of rehabilitative strategies after aggressive anti-cancer therapy.

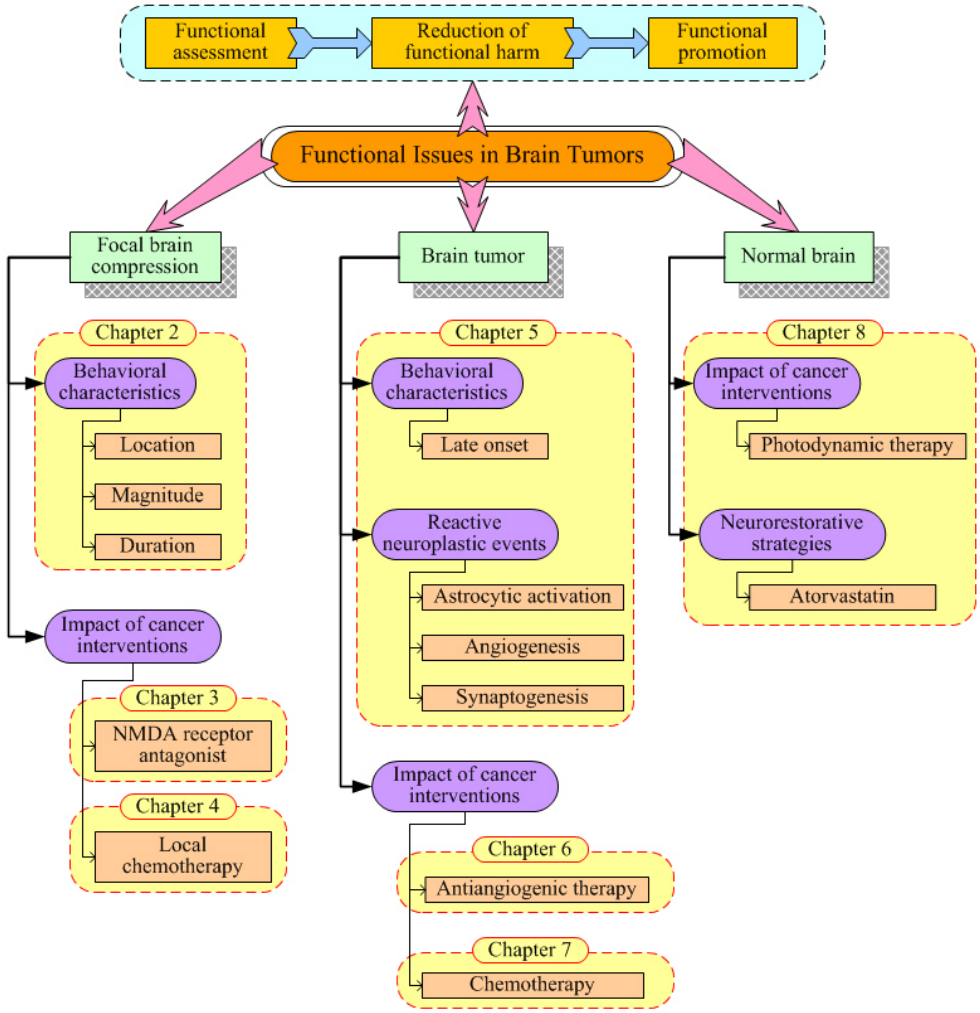

Figure 1.1: Overview of the dissertation.

To fulfill this aim, the following related experiments were conducted: (a) development of a mass compression model with epidural implantation of a hemisphere-shaped bead over the sensorimotor cortex and assessment of the behavioral deficits following varied location, magnitude and duration of the focal compression (Chapter 2); (b) evaluation of the impacts of two examples of novel brain tumor treatments - an NMDA glutamate antagonist MK801 (Chapter 3) and local fluorouracil chemotherapy

(Chapter 4) on neurorestoration using the mass compression model; (c) measurement of the functional deficits in orthotopic rodent glioma models and investigation of the tumor-induced brain plasticity mechanisms (Chapter 5); (d) evaluation of the functional outcomes after anti-cancer treatments, including antiangiogenic treatment (Chapter 6) and systemic chemotherapy (Chapter 7) as examples, administered in the dormant stages of brain tumors; and (e) measurement of the functional responses after photodynamic therapy in normal brain and evaluation of the functional outcomes of a novel combination therapy with photodynamic therapy and a neurorestorative agent atorvastatin (Chapter 8).

This dissertation is composed of a wide variety of experiments conducted on various models, including a focal brain compression model and a tumor cell implantation model. The dissertation has a seemingly loose structure, but a strict internal logic. First, in many cases, reduction of tumor may result in functional improvement in parallel, and the effects of mass reduction may mask the adverse effects of the treatment on the integrity of brain function. Therefore, a model that can hold tumor size constant independent of treatment may help assess the potential detrimental effects of tumor growth inhibitors on brain plasticity more directly. We then adopted an epiducal bead implantation model which was first developed by Chen et al. in 2003 (Chen et al., 2003b). The hemisphere-shaped plastic bead is like a mechanical tumor, which can induce significant focal brain compression, and can be either left remained or removed when needed. However, before this model can be used to screen for anti-cancer drugs with reduced adverse effects on brain function, we need to characterize the behavioral change pattern of this focal brain compression model. Because location and size are two major factors that determine clinical signs and symptoms of brain tumors and surgical resection is the most important treatment for brain tumors, we then investigated how location, duration and magnitude of the focal compression might affect the behavioral

changes, with two factors fixed and the other one changed once a time. Each time, we changed one single factor, and compared the behavioral responses, when the bead was implanted into varied locations over the sensorimotor cortex (SMC), when the bead was removed at different times, and when different sizes of beads were implanted, respectively. Finally, we found that the model of 2-mm-thick bead remained implanted over the middle SMC is suitable to investigate the potential adverse effects of anti-cancer treatments on functional recovery, because it can reliably induce transient, mild, but significant behavioral deficits in all of the four behavioral tests that we used, including forelimb asymmetry, somatosensory asymmetry, and placing tests. We then used this bead compression model to assess the behavioral responses after treatment with glutamate antagonist MK801 and 5FU local chemotherapy, respectively, as two examples to show "proof of principle", because they are both novel treatments that can reduce glioma growth according to literature (Menei et al., 1996; Lemaire et al., 2001; Rzeski et al., 2001; Takano et al., 2001; Ishiuchi et al., 2002; Fournier et al., 2003; Menei et al., 2004), and may possibly interfere with functional recovery after focal brain compression.

Second, how rats bearing gliomas grown in the SMC and the underlying striatum behave in our sensorimotor tests is unknown, and warrants investigation, because the glioma implantation model is to date the closest model to mimic clinical tumor characteristics in human patients. Therefore, we implanted 9L glioma cells into the SMC of Fischer rats and measured their behaviors repeatedly until they started to die. We found that the average behavioral performance was not significant until very late stage of tumor growth, although some of the animals showed substantial functional impairment earlier. Histological analyses indicated that there were some variabilities in tumor growth rate. Therefore, a closer case-by-case tumor volume-behavior correlation needs to be evaluated to clarify how tumor progression affects rats' behavior. Magnetic resonance

imaging (MRI) was then used to monitor tumor volume right after the behavioral testing. Regression analyses were performed to correlate the behavioral test score with the corresponding tumor volume. To investigate whether a brain tumor is like a lesion which can induce neuroplasticity, immunohistochemistry was performed to assess the expression levels of multiple markers for neurons, astrocytes, endothelial cells, and synaptogenesis in the peri-tumoral area. From testing the glioma-bearing animals, we found a dormant period of tumor growth, in which no significant behavioral deficits were exhibited. We then used this glioma implantation model to investigate whether certain cancer therapies can cause worsening of functional deficits in the dormant stage of tumor growth. Antiangiogenic therapy is a relatively new form of cancer treatment using angiogenesis inhibitors that specifically halt new blood vessel growth and starve a tumor by cutting off its blood supply. We had two antiangiogenic agents available in the lab, which are antibodies against vascular endothelial growth factor receptor (VEGFR) -1 and 2, respectively. It has recently been shown in the literature that combination of the two antibodies targeting both VEGFR-1 and VEGFR-2 is more effective than either single antibody to treat cancers (Lyden et al., 2001). However, the two antibodies available in the lab are both designed targeting mouse antigens. We then employed a nude mouse intracranial model using the U87 malignant glioma cell line to investigate the behavioral response after systemic administration of antiangiogenic therapy during the dormant period of tumor growth. BCNU is a classic chemotherapy drug which has been the mainstay of management of malignant glioma in clinic for decades. We used the rat 9L glioma model to investigate the behavioral response after systemic administration of BCNU during the dormant period of tumor growth. We found that both the antiangiogenic agents and BCNU retarded or inhibited the onset of significant behavioral deficits without affecting brain function adversely in the dormant stages of tumor

development. However, the behavioral performances with or without anti-cancer therapy were compared under the conditions of different tumor sizes, due to the tumor reduction effect of the anti-cancer therapies. Therefore, this tumor implantation model is not suitable to detect the potential adverse effects of anti-cancer therapies on neuroplasticity. These experiments, in fact, prove the necessity of using a controlled-rate non-tumor compression/decompression model to detect the potential adverse effects of anti-cancer therapies on neuroplasticity.

Third, not only brain tumors themselves can cause damage, conventional cancer treatment approaches, such as surgical tumor resection, radiotherapy and chemotherapy, can also cause neurological impairment. Usually in the clinic, surgical resection is performed as soon as a brain tumor is diagnosed if allowed. Radiation and chemotherapy may be used in conjunction with surgery. To mimic the aggressive local tumor killing procedure, and to simplify the model, we used a photodynamic therapy on the normal brain to show the principle of direct brain tissue damage by a cancer therapy. A model with severe and stable behavioral deficits is suitable to investigate a treatment's functional restorative effects. We measured the behavioral deficits associated with high-dose photodynamic therapy. We then investigated whether a neurorestorative treatment can promote the functional recovery after photodynamic therapy. Atorvastatin was our first attempt, because atorvastatin has shown significant neurorestorative effects in models of stroke, intracerebral hemorrhage, and traumatic brain injury (Chen et al., 2003a; Lu et al., 2004c; Lu et al., 2004b; Lu et al., 2004d; Lu et al., 2004a; Seyfried et al., 2004; Chen et al., 2005).

To summarize, the goal of this set of experiments was to start to fill a critical behavioral void in the early phases of translational brain tumor research. A longer term hope is for an improved collaboration among scientists in the areas of behavioral

neuroscience, experimental and clinical neuro-oncology, neurosurgery and neurology to find better ways to help patients have maximum functioning and quality of life.

Chapter 2: Mass-induced Brain Tissue Displacement and Behavioral Impairment

This work is published in Journal of Neurotrauma in 2006 (Yang et al., 2006c).

2.1 ABSTRACT

This study was focused on a preclinical model of brain compression injury which has relevance to the pathological condition of a brain tumor. Behavioral impairment as a result of rapid-onset small mass, and the factors involved in lesion formation and neuroplasticity were investigated. An epidural bead implantation method was adopted. Two sizes (1.5 mm and 2.0 mm thick) of hemisphere-shaped beads were used. The beads were implanted into various locations over the sensorimotor cortex (SMC- anterior, middle and posterior). The effects of early vs. delayed bead removal were examined to model clinical neurosurgical or other treatment procedures. Forelimb and hind-limb behavioral deficits and recovery were observed and histological changes were quantified to determine brain reaction to focal compression. Our results showed that the behavioral deficits of compression were influenced by the location, timing of compression release, and magnitude of compression. Even persistent compression by the thicker bead (2.0 mm) caused only minor behavioral deficits, followed by fast recovery within a week in most animals, suggesting a mild lesion pattern for this model. Brain tissue was compressed into a deformed shape under pressure with slight tissue damage, evidenced by pathological evaluation on hematoxylin and eosin (H&E)- and terminal deoxynucleotidyl transferase dUTP nick end labeling (TUNEL)- stained sections. Detectable but not severe behavioral dysfunction exhibited by this model makes it particularly suitable for direct assessment of adverse effects of interventions on

neuroplasticity after brain compression injury. This model may permit development of treatment strategies to alleviate brain mass effects, without disrupting neuroplasticity.

2.2 INTRODUCTION

An additional space-occupying mass within the closed cavity of the skull on the normal brain (mass effect), either from brain trauma, tumor, intracranial hemorrhage, or infection, can block the circulation system for the cerebrospinal fluid, resulting in surrounding brain edema and an even larger mass is formed, which induces compression or displacement of brain tissue. Chen et al. first developed a novel focal compression model with epidural implantation of a plastic bead over the sensorimotor cortex (SMC), and investigated the morphological changes of the surrounding brain tissue (Chen et al., 2003b). Although they reported that no obvious behavioral effects could be detected, it seemed reasonable that if sensitive enough tests were applied, mild deficits might be found in this model, which would enhance its value as a preclinical method to develop single or multi-target interventions that can reduce mass while promoting restorative events that contribute to "quality of life". This study was focused on the examination of behavioral changes in the focal compression model and the neuroplasticity associated with the mass lesion localized in the SMC, using sensitive tests that can detect injury to this region, recovery of function and small variations in trauma extent. Behavioral deficits depend on which regions of the SMC are injured (Barth et al., 1990b; Baskin et al., 2003). This study observed the location-dependent behavioral effects of the compression injury. Furthermore, how different magnitudes of compression affect behavioral deficits without causing severe brain tissue damage was also investigated. In the clinic, surgical removal of the mass is often executed to reduce intracerebral pressure

in patients suffering from brain compression. Therefore, this study determined how different time points for compression release influence functional recovery.

Quality of life after treatment for mass-related insults has not been adequately modeled, particularly functional outcome associated with brain integrity. Without controlling for mass effects specifically, it cannot be determined whether the treatment is maximally benign with respect to surviving brain tissue because the extremely beneficial effects of mass reduction would severely mask any adverse effects of the treatment on brain function. Moreover, because tumors can initiate cascades of pathological and non-pathological events that are independent of mass per se, a model that does not initiate these cascades may allow one to investigate behavior-related mass effects independently and thus may be additionally useful.

2.3 MATERIALS AND METHODS

2.3.1 Subjects

A total of 71 male Sprague Dawley rats (250-350 g) were used. They were housed in pairs in Plexiglas tub cages and were maintained on a 12:12 h light/dark cycle. Prior to the experiment they were tamed by gentle handling, and food and water were available ad libitum.

2.3.2 Materials

Two different sizes of hemispherical plastic beads with different thicknesses were used for focal compression surgeries. One is 4.8 mm in diameter and 1.5 mm in thickness, and the other is 4.8 mm in diameter and 2.0 mm in thickness. A small dent was drilled in the center of the flat surface for the convenience of orientation and removal.

2.3.3 Experimental model

Rats were anesthetized with i.p. injections of Ketamine (90 mg/kg) and Xylazine (10 mg/kg). The epidural bead implantation surgery was performed as described by Chen et al. (2003). Briefly, each animal was secured to the stereotaxic apparatus (Kopf), the scalp was incised and an elliptical hole with 5.8 mm in long diameter and 3.8 mm in short diameter was drilled in the skull over the SMC. The plastic bead, with the flat surface facing upward, was slipped obliquely into the hole very slowly and carefully to avoid damage to the dura. After the bead was placed completely under the skull, it was pulled back along the short axis of the hole and fixed well into the epidural space. The bead can be inserted and fixed because the diameter of the bead is shorter than the long diameter of the skull hole but longer than the short diameter of the skull hole. The bead was moved gently using the dent and a needle until the center of the bead was located on the required coordinates.

To compare the mechanical compression effects at different locations of the SMC, a plastic bead with 1.5 mm thickness was used, and the rats were divided into 3 groups. Group 1 (anterior group, n=6) underwent bead implantation with the compression center ~2 mm rostral to the bregma and 2.5 mm lateral to the midline; Group 2 (middle group, n=10) was given bead implantation with the compression center 0.7 mm rostral to the bregma and 2.5 mm lateral to the midline; Group 3 (posterior group, n=6) received bead implantation with the compression center ~2 mm caudal to the bregma and 2.5 mm lateral to the midline.

To detect the compression effects alone and to exclude the influence of the surgical procedure of skull removal on the behavioral results, Group 4 (control group, n=9) was designed to be compared with the group subjected to 1.5-mm-thick bead implantation over the middle SMC. The control group received only skull removal within

the same area as the middle group described above, but did not undergo bead implantation.

To determine the effects of magnitude of compression, plastic beads with 2.0 mm thickness were employed and Group 5 (2.0 mm bead group, n=8) underwent 2.0-mm-thick bead implantation with the same compression center as the 1.5-mm-thick bead implantation over the middle SMC.

After the bead implantation or control procedure, the scalp was sutured.

To examine the effects of compression release at different time points, Group 6 (day 0 removal group, n=9) underwent a 1.5-mm-thick bead implantation over the middle SMC, followed by immediate bead removal, and Group 7 (day 3 removal group, n=7) received a 1.5-mm-thick bead implantation over the middle SMC, followed by delayed bead removal at post-operative (post-op) day 3. The behavioral results of these two groups were compared with those of the group undergoing persistent 1.5-mm-thick bead compression over the same area.

2.3.4 Behavioral tests

Forelimb-use asymmetry test (cylinder test): Rats were placed in a transparent cylinder, which is 30 cm high and 20 cm in diameter. Rats tend to rear and contact the wall of the cylinder with their forepaws spontaneously (Fig. 2.1). The numbers of wall contacts with the ipsilateral (unaffected), the contralateral (affected) and both limbs were recorded by a rater blind to the lesion side. Twenty consecutive behaviors were scored. The extent of forelimb-use asymmetry was calculated as ipsilateral limb use plus 1/2 the number of "both" contacts, divided by the total number of behaviors (equal to 20). Higher scores (>50%) indicate greater behavioral deficits (Schallert and Woodlee, 2005).

Figure 2.1: Example picture of a rat in the forelimb-use asymmetry test.

Somatosensory asymmetry test: Rats were tested in their home cage. Adhesive labels (Avery adhesive backed labels, 113 mm^2) were attached to the distal-radial aspect of both forelimbs (Fig. 2.2 A). Rats tend to remove these uncomfortable stimuli (Fig. 2.2 B). The order of contact (i.e., left vs. right) was recorded in each of 4 trials to determine whether the rat showed a bias. If the animal showed a preference for removing the stimulus from one particular forelimb—that is, if the adhesive stimulus was contacted first on 3 or more of the trials—then additional tests were conducted to determine the magnitude of the somatosensory asymmetry. The size of the unbiased limb stimulus was progressively increased and, at the same time, the size of the biased limb stimulus was decreased by an equal amount (14.1 mm^2). The ratio of the size of the unbiased limb stimulus relative to that of the biased limb stimulus was increased until the bias was neutralized, providing the magnitude of somatosensory asymmetry. A score was given to reflect the two levels between which the animal reversed the original order of contact. If the rat did not show any bias, a score of 0 was assigned for it. If the rat showed a bias

contralateral to the lesion, a negative score was given, while a positive score was assigned to represent a bias ipsilateral to the lesion. Higher scores indicate greater behavioral deficits (Schallert et al., 1982; Schallert and Whishaw, 1984; Schallert et al., 2000; Schallert et al., 2002).

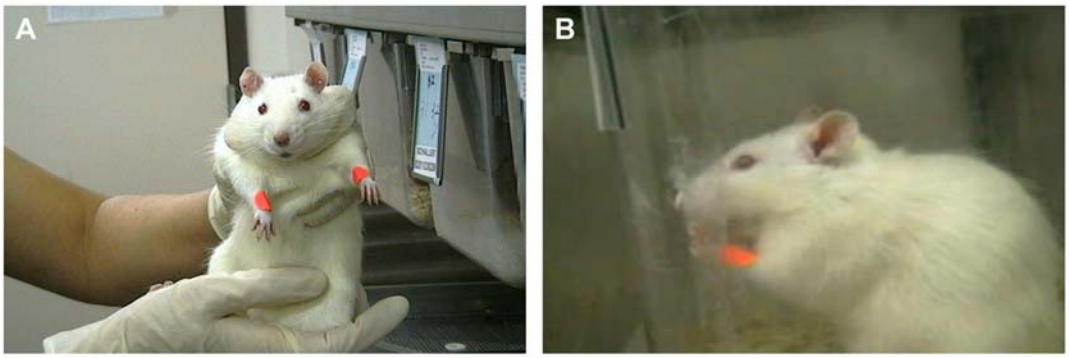

Figure 2.2: Example pictures of a rat in the somatosensory asymmetry test.

Foot-fault test: Animals were placed on an elevated grid floor (45 cm X 30 cm), 2.5 cm higher than a solid base floor, with 2.5 cm X 2.5 cm diameter openings. When animals inaccurately placed a limb, the limb fell through one of the openings in the grid (Fig. 2.3). When the limb fell through and pulled back quickly without touching the solid base, the behavior was called a half fault and counted as 1 foot-fault score. If the limb fell through and touched the base for support, this situation was called a full fault and counted as 2 foot-fault scores. Both foot-fault scores and the number of total steps for both forelimbs with at least 40 movements in a trial, were measured. The asymmetry score was given by subtracting the percent of ipsilateral forelimb faults from the percent of contralateral forelimb faults (Barth et al., 1990b).

Figure 2.3: Example picture of a rat in the foot-fault test.

Tapered ledged beam test: A tapered beam, 165 cm long and 2 cm thick, was placed on top of a wider beam to create a tapered beam with 2 cm wide ledges on each side positioned 2 cm below the top of the beam surface. This arrangement allows rats traversing the beam to use the bottom ledge as a crutch when they misstep (Fig. 2.4). The ledged beam reduces the need for rapidly learning compensatory motor behaviors to prevent falling, and thus reveals behavioral deficits in the rats chronically. If a rat misstepped and its limb touched either side of the beam without using the ledge for support, it was counted as a half fault. If the rat misstepped onto the ledge, it was counted as a full fault. Both step faults and the number of total steps for each hind-limb over 5 trials across the entire beam were measured. The asymmetry score was calculated by subtracting the percent of ipsilateral hind-limb faults from the percent of contralateral hind-limb faults (Schallert et al., 2002).

Figure 2.4: Example picture of a rat in the tapered ledged beam test.

Vibrissae-evoked forelimb placing test: The rat was gently held by its torso, with the tested forelimb hanging freely, and the untested forelimb kept from placing by gentle pressure on the front of the limb. A same-side placing reaction (Fig. 2.5 A and B) was induced by slowly moving the ipsilateral vibrissae toward a countertop until the tip of the vibrissae made contact with the edge, thus eliciting a placing response in the ipsilateral forelimb (Barth et al., 1990a; Jones and Schallert, 1994; Schallert and Woodlee, 2005). Similarly, a cross-midline placing response (Fig. 2.5 C and D) was induced by turning the rat sideways and brushing its contralateral vibrissae against the surface of the table, thus eliciting a placing response in the opposite forelimb (Woodlee et al., 2005). A score was given indicating the percent of successful placing responses during 10 trials for both forelimbs in either of these two placing tests (Schallert et al., 2000; Schallert et al., 2002; Hua et al., 2005a).

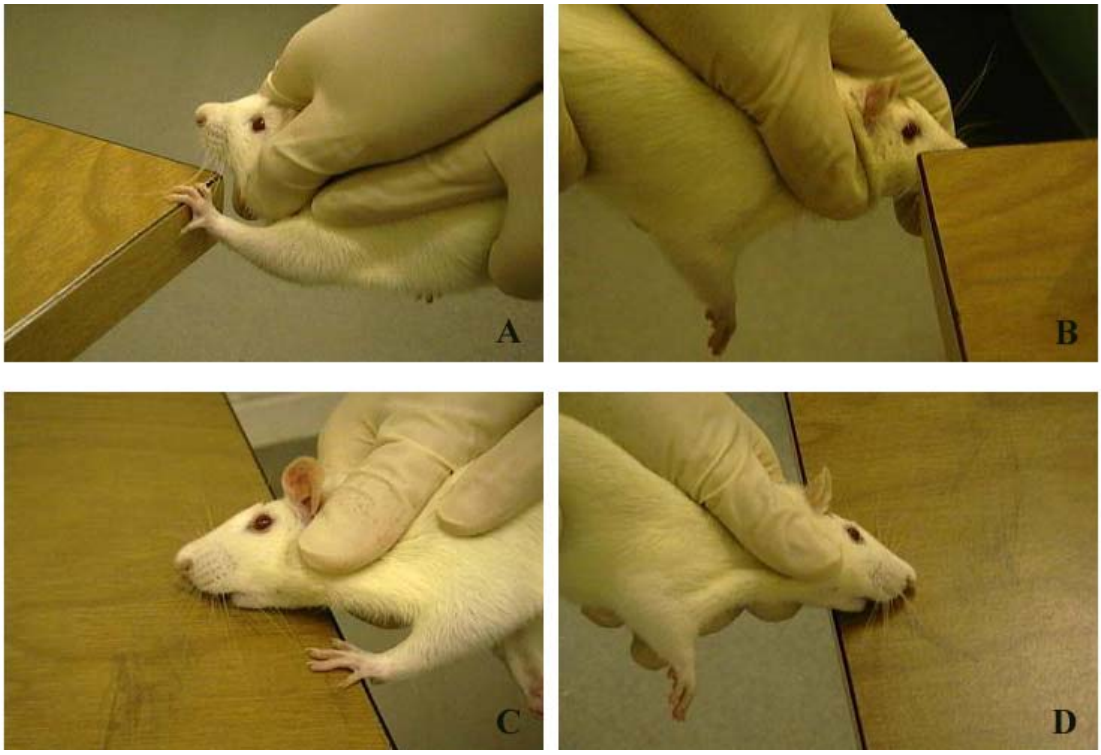

Figure 2.5: Example pictures of a rat in the placing tests.

(A and B) Examples of a successful (A) and a failed (B) placing response in the same-side placing test. (C and D) Examples of a successful (C) and a failed (D) placing response in the cross-midling placing test.

2.3.5 Tissue processing and analysis

Rats were anesthetized with an overdose of pentobarbital (75 mg/kg, i.p.) and perfused through the left ventricle with neutral buffered 10% formalin as a fixative following vascular washout with a 0.1 M heparinized phosphate buffer rinse. Brains were removed and postfixed at 4^{o}C in the same fixative.

The brain tissue from rats sacrificed at post-op day 7 was processed, embedded and cut into seven 2-mm-thick coronal blocks. Six-µm-thick paraffin sections from each block containing the area of bead compression were obtained and stained with

hematoxylin and eosin (H&E) for evaluation of pathological changes. For in situ apoptosis detection, the paraffin sections were stained using terminal deoxynucleotidyl transferase dUTP nick end labeling (TUNEL) apoptosis tag kit (Chemicon) according to the manufacturer's instructions and counter-stained with hematoxylin.

The brains from rats sacrificed at post-op day 28 were cut into 50-μm-thick sections on a vibratome. Every fourth section was mounted on slides and stained with toluidine blue for examination of anatomical changes and location. The areas containing the compressive lesion were scanned into the computer. A schematic diagram of a cross section from the compressed area is shown in Figure 2.6. The cortex thicknesses at the compression center and the corresponding contralateral hemisphere were measured as lines ab and cd, respectively, in figure 2.6. The hemisphere widths for both the lesioned and corresponding contralateral unlesioned sides were measured as lines ef and gh, respectively, in figure 2.6. Both the hemisphere areas and the cortex areas for both the lesioned and corresponding contralateral unlesioned sides were measured by tracing the demarcation on the computer screen using an NIH image analysis program (ImageJ, NIH). The hemisphere volumes (mm^3) and the cortex volumes (mm^3) were calculated by multiplying the appropriate area by the section interval thickness. The data are presented as the percentage of the lesion side to the corresponding contralateral side for each parameter.

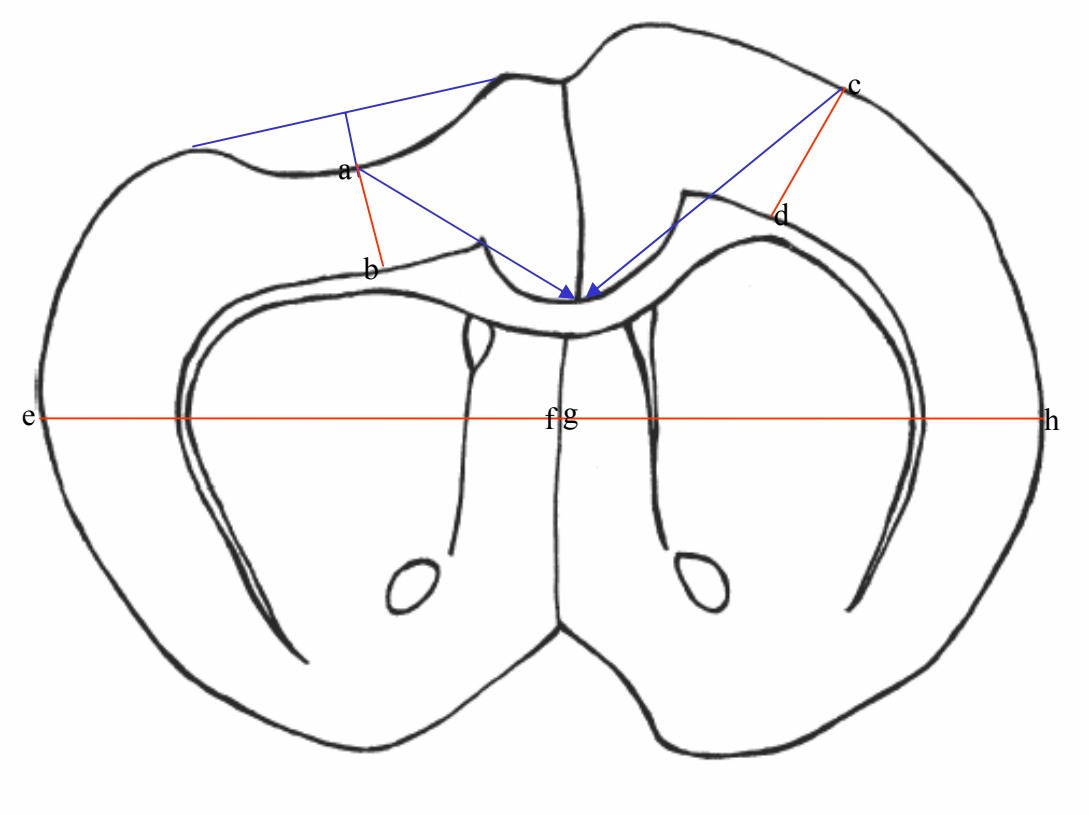

Figure 2.6: Schematic diagram of a cross section from the compressed area.

2.3.6 Statistical analysis

Statistical analyses were performed using SPSS 11.5 statistical software (SPSS, Inc., Chicago, Illinois, US). Repeated-measures analysis of variance (ANOVA) was applied to examine behavioral data across days, and the simple main effects at a specific test day were determined with one-way ANOVA. When there was a significant overall effect, post-hoc analyses were carried out. The anatomical data from different lesion groups were also compared by one-way ANOVA. Data are presented as mean ± standard error of the mean (SEM).

2.4 RESULTS

2.4.1 SMC lesion extent and placement

Figure 2.7 shows the brains removed 28 days after the 1.5-mm-thick bead compression over the anterior (Fig. 2.7 A), middle (Fig. 2.7 B) and posterior (Fig. 2.7 C) SMC, respectively. Sampling slices with Nissl staining from the group of 1.5-mm-thick bead compression over the middle SMC (Fig. 2.7 D) and the group of 2.0-mm-thick bead compression over the middle SMC (Fig. 2.7 E) are shown in Figure 2.7 as well. Both coronal sections were obtained at the site of the approximate compression center of each brain from the corresponding groups sacrificed 28 days after lesions. Both the 1.5-mm-thick and the 2.0-mm-thick bead compression led to brain deformation, in which the midline shifted toward the contralateral side and the brain became wider.

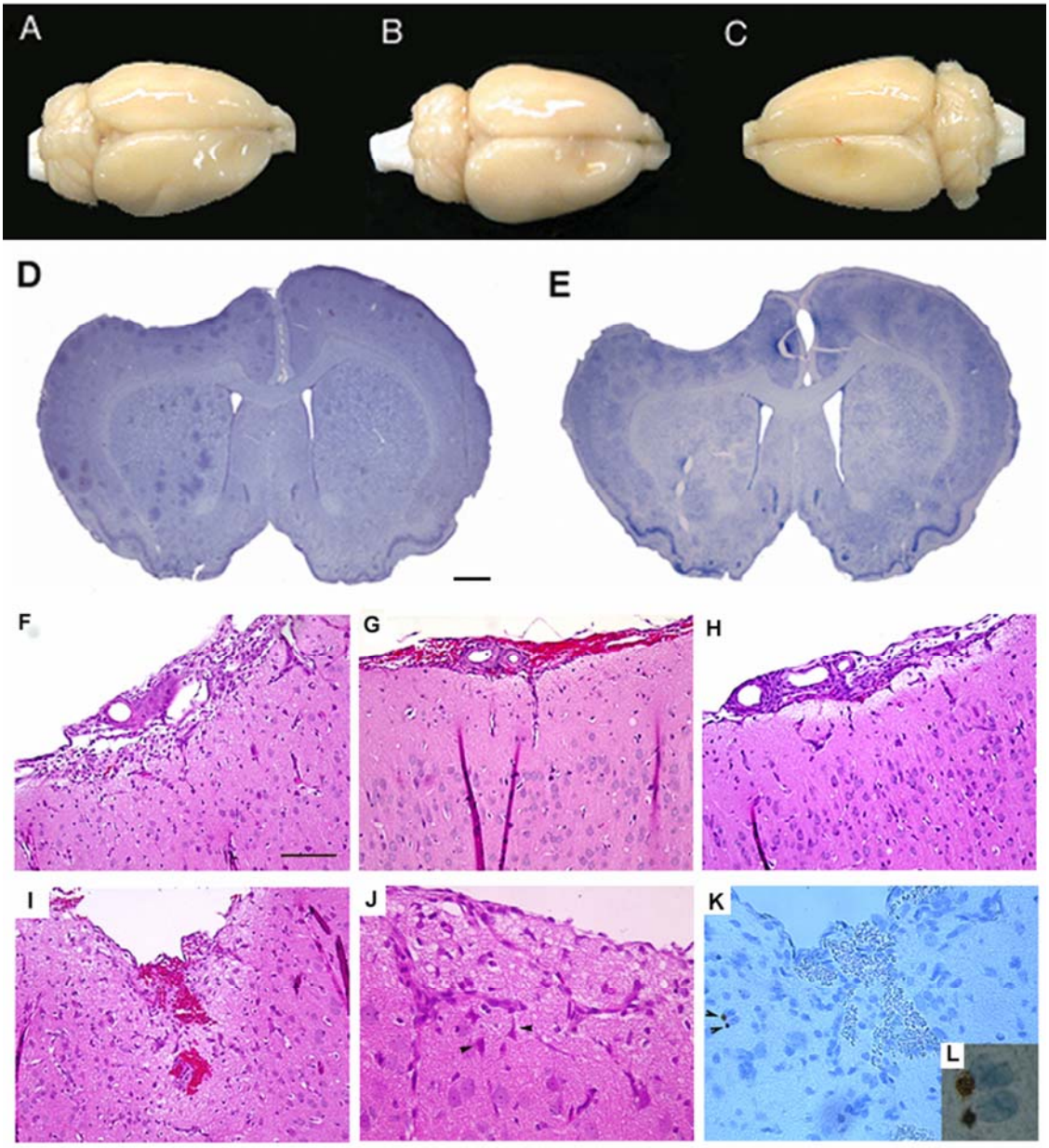

Figure 2.7: Histological images of brain compression.

(A-C) Brains with 1.5-mm-thick bead compression over varied areas of the sensorimotor cortex (SMC). These brains were all removed 28 days after bead implantation. (A) Anterior SMC compression. (B) Middle SMC compression. (C) Posterior SMC compression. (D,E) Slices at the compression center with Nissl staining. These two slices were both sectioned from brains with bead compression for 28 days. (D) 1.5-mm-thick bead compression. (E) 2.0-mm-thick bead compression. (F-L) H&E staining and TUNEL

apoptosis assay. H&E staining images (200 times magnification) show different magnitudes of damage, which includes hemorrhage, edema and cell death to the brain tissue in representative slices from 1.5-mm-thick bead implantation (F); 1.5-mm-thick bead implantation followed by immediate removal (G); 1.5-mm-thick bead implantation followed by removal at post-op day 3 (H); 2.0-mm-thick bead implantation (I). All were sacrificed at post-op day 7. Panel J shows a higher magnification (400 times magnification) of a representative slice from the 2.0-mm-thick bead compression group, with arrow heads indicating samples of necrotic neurons. Hematoxylin and TUNEL counter staining (400 times magnification) shows few apoptosis signals even in the 2.0-mm-thick bead implantation model, sacrificed at post-op day 7 (K). The arrow heads in panel K display samples of apoptotic neurons. Panel L shows a high magnification (1000 times magnification) of dark brown apoptotic neurons. Scale bar = 1 mm (D,E); Scale bar = 100 μm (F-I), 50 μm (J,K), 20 μm (L).

Table 2.1 shows the results for the lesioned hemisphere relative to the unlesioned hemisphere, including cortex thickness at the compression center, mean cortex thickness in the adjacent compression area, hemisphere width at the compression center, mean hemisphere width in the adjacent compression area, and the hemisphere and cortex volumes in the compression area. All data were collected from brains removed 28 days after lesions and subjected to Nissl staining. All three groups of 1.5-mm-thick bead implantation with varied compression locations showed less than 2 percent cortical tissue loss. One-way ANOVA indicated no significant differences among the anterior, middle and posterior SMC compression groups ($F(2,13) = 0.201$; $p = 0.820$). Compression induced by the 2.0-mm-thick bead over the middle SMC resulted in approximately 7 percent of cortical tissue loss. Considering cortex thickness, one-way ANOVA showed no significant differences among the three 1.5-mm-thick bead implantation groups in both cortex thickness at the compression center ($F(2,13) = 2.033$; $p = 0.171$) and the mean cortex thickness in the compression area ($F(2,13) = 3.562$; $p = 0.058$). 2.0-mm-thick bead compression over the middle SMC led to a significantly greater decrease of cortex thickness at the compression center, compared with 1.5-mm-thick bead compression over the same location ($F(1,13) = 4.833$; $p < 0.05$). As for the mean

hemisphere width in the compression area, no significant differences were found among the three 1.5mm thick bead implantation groups ($F(2,13) = 1.960$; $p = 0.180$). Also, no significant differences in mean hemisphere width were revealed between the groups of 2.0-mm-thick and 1.5-mm-thick beads implanted over the middle SMC ($F(1,13) = 0.125$; $p = 0.729$).

Table 2.1: Histological analysis after brain compression.

Ratios of cortex thickness at the compression center, the mean cortex thickness in the compression area, hemisphere width at the compression center, the mean hemisphere width in the compression area, hemisphere volume and cortex volume in the compression area of the lesion side to the contralateral side are shown from different lesion types, including 1.5-mm-thick bead implantation over the anterior SMC, middle SMC and posterior SMC, and 2.0-mm-thick bead implantation over the middle SMC. All the data were collected 28 days after surgeries with sections Nissl-stained. Data are mean ± SEM.

Ratio (Lesion/Contralateral)	*1.5 mm Bead (An)*	*1.5 mm Bead (Mid)*	*1.5 mm Bead (Pos)*	*2.0 mm Bead (Mid)*
Cortex thickness at the compression center	67.79%±0.060	55.86%±0.023	58.00%±0.053	43.74%±0.047
Mean cortex thickness	78.60%±0.023	72.10%±0.009	74.00%±0.028	66.09%±0.029
Hemisphere width at the compression center	109.84%±0.008	103.22%±0.025	103.13%±0.009	107.32%±0.012
Mean hemisphere width	108.29%±0.017	104.95%±0.021	102.58%±0.008	105.77%±0.012
Hemisphere volume	99.58%±0.002	96.58%±0.009	98.84%±0.004	93.93%±0.019
Cortex volume	99.05%±0.009	98.01%±0.013	98.61%±0.013	93.20%±0.024

To investigate early pathological changes following focal compression, 4 rats in each group were sacrificed at post-op day 7. H&E staining and TUNEL apoptosis assay were conducted. As shown in H&E stained sections (Fig. 2.2 F to I), hemorrhage, edema

and necrosis were present in each lesion group, which varied with magnitude, and was related to the extent of compression. Under light microscopy, as shown in Figure 2.2 J, necrotic neurons could be identified as red neurons, exhibiting cytoplastic eosinophilia, or ghost neurons, with complete loss of hematoxylinophilia, due to the features of necrosis, including pyknosis, karyorrhexis and karyolysis (Garcia et al., 1995). Vacuolization was prominent in the tissue area adjacent to the compressive mass. A higher density of blood vessels was also found, presumably reflecting damage-induced angiogenesis. General pathological evaluation indicated that the 2.0-mm-thick bead compression led to greater brain tissue damage than the 1.5-mm-thick bead compression, while the 1.5-mm-thick bead compression released at post-op day 3 displayed reduced brain tissue damage compared with the 1.5-mm-thick bead that remained implanted. The 1.5-mm-thick bead compression released immediately resulted in minor but notable brain tissue damage. With TUNEL staining, only few apoptotic cells were found even in the 2.0-mm-thick bead compression group (Fig. 2.2 K and L), suggesting that little apoptosis is involved in such focal compression lesions.

2.4.2 Behavioral deficits of compression are dependent on implant locations

In the cylinder test at post-op day 4 as shown in Figure 2.8, one-way ANOVA among the four groups revealed a significant main effect ($F(3,27) = 3.862$; $p < 0.05$). Post-hoc analyses indicated a significant difference between the middle SMC bead implant group and the control group ($F(1,17) = 8.303$; $p < 0.05$). However, no significant differences were found either between the anterior group and the control ($F(1,13) = 0.011$; $p = 0.918$) or between the posterior group and the control ($F(1,13) = 0.478$; $p = 0.502$). Also, at post-op day 4, the middle SMC bead implant group showed significantly more behavioral deficits than the anterior SMC bead implant group ($F(1,14) = 7.064$; $p <$

0.05), but there were no significant differences between either the middle group and the posterior group ($F(1,14) = 4.456$; $p = 0.053$), or the anterior group and the posterior group ($F(1,10) = 0.372$; $p = 0.556$). Because focal compression over the middle SMC led to more consistent behavioral deficits, the following experiments used this procedure to investigate the influence of timing and magnitude on compressive effects.

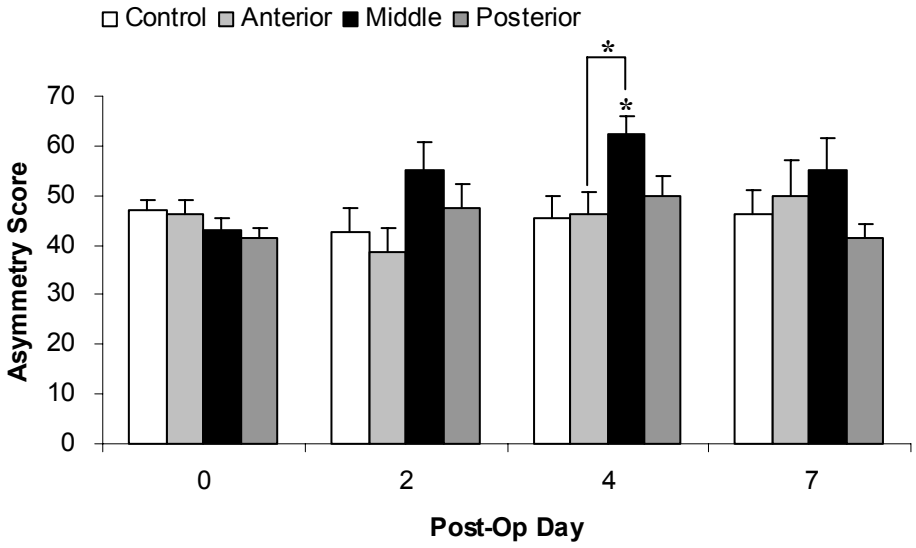

Figure 2.8: Behavioral responses in rats with brain compression in varied locations.

Animals with 1.5-mm-thick bead compression over the middle SMC, but not those undergoing either anterior or posterior SMC focal compression were found to exhibit significant forelimb-use asymmetry compared to the control. Data are mean ± SEM. * indicates a significant difference from control or between different conditions with $p < 0.05$.

2.4.3 Behavioral deficits are dependent on the timing of compression release

Compared with the control group in the cylinder test (Fig. 2.9 A), the group with the 1.5-mm-thick bead removed at post-op day 3 showed significant behavioral deficits at post-op day 2 ($F(1,14) = 7.762$; $p < 0.05$), but no significant differences at post-op day 4 and day 7, reflecting that compression release in the early stage can accelerate the

functional recovery. When removed immediately after implantation, the 1.5-mm-thick bead did not induce any behavioral deficits in the cylinder test at each time point compared with the control group.

In the somatosensory asymmetry test (Fig. 2.9 B). One-way ANOVA showed that 1.5-mm-thick bead implantation caused significant behavioral deficits at post-op day 7, compared with the control group ($F(1,17) = 7.382$; $p < 0.05$). Repeated-measures ANOVA showed significant differences between the group with the 1.5-mm-thick bead removed at post-op day 3 and the group with the 1.5-mm-thick bead left in place ($F(1,15) = 6.810$; $p < 0.05$). Simple main effects revealed significant group differences at post-op day 4 ($F(1,15) = 12.937$; $p < 0.01$). In contrast to the cylinder test results, the immediate bead removal group showed significant somatosensory asymmetry at post-op day 7, compared with the control group ($F(1,16) = 8.965$; $p < 0.01$), suggesting that even transient compression can cause at least some lasting, or delayed, behavioral deficits.

A

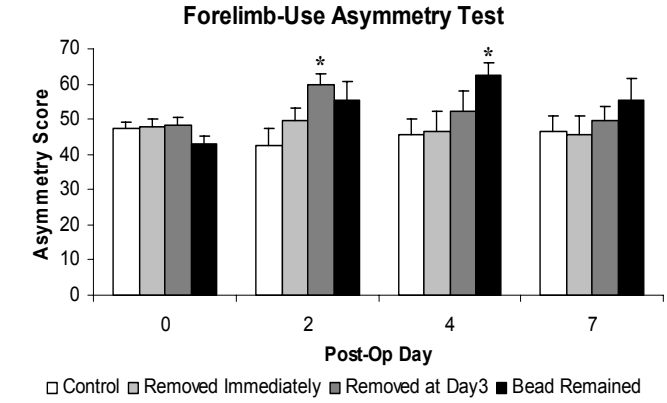

B

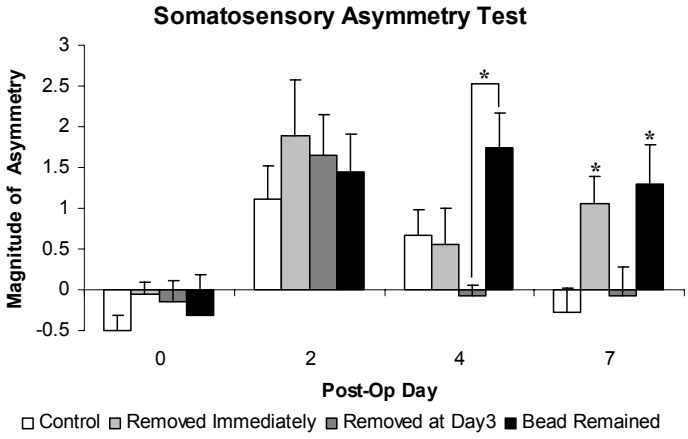

Figure 2.9: Behavioral responses in rats with brain compression released at different times.

Forelimb-use asymmetry (A) and somatosensory asymmetry (B). 1.5-mm-thick bead implantation caused significant behavioral deficits compared to the control group in both the cylinder test and the somatosensory asymmetry test. Bead removal at post-op day 3 resulted in improved functional recovery in both the cylinder test and the somatosensory asymmetry test. Bead implantation followed by immediate removal caused no behavioral deficits in the cylinder test, but significant deficits in the somatosensory asymmetry test. Data are mean ± SEM. * indicates a significant difference from control or between different conditions with $p < 0.05$.

2.4.4 Behavioral deficits of compression depend on the magnitude of compression

One-way ANOVA revealed that 2.0-mm-thick bead compression resulted in greater behavioral deficits than 1.5-mm-thick bead compression at post-op day 2 ($F(1,12) = 5.626$; $p < 0.05$) in the somatosensory asymmetry test (Fig. 2.10 A; $F(1,16) = 4.739$; $p < 0.05$), the foot-fault test (Fig. 2.10 B; $F(1,14) = 6.792$; $p < 0.05$), and the hind-limb ledged tapered beam test (Fig. 2.10 C; $F(1,12) = 6.861$; $p < 0.05$). The 1.5-mm-thick bead group did not show any placing deficits, while the 2.0-mm-thick bead implantation caused significant deficits in contralateral forelimb placing. In the same-side placing test (Fig. 2.10 D), repeated-measures ANOVA showed significant differences between the 1.5-mm-thick bead group and the 2.0-mm-thick bead group ($F(1,16) = 55.591$; $p < 0.001$) as well as a significant time effect ($F(6,96) = 24.581$; $p < 0.001$) and a significant time by group effect ($F(6,96) = 24.581$; $p < 0.001$). Follow-up tests of simple main effects revealed significant group differences at post-op day 1 ($p < 0.001$), day 2 ($p < 0.001$), day 3 ($p < 0.01$) and day 4 ($p < 0.05$). The cross-midline placing test also showed a similar behavioral pattern (Fig. 2.10 E). In repeated-measures ANOVA, there was a significant group effect ($F(1,16) = 5.153$; $p < 0.05$), a significant time effect ($F(6,96) = 5.348$; $p < 0.001$) and a significant time by group effect ($F(6,96) = 5.348$; $p < 0.001$). Follow-up tests of simple main effects revealed significant group differences at post-op day 1 ($p < 0.01$) and day 2 ($p < 0.05$). In the cylinder test, no significant differences were found between the 1.5-mm-thick and 2.0-mm-thick bead implantation (data not shown).

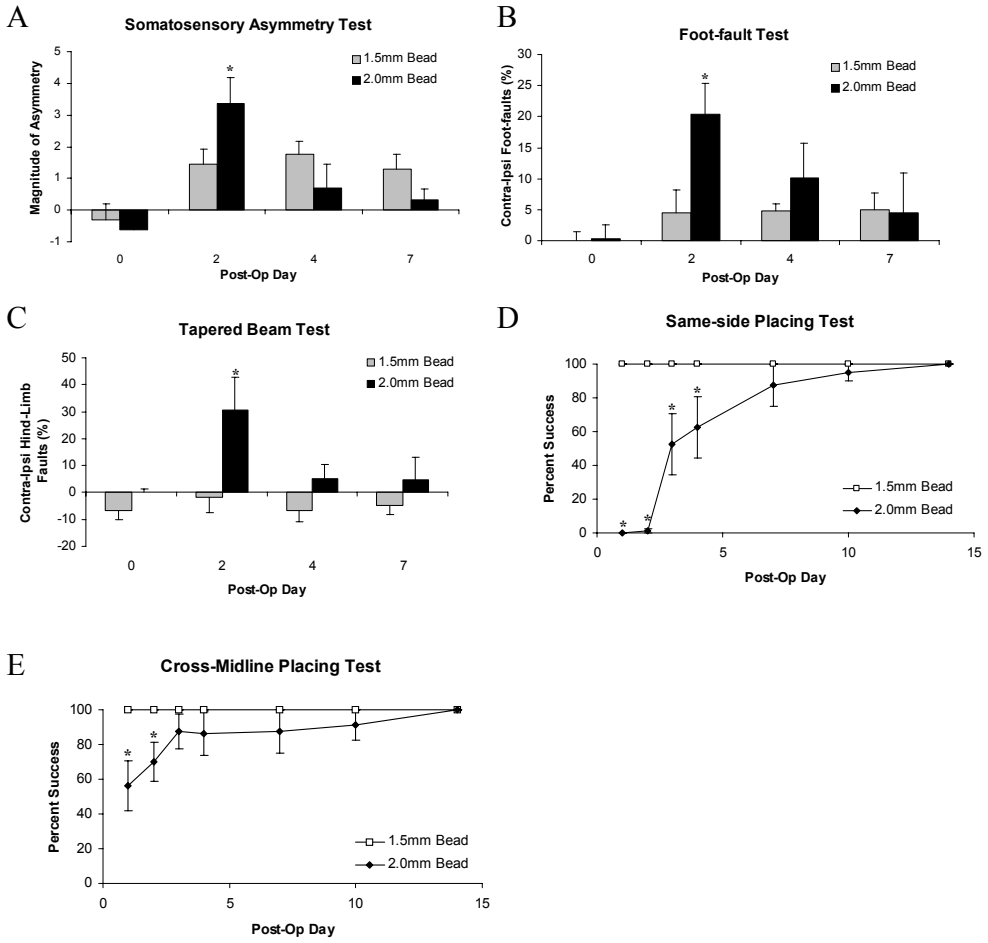

Figure 2.10: Behavioral responses in rats with different magnitudes of brain compression.

Somatosensory asymmetry (A), foot-faults asymmetry (B), hind-limb faults asymmetry as measured in the tapered beam test (C), same-side placing (D) and cross-midline placing (E) with the contralateral forelimb following different size bead implantation. The 2.0-mm-thick bead was found to cause greater behavioral deficits than the 1.5-mm-thick bead in all the above tests. Data are mean ± SEM. In A-C, a positive number represents a bias ipsilateral to the lesion and a negative number represents a bias contralateral to the lesison. * indicates a significant difference between different lesion groups with $p < 0.05$.

2.5 DISCUSSION

Besides the bead model that we used in this study, two other models of focal cerebral compression using different devices have been reported in the literature. One is the balloon model, used to examine the intracranial pressure and cerebral blood flow changes in compressed brain tissue (Abe et al., 1984; Douzinas et al., 1999; Im and Park, 2002). Another one is the piston model, used to determine the pathological and behavioral effects of acute epidural pressure leading to transient cerebral ischemia (Kundrotiene et al., 2002; Kundrotiene et al., 2004b; Kundrotiene et al., 2004a; Moreira et al., 2005; Moreira et al., 2006; Moreira et al., 2007). In 2003, Chen et al. first developed this bead model and used it to investigate how epidural compression affects neuronal morphology. However, no gross behavioral deficits were detected (Chen et al., 2003b). This bead model can well mimic mass lesions with the bead remaining implanted epidurally for a long time, which allows for the implementation of various interventions and chronic behavioral measurements using sensitive tests. Because location, duration and magnitude are the primary factors determining brain mass effects, we further modified the design of the bead by varying its thickness and adding a dent on the flat upper surface for more accurate orientation and more convenient translocation.

The results of the present study suggest that displacement of brain tissue occurs as a result of its elastic property under the insult of focal compression. In general, the brain can adapt to compressive force through deformation (i.e., midline shift and extension within the skull). Our data showed that although the thickness of the cortex under compression shrinked significantly, only a small amount of brain tissue loss developed—that was, 2% and 7% of tissue loss a month after 1.5-mm-thick and 2.0-mm-thick bead implantation, respectively. A previous study showed that total dendritic length as well as dendritic spines on all dendrites were reduced, while the densities of neurons and

capillaries increased following compression (Chen et al., 2003b). Based on the increased densities of neurons and vessels, it was concluded that no cell death was involved in the compression of particles 1.5 mm in thickness (Chen et al., 2003b). In our study, H&E staining revealed necrotic cell death and angiogenesis, suggesting ischemia and ischemia-related neuroplasticity. In this case, H&E staining may be a sensitive method of detecting pathological changes.

Previous findings of spine loss accompanied by brain compression suggest that synaptic function may be compromised (Chen et al., 2003b). In the present study, our main interest focused on the behavioral changes after focal compression. To detect the influence of location, magnitude and duration of brain compression on behavioral deficits, we changed one factor and fixed the others. We found that a bead implanted over the middle part of the SMC caused reliably detectable behavioral deficits, compared with implantation over either the anterior or the posterior part of the SMC, whereas the shrinkage of the cortical thickness and the loss of cortical volume revealed no significant differences among these three groups. Several previous studies have found that location could be an important variable in behavioral responses in different kinds of lesion models. Varying the location of brain injury in the region of the SMC produced different behavioral outcomes and delayed subcortical degenerative patterns that were influenced by pharmacological interventions (Barth et al., 1990b; Jones and Schallert, 1992). Baskin et al., using similar tests, recently showed insult-location-dependent behavioral variation in a mouse traumatic brain injury model. Trauma centered on the middle SMC location appeared to cause the most severe and persistent behavioral deficits (Baskin et al., 2003).

Our data revealed that behavioral deficits depend on the magnitude of brain compression. In our experiment, the 2.0-mm-thick bead caused more brain tissue loss and greater behavioral deficits compared with the 1.5-mm-thick bead after implantation.

Note, though, that while both the 1.5-mm-thick and 2.0-mm-thick bead compression induced behavioral deficits in the cylinder test and the somatosensory asymmetry test, only the 2.0-mm-thick bead implantation caused dysfunction in the vibrissae-evoked placing test, which typically can detect only larger injuries. There is extensive evidence, of course, that behavioral deficits depend on the magnitude of subtotal injury. For example, a relationship exists between the extent of dopamine depletion and behavioral deficits in a parkinsonian animal model (Schallert and Tillerson, 2000; Bergstrom et al., 2001), and also, behavioral asymmetries tend to rely on the size of the lesion in a focal cortical ischemia model (Lindner et al., 2003; Allred and Jones, 2004). Here, we show a relationship between behavioral changes and the extent of brain compression.

Early removal following 1.5-mm-thick bead compression at post-op day 3 showed functional improvement, compared with persistent compression using the same size bead, suggesting that early release of brain compression may be beneficial to functional recovery. After the 1.5-mm-thick bead was removed at post-op day 3, the shape of the brain appeared to recover to its original state by post-op day 28. Concurrent with our behavioral findings, Chen's recent study reported that decompression for 14 days resulted in near complete to partial recovery of the cortical thicknesses and the dendritic length of pyramidal neurons, and also, the recoverability was dependent on duration of preceding compression (Chen et al., 2004). It would be important in the future to assess whether motor experience might influence molecular, structural and functional outcome (Jones and Schallert, 1994; Keyvani and Schallert, 2002; Kleim et al., 2003).

After a month's observation, we found that rats with both 1.5-mm-thick and 2.0-mm-thick bead compression showed only minor behavioral deficits and recovered within two weeks, suggesting a mild lesion pattern for this model. We removed the same area of skull as a control operation, which showed transient detectable behavioral asymmetries in

the somatosensory asymmetry test, but the response was normal in the cylinder test. This result is consistent with previous findings that even skull removal can result in behavioral asymmetries (Adams et al., 1994). The effects of transient brain compression were also investigated. Animals with transient 1.5-mm-thick bead implantation followed by immediate removal showed considerable behavioral asymmetries in the somatosensory asymmetry test, but no detectable deficits in the cylinder test, indicating that even transient compression can lead to detectable behavioral deficits. It may seem paradoxical that significant somatosensory asymmetry was detected in the immediate removal group, compared with the control at post-op day 7, while the day-3 removal group had recovered by day 7. The mechanism to explain this phenomenon remains obscure so far, although secondary damage may possibly play a role in exaggerating brain injury following transient compression through bead-removal induced swelling and ischemia initiated at a critical time point. Chen et al (2004) found that decompression after 3 days or months led to varied extent of recovery of the dendritic length. Perhaps removing the bead early after the implantation can be especially traumatic. Results from earlier investigations showed behavioral deficits up to 7 days on the beam walking test after transient focal compression with a piston for 30 min (Kundrotiene et al., 2002; Kundrotiene et al., 2004b). Taken together, our behavioral data from control operations and transient focal compression indicate that the somatosensory asymmetry test is sensitive even for a slight insult to the SMC.

The bead model discussed here may be applied in evaluating treatment effects on neuroplasticity after mass compression in brain tumors, hematoma and traumatic head injuries. Exogenous NGF has been reported to enhance restoration of the density of dendritic spines on pyramidal neurons subjected to compression (Chen et al., 2004). Treatments to remove compressive masses either by pharmaceuticals or by surgery may

not promote neuroplasticity or may even damage the self-repair mechanisms involved in mass lesions depending on the timing. The mild lesion pattern makes this model specifically suitable to examine directly whether therapies designed to shrink mass would adversely affect brain plasticity and functional recovery independent of mass reduction, thereby facilitating an improvement of therapeutic strategies.

Chapter 3: Interruption of Functional Recovery by the NMDA Glutamate Antagonist MK-801 after Compression of the Sensorimotor Cortex

This work is published in Experimental Neurology in 2006 (Yang et al., 2006b).

3.1 ABSTRACT

Glutamate antagonists have recently been shown to limit tumor growth, providing potential new therapeutic strategies against brain tumors. Here we demonstrate that long-term systemic administration of the glutamate NMDA receptor antagonist MK801, after a delay, adversely reverses functional recovery in rats with compressive mass lesions of the sensorimotor cortex. Our data suggest that the controlled focal cortical compression model may be a valuable pre-clinical tool to screen compounds for the treatment of brain tumors. It may be possible to use this model to develop interventions that maintain anti-cancer effects but with diminished harm to bystander tissue and brain plasticity.

3.2 INTRODUCTION

Recent findings suggest a correlation between extracellular glutamate release and glioma expansion, adding brain tumor to the wide variety of central nervous system (CNS) diseases that involve excitotoxicity, such as stroke (Benveniste et al., 1984; Butcher et al., 1990), traumatic brain injury (Faden et al., 1989), Parkinson's disease and Alzheimer's disease (Olney et al., 1990; Doble, 1999; Miguel-Hidalgo et al., 2002). Excitotoxicity facilitates brain tumor growth in part by actively killing normal tissue in the vicinity of the tumor, thereby, easing tumor growth (Ye and Sontheimer, 1999; Takano et al., 2001; Sontheimer, 2003). Blockage of either N-methyl-D-aspartate

(NMDA) or alpha-amino-3-hydroxy-5-methyl-4-isoxazolepropionic acid (AMPA) subtype glutamate receptors limits glioma growth in vitro and in vivo, by inhibiting proliferation and migration of tumor cells as well as inducing tumor cell death (Rzeski et al., 2001; Takano et al., 2001; Ishiuchi et al., 2002). Thus, the development of novel, well-tolerated drugs to modulate glutamate release and activation of its receptors may provide therapeutic opportunities for brain cancers (Planells-Cases et al., 2002).

There is contradictory evidence in a large body of literature on the role of glutamate antagonists, which can either facilitate (Faden et al., 1989; Barth et al., 1990a; Sun and Faden, 1995; Barth et al., 1998; Kundrotiene et al., 2004b) or inhibit (Barth et al., 1990a; Kozlowski et al., 1994; Kozlowski et al., 1997; Barth et al., 1998; Kozlowski and Schallert, 1998; Felt et al., 2002; Biegon et al., 2004) optimal functional outcome after brain injury. The underlying mechanisms of these discrepancies seem to be related to the pattern and time of drug delivery and which anti-glutamate compound is used. Since the anti-tumor efficacy of the anti-glutamate drugs is dependent on persistent depression of glutamate activity (Chung et al., 2005), long-term drug administration is likely required for the management of brain tumors.

Assessment of quality of life has become increasingly important in clinical trials to evaluate the benefits and risks of new brain tumor treatments, while pre-clinical research on the functional impact of cancer treatment is scanty. Therefore, we sought to investigate the effects of long-term exposure of MK801, an NMDA glutamate antagonist, which is effective in slowing brain tumor growth (Rzeski et al., 2001; Takano et al., 2001), on functional recovery from mass compression, partly characteristic of some rapid-expanding brain tumors. In order to disentangle the potential detrimental effects of an anti-tumor treatment on brain function from its beneficial mass reduction effects, an approach using epidural implantation of a plastic bead overlying the sensorimotor cortex

(SMC) was used (Yang et al., 2006c). This controlled mass compression model, without the expansion property of an actual tumor, allows us to directly examine whether a promising brain tumor treatment, such as MK801, might harm bystander tissue and brain plasticity.

3.3 MATERIALS AND METHODS

3.3.1 Subjects

Twenty-seven male Sprague-Dawley rats, weighing 150-200 g were used in this study. Animals were randomly assigned to the following groups: (1) animals receiving bead implantation followed by 1 mg/kg MK801 (Sigma) i.p. (Bead+MK801, n=8) or (2) the same volume saline i.p. (Bead+Vehicle, n=7) and (3) animals undergoing control operations followed by 1 mg/kg MK801 i.p. (Control+MK801, n=6) or (4) saline i.p. (Control+Vehicle, n=6) beginning on post-operative (post-op) day 1, three times a week, until 4 weeks after surgery. Control animals were administered MK801 to determine whether the drug itself can cause detectable behavioral changes. All injections were given after behavioral testing to ensure that drug intoxication effects would not affect the test results.

3.3.2 Experimental model

The plastic hemispherical bead used for focal compression surgeries was 4.8 mm in diameter and 2.0 mm in thickness. The unilateral epidural bead implantation surgery (Chen et al., 2003b, 2004; Yang et al., 2006c) was performed as described in Chapter 2. The center of the bead was located 1.0 mm rostral to the bregma and 2.5 mm lateral to the midline. Control animals received all surgical procedures, including skull removal, except for bead implantation.

3.3.3 Behavioral tests

Rats were dynamically evaluated for neurobehavioral deficits over a 4-week period. Behavioral tests included vibrissae-evoked forelimb placing tests (both same-side placing and cross-midline placing), a forelimb-use asymmetry test, and a somatosensory asymmetry test (Schallert et al., 2000; Schallert et al., 2002; Schallert and Woodlee, 2005; Woodlee et al., 2005; Yang et al., 2006c), with method details described in Chapter 2.

3.3.4 Tissue processing and analysis

Four weeks after the surgery, all rats were given a lethal dose of sodium pentobarbital anesthesia (75 mg/kg, i.p.) and perfused transcardially with neutral buffered 10% formalin. The brain tissue was processed, embedded and cut into seven 2-mm-thick coronal blocks. Six-μm-thick paraffin sections from each block containing brain tissue under bead compression were obtained and stained with hematoxylin and eosin (H&E) for light microscopic examination and image analysis. The hemisphere volume and cortex thickness for both the affected and corresponding contralateral unaffected sides of the brain were measured with a Global Lab Image analysis program (Data Translation, Malboro, MA). The data are presented as the percentage of the affected side relative to the corresponding contralateral side for each parameter. Also, the pathological changes were evaluated. The paraffin sections were counter stained with TUNEL (Chemicon) and hematoxylin to determine whether apoptotic death is present in the lesion and affected by treatment.

3.3.5 Statistical Analysis

Behavioral responses across time were analyzed statistically by a repeated-measures ANOVA model, and the simple main effects at a specific test day were determined by a one-way ANOVA model, followed by the Tukey HSD test for post-hoc comparisons when appropriate. The histological data from two different treatment groups were compared with Student's t-tests. Level of significance was set to $p < 0.05$.

3.4 RESULTS

Figure 3.1 A shows a representative slice obtained from the level of compression center with H&E staining from the brain with bead compression for 28 days. Bead compression caused slight loss of brain tissue and significant shrinkage of cortex thickness in the compression area, but no significant differences were found between the bead+MK801 and bead+vehicle groups. Also, no significant differences were revealed by more detailed pathological observation of H&E stained tissue sections, in which necrosis, edema and angiogenesis indicative of ischemia were found in both groups (Fig. 3.1 B and C). TUNEL apoptosis assay showed very few apoptotic cells in the focal compression area in either the bead+MK801 group or the bead+vehicle group (Fig. 3.1 D).

Repeated-measures ANOVA revealed no statistically significant effects of MK801 in control-operated animals in all behavioral tests. Moreover, there were no significant differences between the control+MK801 group and the control+vehicle group at any time point. Therefore, these two groups were pooled and labeled as controls for all subsequent statistical analyses (Kozlowski et al., 1994; Kozlowski et al., 1997; Kozlowski and Schallert, 1998). Repeated-measures ANOVA showed significant treatment group differences among bead+MK801, bead+vehicle and control groups in both same-side placing ($p < 0.001$) and cross-midline placing ($p < 0.01$) tests. In the

same-side placing test (Fig. 3.1 E), both groups with bead implantation exhibited significant contralateral placing deficits at day 1 following surgery ($p < 0.001$), and the deficits persisted at day 2 ($p < 0.001$), day 3 ($p < 0.001$) and day 4 ($p < 0.01$), compared to the pooled control group. At day 7, no significant differences were found between either group with bead compression and controls. By day 14, all the bead-implanted animals completely recovered their placing abilities. The continuous administration of MK801 led to a reinstatement of placing deficits in the bead+MK801 group, which, in contrast, did not occur in the bead+vehicle group. At post-op day 18, the performance of the bead+MK801 group differed significantly from controls ($p < 0.01$), and further declined until the last testing day (day 28). A similar behavioral change pattern was also revealed in the cross-midline placing test (Fig. 3.1 F). Both groups with bead implantation displayed cross-midline placing deficits at post-op day 1 ($p < 0.01$) and day 2 ($p < 0.05$), but at day 3, they were both not significantly different from the control group. A reinstatement of placing deficits in the bead+MK801 group commenced at day 20, and became significant at day 24 ($p < 0.05$) compared with controls, lasting chronically until the end of the experiment. The proportion of animals in each treatment group exhibiting deficits in contralateral forelimb placing is shown in Table 3.1. In the forelimb-use as well as somatosensory asymmetry tests, animals in both the bead+MK801 and bead+vehicle groups displayed minor but significant behavioral asymmetries, which resolved within a week following surgery, compared with controls (data not shown).

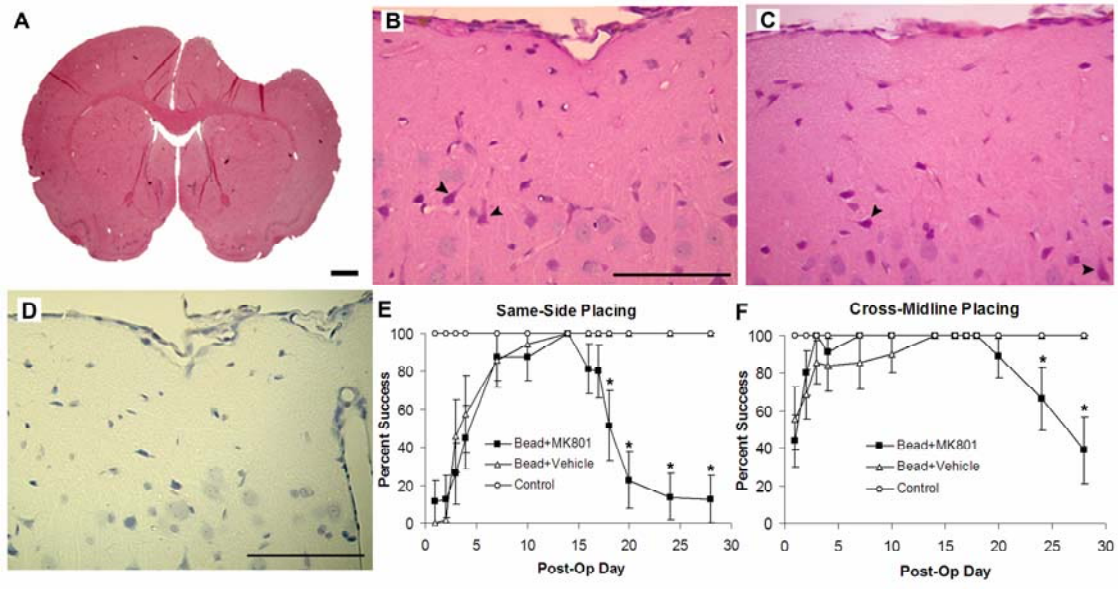

Figure 3.1: Histological and behavioral examinations after MK801 administration in rats with brain compression.

(A) Representative slice at the compression center with H&E staining, sectioned from a brain with bead compression for 28 days. Scale bar, 1 mm in A. (B, C) Photomicrographs with H&E staining (400 times magnification). H&E staining shows damage to the brain tissue, including necrotic neuronal death and edema in both B: bead+MK801 and C: bead+vehicle. Animals were sacrificed 4 weeks following bead implantation. Arrow heads indicate samples of necrotic neurons. Scale bar, 100 μm in B and C. (D) Photomicrograph with TUNEL and hematoxylin counter staining (400 times magnification). TUNEL apoptosis assay shows few apoptotic cells in both bead implantation groups, sacrificed 4 weeks after lesion. Scale bar, 100 μm in D. (E, F) Results of forelimb placing measurements. Percentages of successful placing responses are shown for the contralateral forelimb in both the same-side placing test (E) and the cross-midline placing test (F). Both bead+MK801 and bead+vehicle groups exhibited significant placing deficits following bead implantation. The bead+MK801 group displayed a significant reinstatement of the placing deficit after complete recovery from focal brain compression. Both of the two placing tests revealed a similar behavioral change pattern. * indicates a significant difference between the bead+MK801 and bead+vehicle groups with $p < 0.05$.

Table 3.1: Percentage of animals in each treatment group showing placing deficits.

The majority of animals in the bead+MK801 group exhibited reinstated deficits in both the same-side placing and cross-midline placing tests, whereas, all the animals in the bead+vehicle group exhibited complete recovery.

Placing type	Duration of deficits	Treatment		
		Bead+MK801	Bead+Vehicle	Control
Same-side placing	Short-term	100%	100%	0%
	Long-term	100%	0%	0%
Cross-midline placing	Short-term	87.50%	57.14%	0%
	Long-term	62.50%	0%	0%

3.5 DISCUSSION

Chronic administration of the NMDA antagonist MK801 from an early stage following focal cortical compression did not affect the recovery rate, but instead resulted in a reinstatement of placing deficits after complete recovery. Although the drug administration regimen is different, the timing of the reinstatement of the functional deficits by MK801 is consistent with the previous findings in both adult and neonatal rats (Barth et al., 1990a; Kozlowski et al., 1994; Kozlowski and Schallert, 1998; Felt et al., 2002), suggesting that long-term maintenance of glutamatergic activity at NMDA receptors plays a key role in use-dependent plasticity and post-lesional recovery of brain function regardless of whether the underlying mechanisms are related to changes in homotopic cortex dendritic arbors or to other events which may occur in the lesioned hemisphere. Recent findings demonstrate that overactivation of the glutamate receptors exists only shortly after brain injury (< 1 hour), and is followed by profound and persistent dysfunction (Biegon et al., 2004). Glutamate agonists administered 24 and 48 hours after traumatic brain injury improve the restoration of neurological and cognitive function (Biegon et al., 2004).

Our histology results with H&E staining and TUNEL apoptosis assay, together with the behavioral data, reveal the mild lesion pattern for this focal compression model, which confirm our previous findings (Yang et al., 2006c), and indicate that the exaggeration of behavioral deficits induced by chronic MK801 administration may not be attributed to cell death, at least in the region surrounding the bead. It is possible that the histological assays used in this study were not sufficiently sensitive to detect changes in the compressed tissue following MK801 treatment, or that the changes disappeared and became undetectable after a 4-week period. Recent observations illustrate that NMDA antagonists can trigger apoptotic neurodegeneration in the developing brain (Ikonomidou et al., 1999; Olney et al., 2002) as well as an increase of neurodestruction in the mature brain undergoing slowly progressing neurodegeneration (Ikonomidou et al., 2000).

Pursuit of compounds that would act as glutamate antagonists and have no harmful effects on brain plasticity may be warranted. Memantine, which is also an NMDA antagonist, has been reported to significantly attenuate brain tumor growth (Takano et al., 2001) and is clinically well tolerated (Parsons et al., 1999). Also, cytostatic agents that inhibit cystine uptake suppress glioma release of glutamate, but do not influence astrocytes or neurons (Chung et al., 2005). Our results support the use of a controlled focal cortical compression model to screen promising compounds pre-clinically, which may lead to improved pharmaceutical designs that limit brain tumor growth without harm to bystander tissue and brain plasticity after injury potentially associated with tumor progression and aggressive therapy.

Chapter 4: Local Fluorouracil Chemotherapy Interferes with Neural and Behavioral Recovery after Brain Tumor-like Mass Compression

This work is published in Behavioural Brain Research in 2006 (Yang et al., 2006a).

4.1 ABSTRACT

In this study, we investigated the impact of intracerebral delivery of chemotherapy on functional recovery from focal cortical tissue displacement, characteristic of brain tumors. Unilateral focal brain compression was induced by epidural implantation of an inverted hemisphere-shaped bead over the sensorimotor cortex. Microinjections of a total of 1 mg chemoagent fluorouracil or the same volume of saline were made into the compressed cortex. Behavioral tests of forelimb sensorimotor function were conducted during four weeks' observation. Rats subjected to any of the three types of lesions, saline microinjection plus cortical compression, chemoagent microinjection alone, or chemoagent microinjection combined with cortical compression, demonstrated significant behavioral deficits in several sensorimotor tasks, compared with saline-microinjected control animals. In placing tests, behavioral deficits elicited by each single treatment were worsened by combined treatment with chemoagent microinjection and focal cortical compression. Concurrently, local delivery of chemoagent into the compressed cortex induced increased cortical tissue loss, necrosis and apoptosis. These data indicate that local chemotherapy exacerbates compression-induced neurological impairment, and a model of controlled focal cortical compression may provide a valuable means to improve anti-cancer therapeutic designs with reduced deterioration of brain function.

4.2 INTRODUCTION

Fluorouracil (5FU) is an antimetabolic drug. The mechanism of action of 5FU is associated with inhibition of thymidylate synthase and incorporation of 5FU into DNA and RNA, affecting cell proliferation and survival (Noordhuis et al., 2004). 5FU has been widely used in the investigation of interstitial chemotherapy of brain tumors. There are two potential reasons. First, 5FU is hydrophilic, and does not readily cross the blood brain barrier (BBB). When systemically administered, 5FU has very little effect on malignant gliomas and other tumors implanted in the brain (Shapiro, 1971; Levin et al., 1984; Shapiro et al., 1992); however, it shows some effect on the same malignant brain tumors implanted in the flank (Levin et al., 1972; Neuwelt et al., 1984), indicating that its lack of effectiveness is due to its limited concentration inside the tumor. Direct drug delivery of chemotherapy such as 5FU to the brain tumor can increase the drug level in the tumor area and furthermore can decrease the systemic undesired side effects (Menei et al., 1996; Lemaire et al., 2001; Fournier et al., 2003; Menei et al., 2004). Second, 5FU has relatively less direct neurotoxicity, compared to other commonly used chemotherapy drugs. 5FU is a pyrimidine, which acts on the synthesis of nucleic acids, killing cells that are actively duplicating DNA (Menei et al., 1996). However, even systemic chemotherapy can lead to central neurotoxicity, such as cerebellar syndrome, seizures, aphasia, global motor weakness and bulbar palsy, as well as leukoencephalopathy and progressive dementia (Hook et al., 1992; Figueredo et al., 1995; Barbieux et al., 1996; Bygrave et al., 1998; Bofill et al., 2000; Pirzada et al., 2000; Elkiran et al., 2004). Therefore, there is a good reason to doubt whether regional chemotherapy can initiate functional impairment in a healthy brain, while in a damaged brain, whether it can exaggerate secondary degeneration and impede functional recovery following focal cortical tissue displacement characteristic of brain tumors.

Although in standard tumor implant models reducing tumor size by local chemotherapy will likely retard or prevent deterioration of function dramatically while limiting unwanted effects associated with systemic delivery, tumor shrinkage could mask treatment-related adverse effects on the integrity of brain tissue. Therefore, a model that holds tumor size constant independent of treatment may be useful to assess potential detrimental effects of tumor growth inhibitors on brain plasticity more directly. In this study, the chemoagent 5FU or saline was infused into the region surrounding a false tumor located in the sensorimotor cortex. Injury to the compressed brain, and recovery of function, were detected using sensitive behavioral tests.

4.3 MATERIALS AND METHODS

4.3.1 Animals

A total of 41 adult male Sprague Dawley rats were used in this study. Twenty-five rats were randomly assigned to one of the four groups: 5FU+bead (n=7), saline+bead (n=6), 5FU only (n=6), and saline only (n=6), which were retained for four weeks while behavioral tests were conducted. Another 16 rats with 4 assigned to each of the same four groups were sacrificed 24 hours following surgery to assess the acute histological changes.

4.3.2 Experimental model

Rats were anesthetized with ketamine (90 mg/kg) and xylazine (10 mg/kg) administered intraperitoneally (i.p.). After the head was fixed on a stereotaxic frame (Kopf) and the skull was exposed, an elliptical hole over the sensorimotor cortex (SMC) with approximately 5.8 mm in long diameter and 3.8 mm in short diameter was drilled.

4.3.2.1 Local delivery of 5FU

A total of 1 mg 5FU (solution containing 50 mg/ml 5FU dissolved in water for injection, purchased from pharmacy of the University of Texas at Austin) in a 20 μl volume was equally divided into three trajectory microinjections, delivered into the SMC, 2.5 mm lateral to midline, and 2.5 mm deep below dura, with A/P coordinates at 2.5 mm, 1.0 mm, and -0.5 mm respectively relative to bregma. To reduce fluid backflow, drug infusion was conducted slowly at a speed of 1 μl per min and the needle was retained in position for 3 mins followed by very slow withdrawal after each injection. The dose of 5FU was selected based on literature, in which 5FU can shrink brain tumors at similar doses (Menei et al., 1996; Lemaire et al., 2001; Fournier et al., 2003). Microinjections with the same volume of saline served as a control operation.

4.3.2.2 Bead implantation

After intracerebral microinjections, the plastic hemispherical bead, which is 4.8 mm in diameter and 2.0 mm in thickness, was implanted epidurally over the SMC, according to previous studies (Chen et al., 2003b, 2004; Yang et al., 2006b; Yang et al., 2006c). The bead, with the flat surface facing upward, was fixed on the required coordinates with the center at 1.0 mm rostral to bregma and 2.5 mm lateral to midline (Fig. 4.1 A). Fig. 4.1 B shows a representative brain after 28 days of bead compression.

4.3.3 Behavioral testing

An array of behavioral tests sensitive to focal insults to the SMC, including two different types of vibrissae-evoked forelimb placing tests (same-side and cross-midline placing), as well as a forelimb-use asymmetry test and a somatosensory asymmetry test,

were performed before and after surgical procedures. Please refer to Chapter 2 for more method details.

4.3.4 Histological assessment

Rats were anesthetized and perfused intracardially with physiological saline solution followed by 4% paraformaldehyde. Brains were removed, processed, embedded in paraffin, and cut into seven 2-mm-thick coronal blocks (Fig. 4.1 B). Six-μm-thick sections taken approximately every 0.5 mm from each block containing the area of bead compression were stained with hematoxylin and eosin (H&E). A total of 12 equally spaced sections with 0.5 mm interval for each rat were imaged with 2.5 times magnification for lesion volume measurement. The hemisphere contours were traced on each coronal section and the areas of both hemispheres were measured using the MCID computer imaging analysis system (Imaging Research, Inc., St. Catharines, Ontario, Canada). The hemisphere volumes in the compression area were estimated by the sum of the values produced by multiplying the appropriate area by the section interval thickness. Lesion volume was presented as both an absolute volume of the tissue loss and a volume percentage of the lesioned hemisphere compared with the contralateral hemisphere. The compression center was defined as the most intensively compressed region of the brain as indicated in Fig. 4.1 B. To study the pathological characteristics and the morphological changes of the compressed brain tissue under local chemotherapy, H&E-stained brain tissue collected from the approximate compression center 24 hours or 28 days following bead compression with or without 5FU administration was examined. To study the impact of local chemotherapy on normal brain tissue, the 2-mm-thick coronal blocks were further cut until needle tracks were found. In situ apoptosis detection was conducted with the TUNEL ApopTag kit (Chemicon) in conjunction with hematoxylin

counterstaining. Serial five 6-μm-thick sections obtained at the approximate coronal level of the compression center were analyzed for each animal that received bead implantation with the presence or absence of 5FU delivery. For quantification of TUNEL immunoreactivity, images of TUNEL-immunostained coronal sections were scanned using a X20 objective (0.296 mm^2 field of view) via the MCID program. The number of TUNEL positive cells was counted throughout the entire neocortex in the affected hemisphere after compression on each section. During the calculation, TUNEL positive cells were confirmed at a higher magnification (X40 objective).

4.3.5 Statistical analysis

The behavioral data from each test were subjected to an overall repeated-measures ANOVA, followed by post-hoc analyses when appropriate. The histological data from two different treatment groups were compared with Student's t-tests. Data are presented as mean ± standard error.

4.4 RESULTS

4.4.1 Local delivery of 5FU exaggerates brain tissue loss after brain compression

The volume percentage of the compressed cerebral hemisphere relative to the contralateral hemisphere in the compression area was 96.2% for the saline+bead group and 91.6% for the 5FU+bead group after 28 days of bead compression. Student's t-test indicated that 5FU treatment resulted in a significant increase of the volume of tissue loss after focal cortical compression ($p < 0.05$, Fig. 4.1 C). Fig. 4.1 D and E show representative H&E-stained slices collected at the approximate coronal center of the compression from brains removed 28 days after bead implantation with (Fig. 4.1 E) and without (Fig. 4.1 D) 5FU treatment, respectively.

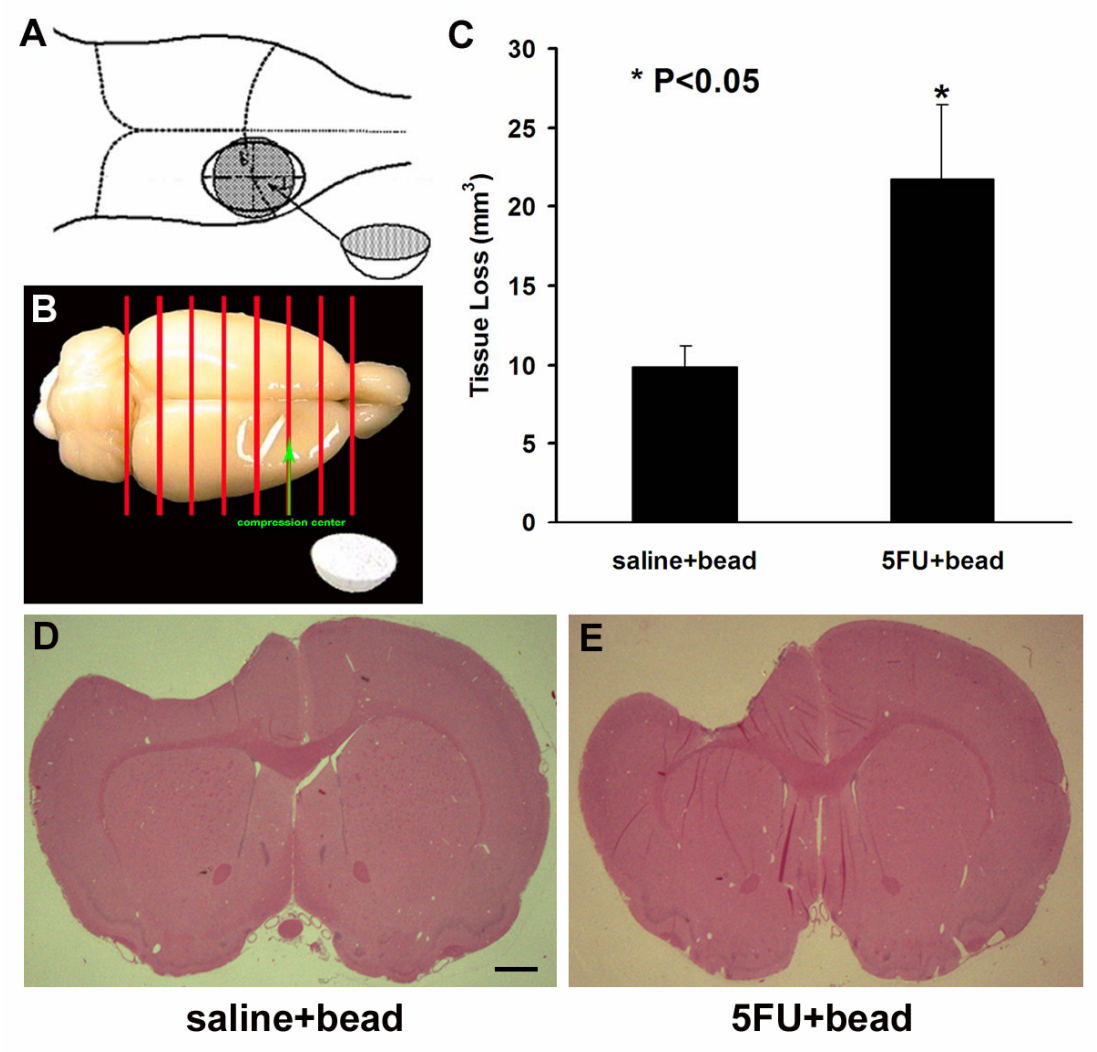

Figure 4.1: Local chemotherapy exaggerates compression-induced tissue loss in the SMC.

(A) Schematic dorsal view of epidural bead implantation over the SMC. (B) A representative brain following bead compression for 28 days. (C) Local chemotherapy leads to a significant increase in cortical tissue loss. (D, E) Representative H&E-stained brain slices collected at the approximate compression center from the saline+bead group (D) and the 5FU+bead group (E), respectively, 28 days after lesions. Scale bar=1mm in D and E.

4.4.2 Local delivery of 5FU induces elevated necrosis after brain compression

Acute and chronic pathological changes were determined with H&E staining. Images (Fig. 4.2 A to D) were obtained at the approximate compression center, which was identified as the deepest region of the compression curve, with the same coronal location as the sections shown in Fig. 4.1 D and E. Following bead compression, lesions were barely visible under 100 power magnification in both the acute (Fig. 4.2 A) and chronic (Fig. 4.2 C) phases. Under 400 power magnification, sporadic red and ghost neurons due to necrosis, and edema, more evident in the acute phase, were found in the compression area compared to the corresponding contralateral area (data not shown). Compared with those undergoing only control injections into the compressed tissue, local delivery of 5FU induced a substantial decrease of the tissue density, representing an increase in the extent of necrosis in the compression area, concurrent with substantial hemorrhage and edema occurring at a very early stage (Fig. 4.2 B) and prominent vacuolation exhibited at a later stage (Fig. 4.2 D).

4.4.3 5FU microinjection causes extended damage around the needle track

5FU microinjection caused extensive acute hemorrhage and chronic vacuolation, with the increased extent of necrotic damage around the needle track, compared with saline microinjection (Fig. 4.2 E to H). Fig. 4.2 F and H indicate the lesion range produced by 5FU microinjections into normal brain tissue.

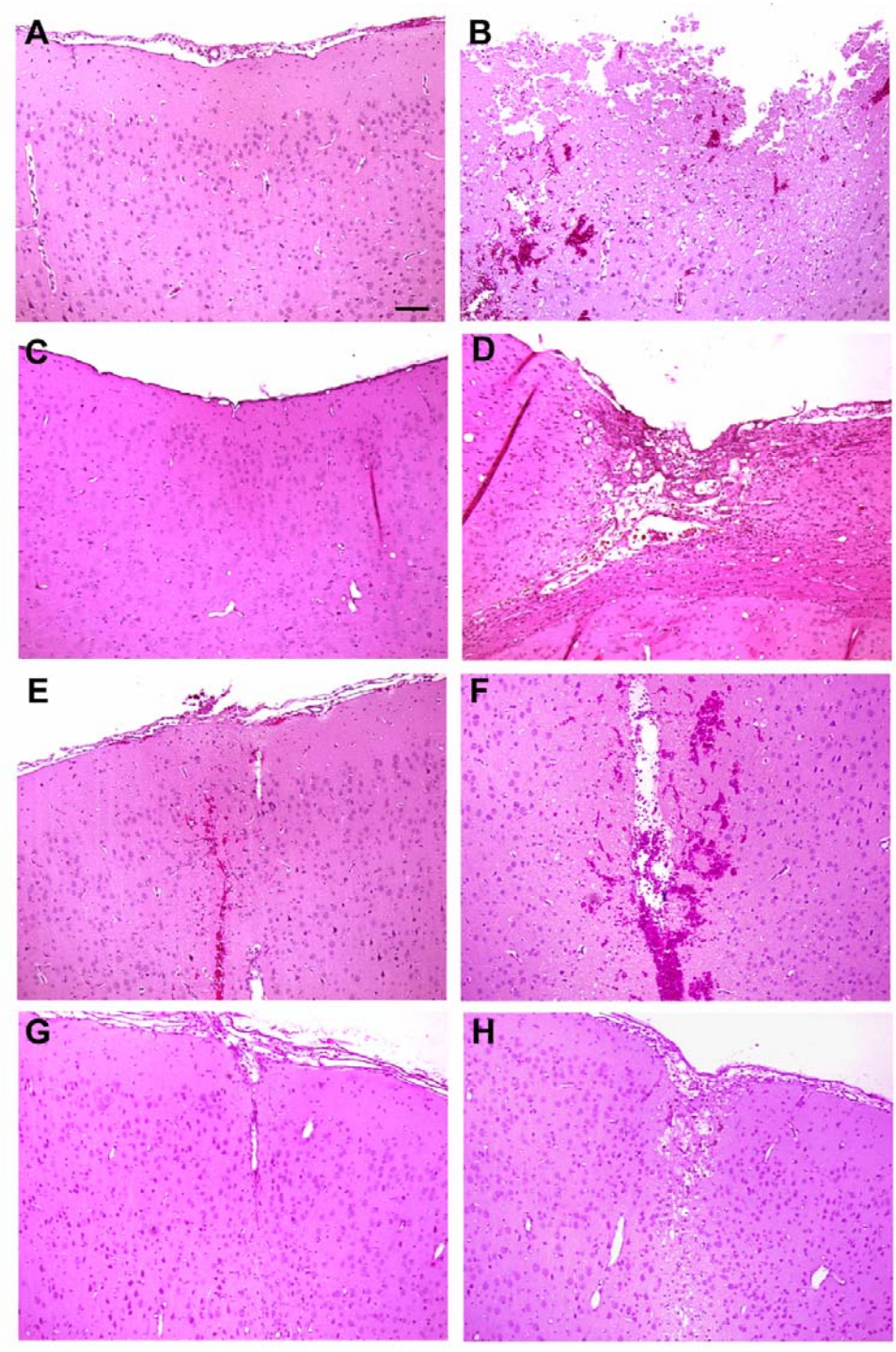

Figure 4.2: Local chemotherapy induces increase in necrosis following either focal cortical compression or needle damage.

(A to D) Representative H&E-stained images under 100 times magnification collected at the approximate compression center in the lesioned hemisphere of rats sacrificed 24 hours after saline+bead (A), or 5FU+bead (B); 28 days following saline+bead (C) or 5FU+bead (D). Compression borders were included in panel A to D. (E to H) Representative H&E-stained images under 100 times magnification collected around the needle track in the lesioned hemisphere of rats sacrificed 24 hours after saline (E) or 5FU (F) microinjection; 28 days following saline (G) or 5FU (H) microinjection. Bar=100 μm in A.

4.4.4 Local delivery of 5FU induces elevated apoptosis after brain compression

In the TUNEL assay, very few TUNEL-positive cells were found after bead compression alone in both the acute (Fig. 4.3 A) and chronic (Fig. 4.3 C) phases. A significant 5FU-induced increase in the total number of apoptotic cells in the compressed cortex was observed after 24 hours ($p < 0.001$, Fig. 4.3 A, B, and E) as well as 28 days ($p < 0.05$, Fig. 4.3 C, D, and E) of focal cortical compression.

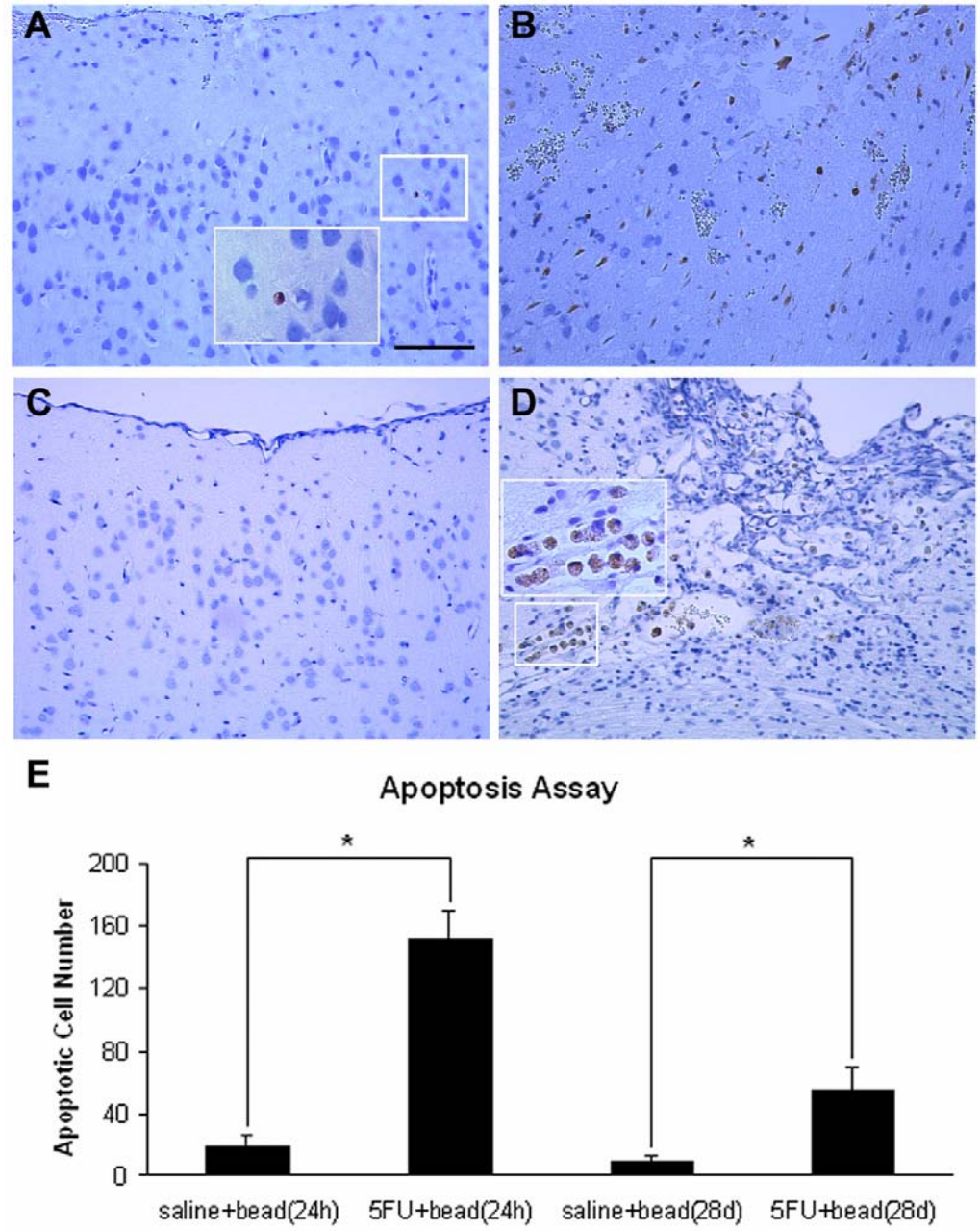

Figure 4.3: Local chemotherapy leads to increase in apoptosis following focal cortical compression.

(A to D) Representative TUNEL&Hematoxylin-counterstained images under 200 times magnification collected at the approximate compression center in the lesioned hemisphere of rats sacrificed 24 hours after saline+bead (A), or 5FU+bead (B); 28 days following saline+bead (C) or 5FU+bead (D). Compression borders were included in all

four images. Magnified views (400 times magnification) of the selected TUNEL-positive cells are shown in panel A and D. No TUNEL-positive cells were found in panel C. (E) The apoptotic cell number was significantly increased in the compressed cortex with the presence of chemotreatment both 24 hours and 28 days after lesions. Bar=100 μm in A. * indicates a significant difference between different conditions with $p < 0.05$.

4.4.5 Local delivery of 5FU exacerbates compression-induced functional deficits

In the same-side placing test (Fig. 4.4 A), saline-treated control animals did not show any placing deficit. Other animals that received 5FU treatment alone ($p < 0.001$), or saline injection plus bead compression ($p < 0.001$), or 5FU treatment plus bead compression ($p < 0.001$), all displayed significant placing deficits, compared to control animals, respectively. Animals that received 5FU treatment in combination with bead compression demonstrated significantly greater placing impairments, when compared with either animals that underwent saline microinjection combined with bead compression ($p < 0.001$) or those receiving 5FU treatment alone ($p < 0.01$).

In the cross-midline placing test (Fig. 4.4 B), no animals in the non-bead control group showed deficits, in contrast to some animals in the saline+bead group; however, these groups did not differ significantly. Both the 5FU group ($p < 0.05$) and the 5FU+bead group ($p < 0.001$) showed significant deficits, when respectively compared with the control group. Also, animals in the 5FU+bead group displayed significantly worse placing impairments than those either in the saline+bead group ($p < 0.001$) or in the 5FU group ($p < 0.01$).

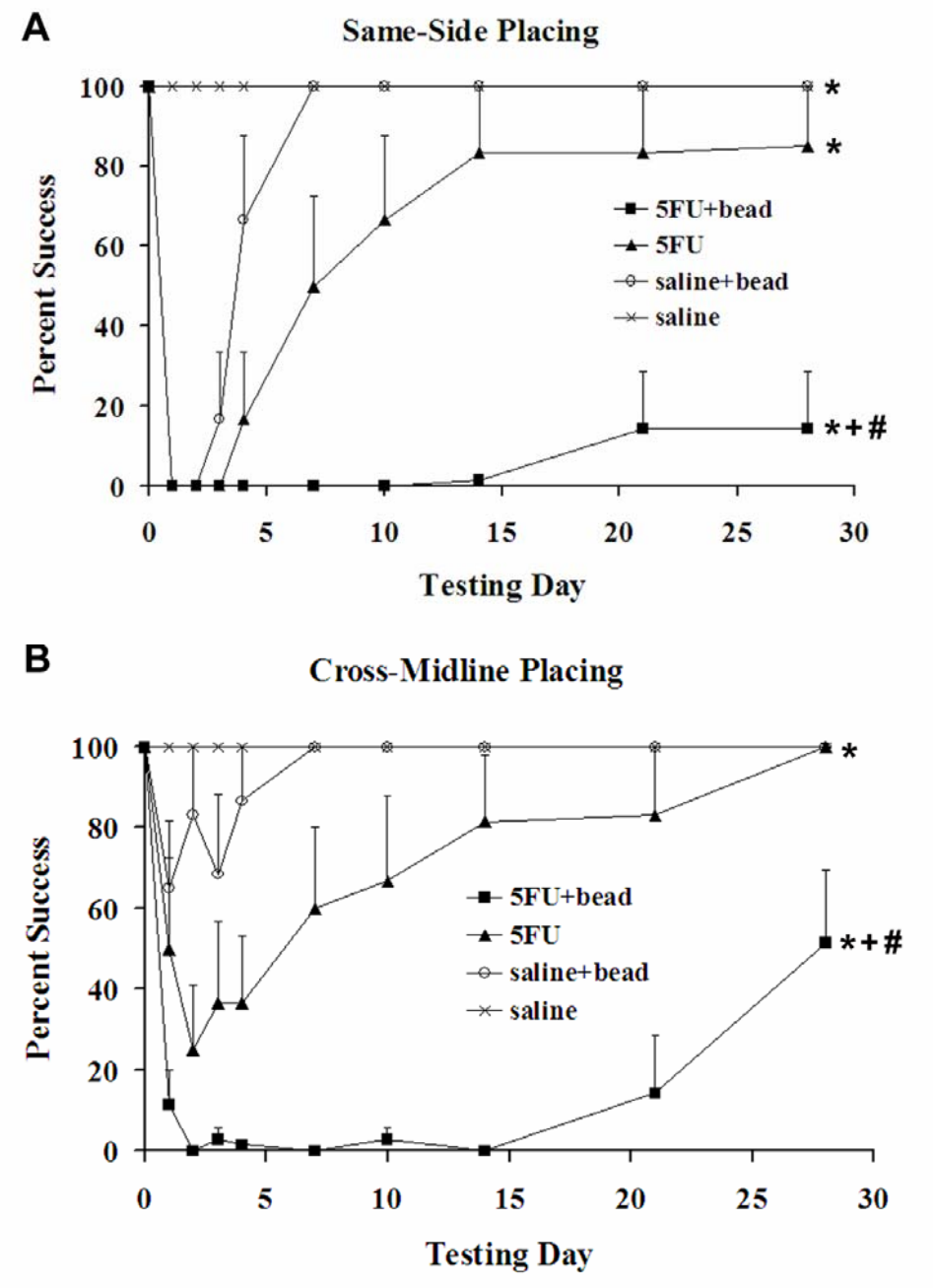

Figure 4.4: Local chemotherapy exacerbates compression-induced placing deficits.

The 5FU+bead group showed significant worse placing deficits than either the saline+bead group or the 5FU group, in both the same-side placing test (A) and the cross-midline placing test (B). * indicates a significant difference between any of the other lesion groups and the saline-treated control; + indicates a significant difference between

the 5FU+bead group and the saline+bead group; # indicates a significant difference between the 5FU+bead group and the 5FU group.

In the forelimb-use task (Fig. 4.5 A), saline microinjection led to a transient behavioral asymmetry, revealed by analysis of within-subjects effect (time effect) in repeated-measures ANOVA ($p < 0.05$), implicating that even the needle damage can detectably affect the behavioral performance. Each of the other treatment groups, including the 5FU group ($p < 0.01$), the saline+bead group ($p < 0.01$), and the 5FU+bead group ($p < 0.001$), showed a significant difference compared to the control group. Forelimb-use asymmetry in the 5FU+bead group was significantly more severe than in the saline+bead group ($p < 0.01$), but the 5FU+bead and the 5FU groups did not differ.

In the forelimb somatosensory asymmetry test (Fig. 4.5 B), animals that received saline microinjection alone did not show any impairment. The saline+bead and the control group did not differ overall, although the two groups were significantly different from each other at day 2 ($p < 0.01$) and day 3 ($p < 0.05$). Animals that received either 5FU treatment alone ($p < 0.01$) or both 5FU treatment and bead compression ($p < 0.001$) displayed significant deficits, when compared with control animals. The 5FU+bead group showed a significantly increased somatosensory deficit relative to the saline+bead group ($p < 0.01$), but no significant difference relative to the 5FU group.

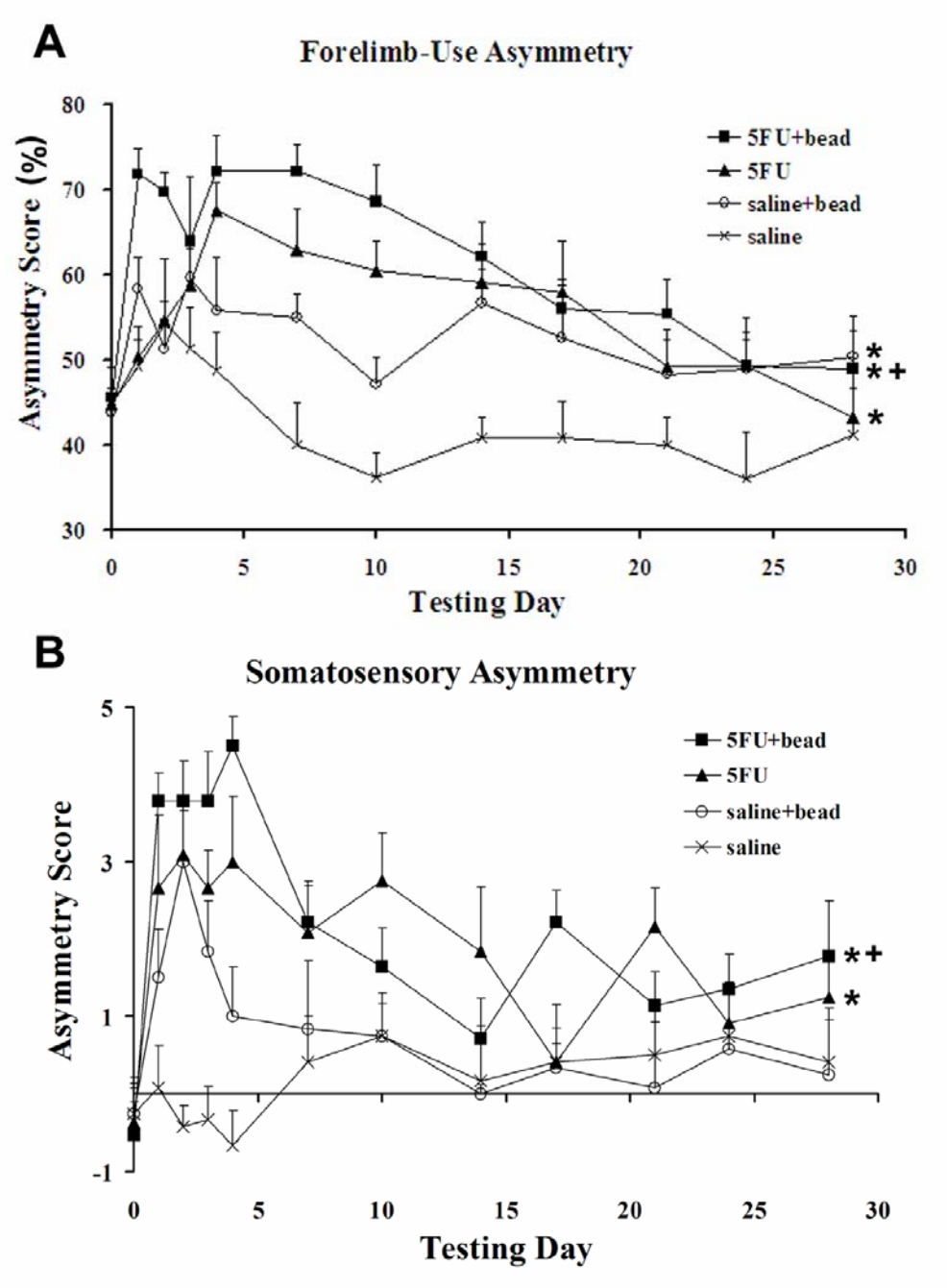

Figure 4.5: Local chemotherapy exacerbates compression-induced behavioral deficits in both the forelimb-use and the forelimb somatosensory asymmetry tests.

The 5FU+bead group demonstrated significantly greater asymmetries than the saline+bead group, but no significant differences compared to the 5FU group, in both the

forelimb-use asymmetry test (A) and the somatosensory asymmetry test (B). * indicates a significant difference from control; + indicates a significant difference between the 5FU+bead group and the saline+bead group.

4.5 DISCUSSION

The neurotoxicity or disruption of neuroplasticity associated with the aggressive anti-cancer regimens potentially makes treatment a source of brain insult together with the tumor itself. Although radiation and chemotherapy are often blamed in the clinic for the accompanied neurological and cognitive side effects (Shapiro and Young, 1984; Macdonald, 1991; Vigliani et al., 1999), little preclinical research has addressed treatment impact specifically on non-tumor tissue. Here, we demonstrate that under conditions of focal cortical compression, which controls for drug induced changes in expansion or shrinkage of mass, local delivery of chemotherapy exacerbates functional impairments.

Because most brain tumors do not tend to metastasize or spread to other parts of the body, the newly renovated local chemotherapy carried out through various delivery devices may be an effective way to reduce the systemic side effects and increase the amount of available drug in the tumor area. However, to date, although more specific drug delivery pathways for cancer treatment are being pursued, drug distribution to the surrounding and remote normal brain tissue may be unavoidable, and remains a potential concern. To our knowledge, there are no published data indicating the extent of 5FU diffusion after intracerebral microinjections. It would be interesting to investigate whether mechanical compression can influence the interstitial diffusion of 5FU in brain tissue. It is possible that diffusion could be more limited in compressed tissue, but still the drug might diffuse beyond the immediate peri-compression brain region. It remains to

be determined whether the adverse effects of 5FU include compromise to remote brain regions in this model.

5FU has been widely used in local chemotherapy research (Menei et al., 1996; Lemaire et al., 2001; Fournier et al., 2003; Menei et al., 2004), in part because the frequency of neurotoxicity following its systemic administration is generally low. The dose of 5FU (1 mg per rat) applied regionally in the present study is roughly comparable to that being used to shrink brain tumors in rats in previous reports (Menei et al., 1996; Lemaire et al., 2001; Fournier et al., 2003).

Consistent with our prior findings (Yang et al., 2006b; Yang et al., 2006c), the 2.0-mm-thick bead compression produced mild injury. Not only local delivery of 5FU into the compressed brain exacerbated functional deficits, but 5FU into the normal brain did too. Histologically, 5FU significantly increased the loss of brain tissue following brain compression. 5FU induced significant vacuole formation suggesting a severe degree of cell necrosis, and also, apoptotic neurons were present both in the compressed area and around the needle. Previous observations demonstrate that metabolites of 5FU can induce vacuolation due to myelin splitting and destruction, and cause necrosis/softening-like change as well (Okeda et al., 1984; Okeda et al., 1988; Okeda et al., 1990; Akiba et al., 1996). Although myelin is more vulnerable than neurons, these pathological changes can develop where the toxic substance readily deposits and accumulates (Okeda et al., 1984). In addition, the central nervous system is among the organs that 5FU tends to be retained over long time periods (Zhang et al., 1992). Furthermore, when examining the effects of chemotherapeutic agents in combination with osmotic blood-brain barrier (BBB) modification, remarkable neurotoxicity was found, suggesting that limited entry of drug into the brain by an intact BBB may account

for the reduced neurotoxicity associated with the usual systemic administration of most chemotherapeutic agents (Neuwelt et al., 1983a; Neuwelt et al., 1983b).

Although local delivery of chemotherapy drugs has been widely investigated, neurotoxicity has not been reported at the preclinical level (Menei et al., 1996). However, when it was applied to clinical trials, worsening of preexisting neurological symptoms was found (Menei et al., 2004). This problem exists extensively in brain cancer therapeutic development, in part because of the lack of functional outcome measurement in the preclinical evaluation of treatment effects. Gross observations, such as measure of body weight, feeding activity and locomotion, are not sufficient to reveal the changes in brain function. More importantly, in growing-tumor transplant models, the therapeutic effects of tumor shrinkage per se may obscure anti-plasticity or other harm to surrounding brain tissue. With a mild lesion pattern and without the invasive and growing properties of an actual tumor, controlled mass compression models can allow investigators to detect directly the potential adverse effects of brain tumor treatment on neuroplastic mechanisms.

Our data suggest that compressed brain tissue may be more vulnerable to chemodrug-induced impairment. Therefore, it is important to choose the optimal time to initiate chemotherapy. It is possible that chemotherapy carried out after neurosurgical decompression and delayed until surgically induced edema and blood-brain barrier opening have resolved may lessen the intensity of chemo-associated neural damage.

Chapter 5: Sensorimotor Deficits Associated with Brain Tumor Progression and Tumor-induced Brain Plasticity Mechanisms

This work is published in Experimental Neurology in 2007 (Yang et al., 2007b).

5.1 ABSTRACT

The objective of this study was to investigate functional deficits and reactive peri-tumoral brain plasticity events in glioma-bearing rats. 9L gliosarcoma cells were implanted into the forelimb region of the sensorimotor cortex in Fischer rats. Control animals underwent the same operation without tumor implantation. Sensitive tests for detecting sensorimotor dysfunction, including forelimb-use asymmetry, somatosensory asymmetry, and vibrissae-evoked forelimb placing tests, were conducted. We found that tumor-bearing animals exhibited significant composite behavioral deficits on day 14 post-tumor injection compared to surgical controls. With the assistance of magnetic resonance imaging, we demonstrated a significant correlation between tumor volume and magnitude of somatosensory asymmetry, indicating that the somatosensory asymmetry test can provide an effective and efficient means to measure and predict tumor progression. Histopathological assessments were performed after the rats were sacrificed 14 days following tumor implantation. Immunostaining revealed that densities of microtubule-associated protein 2, glial fibrillary acid protein, von Willebrand factor, and synaptophysin were all significantly upregulated in the peri-tumoral area, compared to the corresponding region in surgical controls, suggesting synaptic plasticity, astrocyte activation and angiogenesis in response to tumor insult. Understanding the behavioral and bystander cellular events associated with tumor progression may lead to improved

evaluation and development of new brain tumor treatments that promote, or at least do not interfere with, functional adaptation.

5.2 INTRODUCTION

Functional assessment of cancer therapy is essential in translational research and the first step is to establish a simple method for measurement of behavioral changes in animal tumor models. This study employed an array of sensorimotor behavioral tests to determine focal functional deficits in rats following implantation of glioma cells into the forelimb region of the sensorimotor cortex (SMC). Due to the variabilities in both tumor growth and behavioral response, a closer analysis using magnetic resonance imaging (MRI) was conducted to examine the correlation between tumor size and functional impairment.

Both clinical observation and experimental research demonstrate the lack of severe functional deficits until the late stage when the tumor grows large, suggesting tolerance to tumor growth (Whittle and Marston, 1997; Yang et al., 2007b). Cerebral ischemia (Stroemer et al., 1992, 1993; Parent et al., 2002; Zhang et al., 2004b; Zhang et al., 2004a; Zhang et al., 2007a; Zhang et al., 2007b), mechanical compression (Kundrotiene et al., 2002; Kundrotiene et al., 2004b; Moreira et al., 2005; Moreira et al., 2006; Yang et al., 2006b; Yang et al., 2006c; Yang et al., 2006a; Moreira et al., 2007), denervation (Gomez-Pinilla et al., 1992; Kadish and Van Groen, 2003) and excitotoxicity (Pollard et al., 1994) all induce brain plasticity that likely fosters functional recovery (Cramer and Chopp, 2000; Keyvani and Schallert, 2002). Brain plasticity may be most effective when the injury is minor and slowly increases over time, as observed in models of progressive neural degeneration (Fleming et al., 2005). Tumors likewise may gradually upregulate compensatory events, leading to their “stealth” nature. Peri-tumoral plasticity

may be vulnerable to tumor resection or anti-mitotic, anti-angiogenic, anti-growth factor and related treatments used to reduce brain tumor expansion. Normal brain cells, especially progenitor cells and oligodendrocytes, are more susceptible to chemotoxicity than cancer cells, and systemic administration of chemotherapeutic agents leads to reduced cell division and increased cell death in the adult mouse brain even long after drug exposure (Dietrich et al., 2006). Understanding how peri-tumoral neurons resist dying is important, as protection of the surrounding normal tissue and preservation of function is a major goal and a great challenge in glioma management. To begin to address this issue, markers for neurons, astrocytes, endothelial cells, and synaptogenesis were used to examine reactive peri-tumoral plasticity in the rat glioma implantation model.

5.3 MATERIALS AND METHODS

5.3.1 Experiment 1

The goal of Experiment 1 was to examine forelimb sensorimotor function during the growth of tumors placed in the forelimb region of the sensorimotor cortex, and to investigate peri-tumoral plasticity-related events using immunohistochemistry.

5.3.1.1 Animals

A total of 18 adult male Fischer rats (Charles River Breeding, Wilmington, MA) weighing 180-250 g were used in Experiment 1.

5.3.1.2 Experimental model

Animals were randomly assigned to either the tumor-bearing group (n=9) or the control group (n=9).

9L gliosarcoma cell culture: 9L gliosarcoma cells (ATCC, Manassas, VA, USA) were maintained in monolayer culture (37°C, 5% CO_2, 95% O_2) in minimum essential media (MEM) with Eagle's salts, supplemented with 10% fetal bovine serum, penicillin and streptomycin (Gibco, Grand Island, NY). Cells were subcultured and used for implantation when they reached an exponential phase of growth. To harvest, cells were incubated with 0.05% trypsin-ethylenediaminetetraacetic acid (trypsin-EDTA, 0.53 mM, Gibco) for 5 min, and then MEM was added to make a single cell suspension. After the suspension was centrifuged at 1000 rpm (4°C) for 5 min, the media was removed and the cells were re-suspended in phosphate buffered saline (PBS). Cell viability was determined by trypan blue exclusion (non-viable cells stain blue). The number of unstained cells was counted using a hemacytometer under a microscrope and then the suspension was diluted with PBS to a final concentration of 10^7 cells/ml (Chopp et al., 1996a; Chopp et al., 1996b; Jiang et al., 1997; Jiang et al., 1998).

9L cell implantation in Fischer rats: Rats were anesthetized with ketamine (80 mg/kg, i.p.) and xylazine (13 mg/kg, i.p.) and then placed in a stereotaxic device. After the scalp was incised and the cranium was exposed, a circular craniotomy, 2 mm in diameter, was made over the parietal cortex, 1.0 mm anterior to the bregma, and 2.5 mm lateral to the midline. Fifty thousand 9L gliosarcoma cells in 5 µl PBS were injected intracerebrally with a 10 µl Hamilton syringe to a depth of 2.5 mm beneath the dura during a 5-min interval (Chopp et al., 1996a; Chopp et al., 1996b; Jiang et al., 1997; Jiang et al., 1998). The needle was then retracted over a 6-min period. The craniotomy was covered with a piece of polyvinyl chloride film glued to the surrounding intact bone. The incision was closed with 4-0 silk sutures (Ethicon, Somerville, NJ).

Control animals were treated identically to the tumor-implanted rats, having scalp incision, skull removal, needle insertion and withdrawal, but without tumor cell injection.

5.3.1.3 Behavioral testing

Behavioral tests, including forelimb-use asymmetry, somatosensory asymmetry, and vibrissae-evoked forelimb placing tests, were carried out before and after surgical procedures. Please refer to the method details in Chapter 2.

5.3.1.4 Histological assessment

Tissue preparation: The tumor-bearing animals dying during the experiment were subjected to immediate sacrifice. Rats surviving until day 14 after tumor implantation were sacrificed at day 14. Rats were anesthetized and perfused intracardially with physiological saline solution followed by 4% paraformaldehyde. Brains were removed, processed, embedded in paraffin, and cut into seven 2-mm-thick coronal blocks.

Measurement of tumor volume: Six-μm-thick coronal sections taken approximately every 0.5 mm from each block containing the tumor were stained with hematoxylin and eosin (H&E). H&E-stained sections were viewed with 2.5 times magnification and were scanned into the computer. The tumor area (mm^2) was measured by tracing the demarcation of the tumor on the computer screen using the Global Lab Image analysis program (Data Translation, Marlboro, MA). The volume of the tumor (mm^3) was estimated by summing the values produced by multiplying the respective tumor area by the section interval thickness.

Immunofluorescence staining: Microtubule-associated protein 2 (MAP2), glial fibrillary acid protein (GFAP), von Willebrand factor (vWF), and synaptophysin were used as markers for neurons, astrocytes, endothelial cells, and synaptogenesis, respectively.

A series of 6-μm-thick sections at 50 μm intervals were cut from the block containing the maximum cross-sectional tumor area. Double immunofluorescence

staining of MAP2 (mouse monoclonal, 1:200 dilution; Chemicon, Temecula, CA) with GFAP (rabbit polyclonal, 1:10,000 dilution; Dako, Carpenteria, CA) and double immunofluorescence staining of vWF (rabbit polyclonal, 1:400 dilution; Dako, Carpinteria, CA) with synaptophysin (mouse monoclonal, 1:1,000 dilution; Chemicon, Temecula, CA) were carried out on the 6-μm-thick sections. Fluorochromes fluorescein isothiocyanate (FITC; Jackson Immuno.) and Cy3 (Jackson Immuno.) were used for double-label imunoreactivity. The sections were counterstained with 4',6-diamidino-2-phenylindole (DAPI, Dako).

After dehydration, sections were boiled in 1% citric acid buffer (PH 6.0) for 10 min, and cooled down to room temperature. Subsequently, the sections were incubated in 1% BSA to block the non-specific signals. The sections were incubated overnight at 4 ^{o}C in primary antibody (anti-MAP2 or anti-vWF antibody), followed by incubation with FITC-conjugated secondary antibody for 1 h at room temperature. The sections were incubated with primary antibody (anti-GFAP or anti-synaptophysin antibody) overnight at 4 ^{o}C and subsequently with Cy3-conjugated secondary antibody at room temperature for 1 h. Each of the above steps was followed by four 5-min rinses in PBS. The sections were counterstained with DAPI. Finally, the sections were mounted with Vectashield Hardset medium (Vector). Sections were visualized under a fluorescent microscope.

Quantification of immunofluorescence: Semi-quantitative measurements of MAP2, GFAP, vWF and synaptophysin immunoreactivity were conducted on five 6-μm-thick coronal sections that contain the tumor from each tumor-bearing brain and on five sections in the same region as the tumor from each surgical control. Images of corresponding immunostained sections were visualized at 400 times magnification with a fluorescent microscope and analyzed with MCID image analysis program. For quantification of immunoreactivity of MAP2, GFAP, and synaptophysin, five fields from

the peri-tumoral area of tumor-bearing animals and five fields from the operated hemisphere of control animals were selected. Densities of MAP2, GFAP, and synaptophysin (% of positive pixel) were calculated by dividing the positive pixels measured in the peri-tumoral area and the similar region in controls by the field of view (327680 pixels), respectively. For quantification of immunoreactivity of vWF, five fields from the tumors, five fields from the peri-tumoral areas, and another five fields from the surgical controls were selected. Density of vWF (% of positive pixel) was calculated by dividing the positive pixels measured in the tumor, the peri-tumoral area, and the similar region in controls by the field of view (327680 pixels). The corresponding values were averaged for each animal.

5.3.1.5 Statistical analysis

Raw scores from the four behavioral tests, including forelimb-use asymmetry, magnitude of somatosensory asymmetry, same-side placing and cross-midline placing, were converted to make all the testing outcomes consistent with higher scores indicating greater functional deficits, and then standardized with the following formula:

$$y^*_{i,k} = \frac{y_{i,k} - \bar{y}_k}{\hat{\sigma}_k}$$

where $\bar{y}_k$ is the mean and $\hat{\sigma}_k$ is the standard deviation of $y_{i,k}$, $i = 1, 2,\ldots, N$.

Composite scores were produced by summing the four standardized behavioral scores and then adding 4 to avoid the occurrence of negative numbers (Schallert and Lindner, 1990; Lu et al., 2003).

Repeated-measures ANOVA was applied to examine behavioral data across time. One-way ANOVA was used to examine behavioral differences between the two experimental groups at each specific time point. The immunofluorescent data of MAP2,

GFAP, and synaptophysin from the peri-tumoral areas and from the corresponding areas in surgical controls were compared with Student's t-tests, respectively. The immunofluorescent data of vWF from the tumors and the peri-tumoral areas were compared with the corresponding areas in controls with Student's t-tests, respectively. Data are presented as mean ± standard error.

5.3.2 Experiment 2

The goal of Experiment 2 was to determine the correlation between the magnitude of somatosensory asymmetry and the brain tumor volume dynamically measured by MRI.

5.3.2.1 Animals, experimental model, and behavioral testing

Seven animals received the same 9L gliosarcoma cell implantation surgery, and somatosensory asymmetry test as in Experiment 1. The behavioral tests were conducted immediately prior to MRI measurements at day 6, 12, and 16 after tumor implantation.

5.3.2.2 MRI measurement

MRI measurements were performed using a 7 T, 20 cm bore superconducting magnet (Magnex Scientific, Abingdon, UK) interfaced to a BRUKER console (Billerica, MA, USA). During the imaging procedure, the rat was fixed with ear bars and was fitted with a nose mask for anesthesia using a gas mixture of N_2O (69%), O_2 (30%) and Halothane or Isoflurane (0.75-1%). One of two standard magnetic resonance contrast agents (MRCA) was administered via tail vein based on availability: Gadomer-17, or gadolinium-diethylanetriamine pentaacetic acid (Gd-DTPA), with the dosage for both agents 250 μmol/kg, in a 0.15 ml bolus. High-resolution proton spin-lattice relaxation time (T1)-weighted images were obtained using multislice (27 slices) spin-echo [repetition time (TR) = 1000 ms, time to echo (TE) = 7.5 ms, 4 averages] sequences with

a 0.5 mm slice thickness, 32 mm field of view (FOV), and 256 x 192 matrix before and after administration of MRCA, with imaging time approximately 13 min for each sequence.

All MR images were reconstructed using a 128 x 128 matrix. Image analysis was performed with "eigentool" software (Peck et al., 1992; Peck et al., 1996; Ewing et al., 2006). Using the postcontrast T1-weighted image, each slice was examined for the presence of tumor. If a tumor was detected, regions of interest (ROIs) were outlined manually and filled, and the areas were measured. The volume of the tumor in the slice was calculated by multiplying the area by the slice thickness, and all such volumes were summed, thus yielding an estimate of the total tumor volume.

5.3.2.3 Statistical analysis

A multiple regression analysis was conducted to determine the relationship between tumor volume (independent variable) and behavioral score (dependent variable) after adjusting for time (covariate). The significance levels (*p*) of tumor volume as well as time in the multiple regression model were calculated. The correlation coefficient (R) was calculated. An equation $Y = b_0 + \Sigma\, b_i X_i$ was produced to summarize the model, in which Y is the predicted value of behavioral score, X_i represents all the independent variables, including tumor volume and time, b_i represents regression coefficients, and b_0 is the value of Y when all X are zero.

5.4 RESULTS

5.4.1 Experiment 1

5.4.1.1 Late onset of significant behavioral deficits in 9L glioma-bearing rats

Fischer rats implanted with 5 x 10^4 9L glioma cells usually die within 14 to 17 days. In this study, two tumor-bearing animals died at day 11 and 14 respectively, and the rest of them were still alive at day 14 after tumor implantation. All surviving animals were sacrificed after behavioral testing at day 14.

Both repeated-measures ANOVA and one-way ANOVA showed no changes in the general activity of the tumor-bearing rats whose test results were collected. Near-death animals could not perform the behavioral tests. In the somatosensory asymmetry test, both the percentage of the trials that the adhesive label on the ipsilateral limb was contacted first and the asymmetry score, are presented. When the percentage of trials on which the ipsilateral label was contacted first was considered (Fig. 5.1 A), all surviving rats at day 14 displayed a marked bias for contacting the label on the ipsilateral forelimb. Repeated-measures ANOVA revealed a significant time effect ($F(6, 84) = 3.378$; $p < 0.01$). One-way ANOVA showed significant differences between the tumor-bearing group and the control group at day 14 after tumor implantation ($F(1, 14) = 7.828$; $p < 0.05$). In terms of the magnitude of the somatosensory asymmetry (Fig. 5.1 B), all surviving rats at day 14 exhibited an asymmetry with a score as much as, or higher than, 2.5. Repeated-measures ANOVA showed a significant time effect ($F(6, 84) = 6.124$; $p < 0.001$), and a significant time by group effect ($F(6, 84) = 6.578$; $p < 0.001$). One-way ANOVA showed that the tumor-bearing animals displayed significant behavioral deficits at day 14 ($F(1, 14) = 41.702$; $p < 0.001$) in comparison with control animals. In the

same-side placing test (Fig. 5.1 C), two tumor-bearing animals exhibited mild behavioral deficits after surgery, followed by complete recovery within a week, but one of them lost all ability to place its contralateral limb at day 11, and the deficits persisted at day 14. However, one-way ANOVA showed that the average performance of the tumor-bearing group was not significantly different from control subjects at any time point. In the cross-midline placing test (Fig. 5.1 D), the same two tumor-bearing rats displayed minor behavioral deficits after surgery as they did in the same-side placing test, and they both recovered completely before day 4 post-tumor implantation. Two rats in the tumor-bearing group showed severe placing deficits from day 11 on, and so did another rat at day 14 post-tumor implantation. Repeated-measures ANOVA revealed a significant time effect ($F(6, 84) = 2.490$; $p < 0.05$), and a significant time by group effect ($F(6, 84) = 2.490$; $p < 0.05$). One-way ANOVA showed that tumor implantation was associated with significant behavioral deficits at day 14 ($F(1, 14) = 5.801$; $p < 0.05$), compared with the control procedure. Note that all animals involved in this experiment placed 100% successfully with both of their forelimbs in the baseline testing, and the tumor implantation did not influence the placing ability of their ipsilateral forelimbs. In the forelimb-use asymmetry test (Fig. 5.1 E), one-way ANOVA showed no significant differences in the average performance between glioma-bearing rats and control-operated animals throughout the testing period. The test results from the four behavioral tasks were integrated to produce a composite score for each animal at each time point (Fig. 5.1 F). Repeated-measures ANOVA revealed a significant time effect ($F(6, 84) = 4.070$; $p < 0.01$), and a significant time by group interaction ($F(6, 84) = 4.460$; $p < 0.01$). One-way ANOVA showed that tumor progression elicited significant behavioral deficits at day 14 post-tumor implantation ($F(1, 14) = 12.224$; $p < 0.01$), as compared to control.

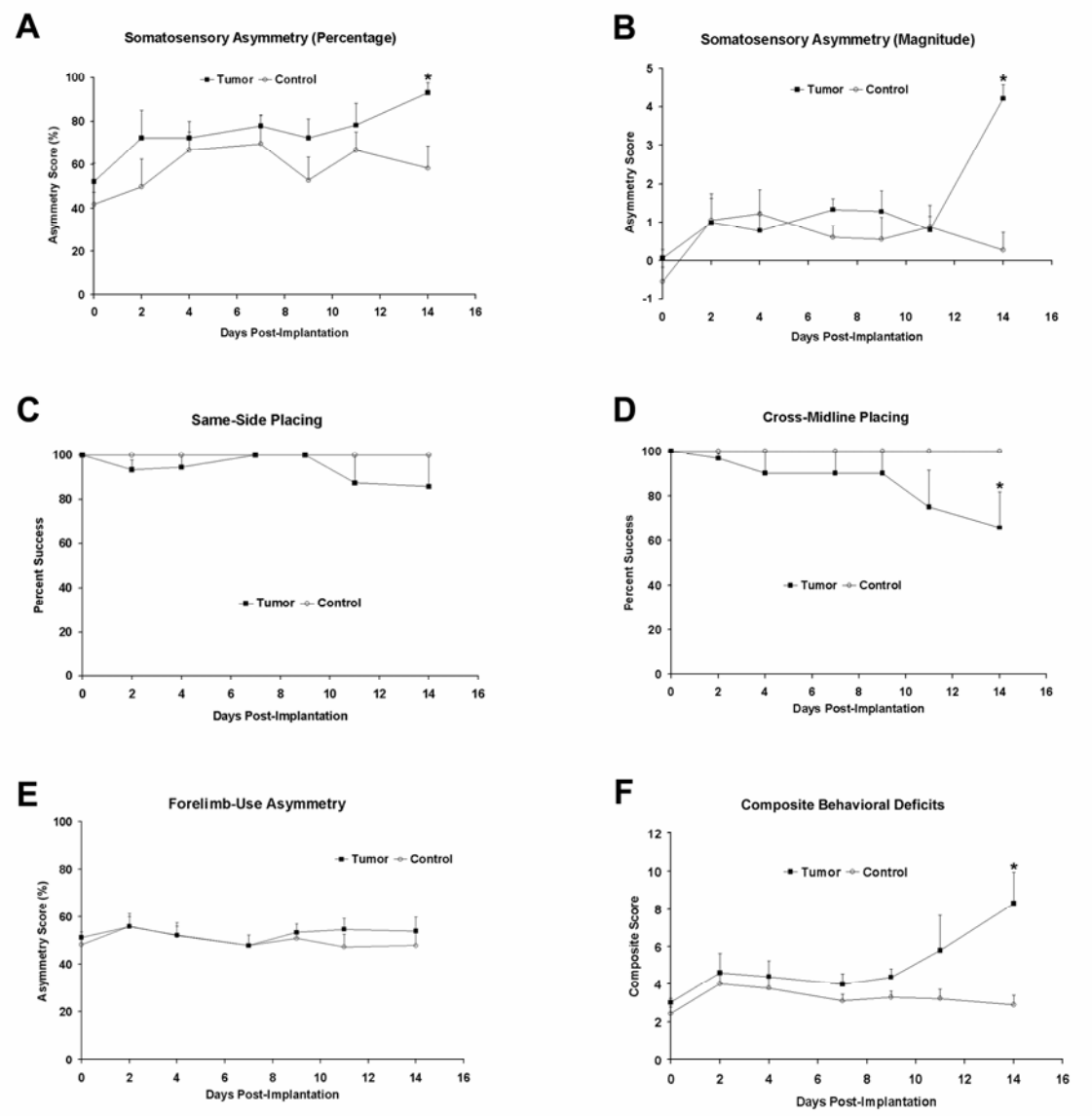

Figure 5.1: Behavioral deficits associated with brain tumor progression.

Significant differences were found between the tumor-bearing group and the control group at day 14 after tumor implantation in both percentage of ipsilateral contact of adhesive label stimuli (A) and magnitude of the somatosensory asymmetry (B). In the same-side placing test (C), the average performance of the tumor-bearing group was not significantly different from that of the control group at any time point. In the cross-midline placing test (D), tumor growth caused significant behavioral deficits at day 14 post tumor cell injection, compared with the control procedure. In the forelimb-use asymmetry test (E), there were no significant differences in the average performance

between glioma-bearing rats and control-operated animals throughout the testing period. Raw scores from the four behavioral tests, including forelimb-use asymmetry, magnitude of somatosensory asymmetry, same-side placing and cross-midline placing, were integrated to produce a composite score for each animal at each time point (F). Tumor progression elicited significant composite neurological deficits at day 14, as compared to control. * indicates significant difference between tumor-bearing animals and surgical controls at the respective time point with $p < 0.05$.

5.4.1.2 Tumor volume and placement

Post-mortem inspection of the tumor-bearing brains confirmed the presence of large striato-cortical tumors in all 9 tumor-implanted animals. The tumor volume was 114.4 ± 35.6 mm^3. Variable midline shift was noted. In tumor-bearing brains, dark purple tumor masses were clearly detected in H&E-stained sections. The peri-tumoral area was identified as an area around the main tumor mass with approximately 0.5 to 1 mm in depth, which was slightly darker than the surrounding normal tissue, consisting of mixed small multi-focal tumors and non-tumor brain tissue.

All 9 control animals had normal brains except for mild damage related to either the burr hole or the needle tract.

5.4.1.3 Reactive peri-tumoral brain plastic events

Quantitative evaluation of the immunohistochemical reactivity was performed by optical density measurements. With DAPI nuclear counterstaining (in blue, Fig. 5.2 A and E, and Fig. 5.3 A and E), the tumor was well demarcated from the surrounding brain tissue, characterized by high nuclear density. The peri-tumoral area contained scattered small foci of tumor. Neither MAP2 (green, Fig. 5.2 F) nor GFAP (red, Fig. 5.2 G) immunoreactivity was found in 9L tumor cells. Student's t-tests revealed a significant increase in both MAP2 ($t(16) = 5.539$; $p < 0.001$; Fig. 5.2 I) and GFAP ($t(16) = 4.083$; $p < 0.01$; Fig. 5.2 J) expression in the peri-tumoral area (Fig. 5.2 F and G), compared with

the similar region in surgical controls (Fig. 5.2 B and C). Fig. 5.2 D is derived from the merging of Fig. 5.2 A, B with C. Fig. 5.2 E, F and G were merged to produce Fig. 5.2 H. Student's t-tests revealed significant increases in vascular density in the tumor region ($t(16) = 4.705$; $p < 0.001$; Fig. 5.3 F and I) and the peri-tumoral area ($t(16) = 4.269$; $p < 0.01$; Fig. 5.3 F and I), compared with the control (Fig. 5.3 B and I), as indicated by the immunoreactivity for vWF (green). We were unable to detect synaptophysin-positive staining (red) in 9L tumor cells (Fig. 5.3 G). The peri-tumoral area displayed significantly increased staining for synaptophysin ($t(16) = 3.739$; $p < 0.01$; Fig. 5.3 G and J), in comparison with the corresponding area in surgical controls (Fig. 5.3 C and J). Fig. 5.3 D was generated by the merger of Fig. 5.3 A, B and C. Fig. 5.3 E, F and G were merged to form Fig. 5.3 H.

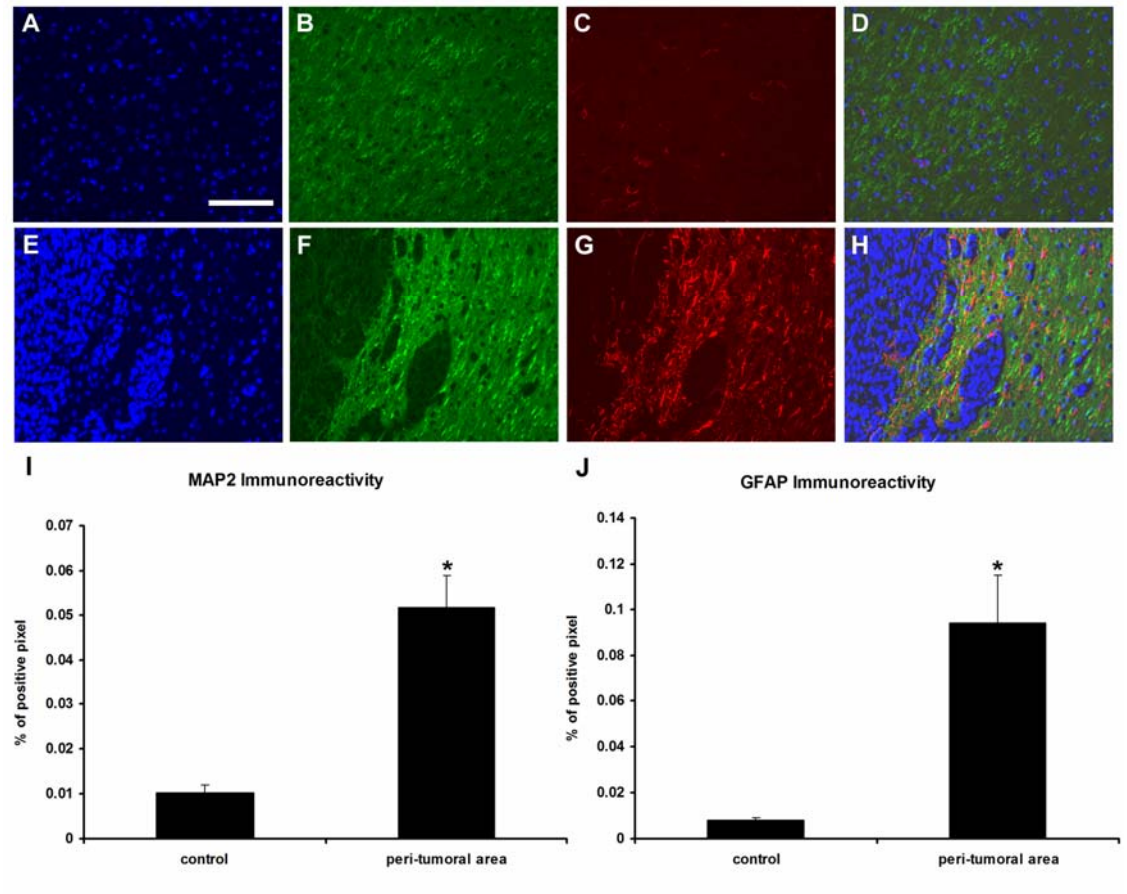

Figure 5.2: Significant increase in MAP2 and GFAP expression in the peri-tumoral area.

Representative images of MAP2 (green) and GFAP (red) double immunostaining with DAPI (blue) counterstaining under 200 times magnification collected from the tumor hemisphere (E-H) and the similar region in controls (A-D), respectively. There was a significant increase in both MAP2 (I) and GFAP (J) expression in the peri-tumoral area, compared with the corresponding region in controls. Bar = 100 μm in A. * $p < 0.05$ versus controls.

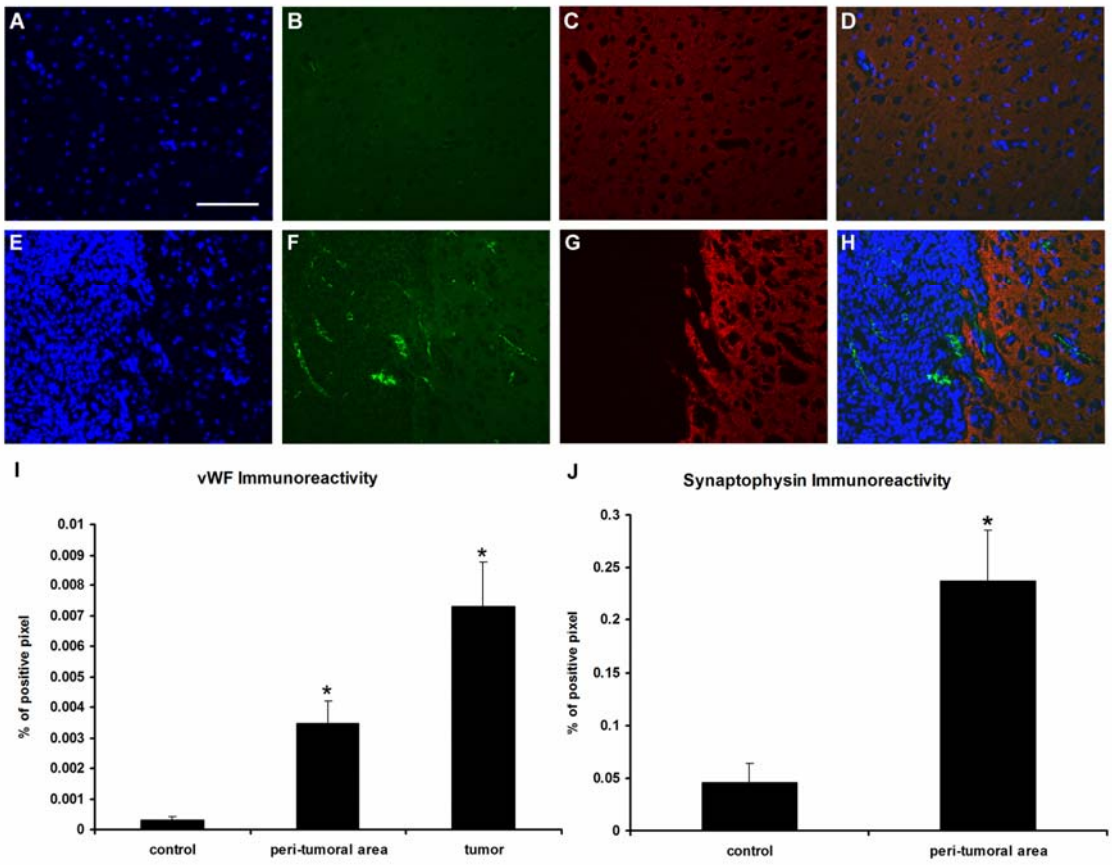

Figure 5.3: Significant increase in vWF and synaptophysin expression in the peri-tumoral area.

Representative images of vWF (green) and synaptophysin (red) double immunostaining with DAPI (blue) counterstaining under 200 times magnification collected from the tumor hemisphere (E-H) and the similar region in controls (A-D), respectively. The vascular density in both the tumor region and the peri-tumoral area significantly increased compared with the corresponding region in controls (I), as indicated by the immunoreactivity for vWF. The peri-tumoral area also displayed significantly increased staining for synaptophysin in comparison with the control (J). Bar = 100 μm in A. * $p <$ 0.05 versus controls.

5.4.2 Experiment 2

5.4.2.1 Significant correlation between magnitude of somatosensory asymmetry and brain tumor volume

Fig. 5.4 A illustrates the tumor volumes in 7 rats repeatedly measured by MRI at different time points. Each line represents an individual rat. Rat # 1, 2, 3 died at day 14 post-tumor implantation, while rat # 4, 5, 6, 7 stayed alive until day 16. Although there was great individual variability in tumor growth rate, the tumors all followed a consistent growth pattern, with faster increase in volume in the later stages.

Behavioral tests were carried out on the same day but prior to MRI measurements to avoid the influence of anesthesia on the behavioral performance. The tumor-bearing rats exhibited a faster behavioral deterioration in the late stage, with a similar trend to tumor progression. Multiple regression analysis showed that the *p*-value of tumor volume after adjusting for time was 0.002, while the *p*-value of time after adjusting for tumor volume was 0.813, indicating that tumor volume was a strong predictor, while time was a poor predictor of the behavioral response in the model. The correlation coefficient between tumor volume and behavioral test score was 0.775, indicating a high degree of correlation and a good fit to a linear model. The correlation coefficient without considering time (R = 0.774) was similar to that with time as a covariate (R = 0.775), also suggesting that time made little contribution to the regression model. Therefore, the time covariate can reasonably be neglected from the regression model. Data were shown in Fig. 5.4 B using bivariate plots with the X axis representing tumor volume and the Y axis representing behavioral score. The equation Y = -0.261 + 0.081 X was produced to summarize the model. A regression line was drawn based on the equation to fit data (Fig. 5.4 B).

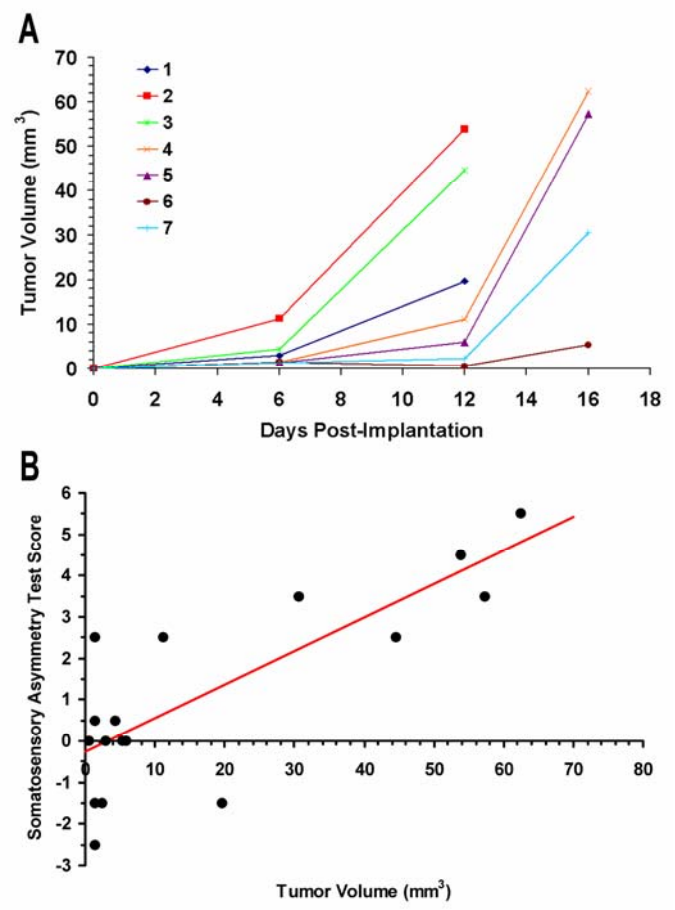

Figure 5.4: Significant correlation between tumor volume and magnitude of somatosensory asymmetry.

(A) Tumor volumes measured by MRI at different time points in 7 glioma-bearing rats. (B) Somatosensory asymmetry scores corresponding to tumor volumes. A regression line based on the equation Y = -0.261 + 0.081 X fits the data well.

5.5 DISCUSSION

We found that 9L glioma-bearing rats did not exhibit significant functional deficits until the presence of very large tumors. Our results are consistent with clinical observations and preclinical studies. Despite the large tumor volume, the development of focal neurological deficits is rarely evident before manifestations of raised intracerebral

pressure (Whittle and Marston, 1997). Whittle and Marston reported that only occasional problems with locomotor function, grooming or general behavioral functions were observed in several hundred cases of rodents implanted with gliomas when the tumors were not very large, and that a subtle progressive loss of motor function was evident in the rat C6 striatal implantation model from 12 days post-implantation during a 22-day test period, detected with the staircase test (Whittle and Marston, 1997).

Among the four behavioral tests that we used in Experiment 1, the somatosensory asymmetry test was the most sensitive for detecting tumor-elicited behavioral deficits. All animals with tumors displayed significant deficits in this test, whereas in the other three tests, only a portion of animals did. The composite behavioral deficit score was influenced primarily by the somatosensory asymmetry. Therefore, in Experiment 2, we examined the correlation between tumor volume and magnitude of somatosensory asymmetry and we found a significant correlation between the two variables with the coefficient of correlation 0.775. Every tumor has a unique growth pattern. In addition to growth rate and size, individual tumors may vary in their extension to neighboring locations, the degree of brain distortion and hydrocephalus, and invasion to the ventricular system. The timing and extent of neuroplasticity-related processes may considerably vary too. Furthermore, there is a subclinical tumor growth stage. These and other events could have degraded the early relationship between behavior and MRI assessment and could explain why, prior to Day 14, the average behavioral deficit was not significant.

Potential mechanisms by which peri-tumoral neurons are damaged and eventually lost are incompletely understood. In the rat C6 striatal implantation model, concurrent metabolic dysregulation and neuroreceptor alterations may contribute to peri-tumoral brain dysfunction (Whittle and Kelly, 2001). An investigation into human diagnostic

resection specimens and postmortem cases of gliomas revealed neuronal loss as well as a sequence of morphological disarray and stress responses in surviving neurons in cerebral cortex infiltrated by diffuse astrocytoma (Goel et al., 2003). In many ways, a brain tumor might be regarded as an injury, not unlike other types of cell loss, and thus would be expected to induce neuroplasticity. The relatively slow growth pattern of brain tumors may share adaptive mechanisms associated with slow degenerative diseases in which adaptive mechanisms prevent early clinical signs. Previous studies showed neurogenic response of the subventricular zone (SVZ) to malignant brain tumors grown in the striatum (Duntsch et al., 2005; Glass et al., 2005; Bexell et al., 2007). In the present study, we observed putative reactive peri-tumoral plasticity-related changes, including markers linked to synaptogenesis, astrocyte activation and angiogenesis.

MAP2 is a cytoskeletal protein localized in the neuronal dendritic compartment. MAP2 plays an important role in neuronal migration and neurite outgrowth by organizing microtubules in developing neurons both for axonal and dendritic morphogenesis (Teng et al., 2001). MAP2 expression coincides with dendritic outgrowth, branching, and post-lesion dendritic remodeling, suggesting that this protein plays a crucial role in plasticity (Johnson and Jope, 1992). Suppression of MAP2 inhibits neurite formation (Dinsmore and Solomon, 1991; Caceres et al., 1992). A previous study demonstrated that MAP2 increased in hippocampal granule cell dendrites following kainite-induced seizures and neuronal loss, suggesting that MAP2 contributes to the stabilization of dendrites after axonal denervation and eventually to the development of new spines and postsynaptic specializations during the reinnervation process (Pollard et al., 1994). Glioma cells release excessive amounts of glutamate and cause excitotoxicity in the vicinity of the tumor (Ye and Sontheimer, 1999; Takano et al., 2001; Sontheimer, 2003). In the current

study, the peri-tumoral increase in MAP2 immunoreactivity may implicate dendritic sprouting and postsynaptic alterations as compensatory responses to tumor insult.

The peri-tumoral increase in GFAP immunoreactivity indicates astrocyte activation. Reactive gliosis has been described as an important outcome of an injury to the nervous system, and plays a crucial role in clearing degenerating terminals (Bechmann and Nitsch, 1997), providing trophic factors (Rowntree and Kolb, 1997; Baba, 1998; Dong and Benveniste, 2001; Keyvani and Schallert, 2002; Kleim et al., 2003), and reestablishing a proper microenvironment for neural tissue repair (Shao and McCarthy, 1994; Aldskogius et al., 1999).

vWF is an endothelial marker, used as an index of vascular density. The peri-tumoral increase in microvessel density reflects the angiogenic process. Normal angiogenesis occurs in developing or healing tissues to provide an adequate supply of nutrients (Papetti and Herman, 2002). Inhibition of angiogenesis impedes astroglial proliferation and brain repair (Krum and Khaibullina, 2003). Although tumor-induced angiogenesis is a pathological condition, it mimics the process of normal angiogenesis, which remodels established primitive networks of blood vessels to support metabolic demands (Papetti and Herman, 2002). Angiogenesis in normal tissue surrounding the tumor may be an adaptive change in response to tissue hypoxia/ischemia and may contribute to tissue recovery. Using a novel three-dimensional quantitative method to analyze laser-scanned confocal microscopy images of dextran-labeled cerebral microvessels, Jiang et al. found significant angiogenesis in tumor and adjacent tissue, identified by increases in the number of vessel branch points coincident with a decrease in the mean vessel length (Jiang et al., 2005).

Synaptophysin is a presynaptic vesicle protein that may be a marker of synaptic density (Leclerc et al., 1989; Masliah et al., 1990; Masliah et al., 1991). An increase in

synaptophysin immunoreactivity has been found in the cortex surrounding an area of infarction (Stroemer et al., 1992). Upregulated synaptophysin staining density occurs in the hippocampus following unilateral enhorhinal cortex lesions in both mice and rats, which may be an indication of terminal sprouting and new synapse formation (Kadish and Van Groen, 2003). It is possible that the peri-tumoral increase in synaptophysin immunoreactivity in the present study reflects axonal sprouting, presynaptic alterations and/or synaptogenesis in response to tumor challenge.

Since we did not control tumor size or block any peri-tumoral events, it remains to be determined whether adaptive mechanisms could prevent or slow the onset of neurological deficits.

In summary, using sensitive behavioral tests, we observed that following tumor implantation in the sensorimotor cortex, rats showed significant functional deficits, but only when tumor growth was extensive. The significant correlation between tumor volume and somatosensory impairment suggests that behavioral markers might help to gauge the extent of tumor progression. We detected a number of peri-tumoral pathological changes that could be reasonably linked to synaptic plasticity, astrocyte activation and angiogenesis. It is possible that peri-tumoral and/or remotely located mechanisms of reactive plasticity may compensate for tumor-associated insult, partially contributing to subclinical tumor extension. Improvements in functional assessment as well as in evaluating pathological events and compensatory adaptations in addition to tumor size may provide useful adjuncts to evaluate potential treatment strategies.

Chapter 6: Functional Outcome after Antiangiogenic Treatment in a Mouse Glioma Model

This work is published in Behavioral Brain Research in 2007 (Yang et al., 2007a).

6.1 ABSTRACT

The objective of the current study was to investigate the functional outcome after treatment with a novel antiangiogenesis regimen, which is a combination of monoclonal antibodies against both vascular endothelial growth factor receptor (VEGFR)-1 (MF1) and VEGFR-2 (DC101) in the orthotopic mouse model of human U87 glioma. We found that the combination antibody therapy retarded tumor progression and delayed the onset of significant behavioral deficits. Histologically, tumor necrosis and apoptosis were increased and tumor cell proliferation was decreased after treatment. In clinical trials for novel interventions, functional end points typically are included in the assessment of potential efficacy. Because certain interventions that successfully treat tumor progression in animal models might interfere with compensatory neuroplasticity, functional measurement may be valuable for improving the clinical relevance of translational brain tumor research.

6.2 INTRODUCTION

Angiogenesis is a process of growing new vessels by remodeling the preexisting ones (Papetti and Herman, 2002). Normal angiogenesis ensures an adequate supply of oxygen and nutrients for developing or healing tissues (Papetti and Herman, 2002). Tumor-induced angiogenesis is a pathological condition in order for tumor growth and propagation to occur, which mimics normal angiogenesis with the same aim of satisfying

the metabolic demands of a tissue, (Carmeliet and Jain, 2000; Papetti and Herman, 2002). However, tumor-induced neovessels exhibit abnormal ultrastructures, which are dilated and tortuous, and exceptionally permeant due to transcellular gaps and fragmented membranes (Papetti and Herman, 2002; Jain, 2005). Two main factors contribute to the leakiness of tumor vessels: vascular endothelial growth factor (VEGF) and angiopoietin (Ang)-2. VEGF not only increases tumor vessel density (Plate et al., 1992; Takahashi et al., 1995), but also increases vascular permeability (Senger et al., 1983; Kevil et al., 1998; Tse et al., 2003), which eases the penetration of tumor cells (Papetti and Herman, 2002). Ang2 antagonizes the Ang1-Tie2 pathway to allow the preexisting vessels to revert to an unstable and plastic state, and to maintain the plastic state in the newly formed vessels, thus facilitating VEGF-induced vessel growth (Stratmann et al., 1998; Holash et al., 1999; Zagzag et al., 1999; Audero et al., 2001; Ding et al., 2001; Papetti and Herman, 2002; Tse et al., 2003).

Antiangiogenic therapy has been considered an alternative or complementary paradigm to conventional cancer treatments. Antiangiogenic therapy is aimed at restraining tumor progression, instead of eliminating all the tumor cells, and is especially suited for administration during the course of the tumor-dormant state (Kohn and Liotta, 1995; Mikkelsen, 1998). However, antiangiogenic treatment has been reported to impede brain repair in a wound lesion model (Krum and Khaibullina, 2003), and therefore may potentially reduce restorative neuroplastic processes associated with tumor and its treatments.

An initial step in developing animal models that could potentially be used to assess the relative effects of different treatment strategies on brain tumor growth vs. neuroplasticity should include assessment of neurological outcome. The primary goal of this study was to use a standard glioma model together with a currently promising

treatment to determine the potential sensitivity of behavioral assays in detecting dysfunction. We investigated the influence of antiangiogenic treatment on brain function in glioma-bearing mice. The combined inhibition of VEGFR1 and VEGFR2 signaling is a powerful antiangiogenic treatment, which has been shown to be more effective than targeting either VEGFR1 or VEGFR2 alone in other cancer types (Lyden et al., 2001). Our results demonstrate that the combination antibody therapy retarded tumor progression and delayed the onset of significant behavioral deficits without detectably affecting brain function adversely in the dormant stages of tumor development.

6.3 MATERIALS AND METHODS

6.3.1 Cell culture

The U87 human glioma cell line was grown in minimum essential media (MEM) with Earle's salts, supplemented with 10% fetal bovine serum, 0.2% phenol red, and 1% each of L-glutamine, MEM sodium pyruvate, nonessential amino acid, and penicillin and streptomycin (Invitrogen Corp., Carlsbad, CA), and incubated in a 5% CO_2 humidified atmosphere at 37^{o}C. Prior to intracranial implantation, cells were dispersed with 0.05% trypsin/EDTA (Invitrogen Corp.) and adjusted to a final concentration of 10^8 cells/ml in PBS.

6.3.2 Experimental model

A total of 23 nude mice (Nu/Nu athymic; Charles River Breeding Laboratories, Wilmington, MA) with a body weight of 15 to 25 g were employed in this study. Fifteen animals received brain implantation of $5X10^5$ U87 tumor cells and 8 animals were assigned to sham surgery. Five microliters of U87 cells ($5X10^5$ cells) were slowly injected into the sensorimotor cortex (SMC) at the following coordinates: 2.0 mm lateral

from the midline, 1.0 mm anterior to the bregma, and 2.5 mm ventral to dura (Jiang et al., 2005). Sham animals were treated identically to the tumor-implanted mice, having scalp incision, but without skull removal.

6.3.3 Antiangiogenic treatment regimen

Seven U87 tumor-bearing mice underwent i.p. injections of MF1 (400 μg/mice) and DC101 (800 μg/mice) every other day from day 8 to day 14 after tumor implantation. The doses of the two agents were based on previous literature (Prewett et al., 1999; Kunkel et al., 2001; Lyden et al., 2001) as well as on information from the manufacturer (Imclone Inc., New York).

6.3.4 Histopathology

6.3.4.1 Tissue preparation

After animals were perfused with 4% paraformaldehyde, brains were removed and cut into 1-mm-thick blocks which then were processed and embedded in paraffin. Six-μm-thick sections were further cut from each of the blocks containing the tumor.

To examine the effect of monoclonal antibodies (mAbs) against VEGFR-1 (MF1) and VEGFR-2 (DC101) on tumor vessel density, animals implanted with U87 cells were administered fluorescein isothiocyanate (FITC)-conjugated dextran ($2x10^6$ molecular weight, Sigma, St. Louis, MO; 1 ml of 5 mg/ml) intravenously (i.v.) 2 mins before they were sacrificed. The brain tissue was cut on a vibratome into 100-μm sections which were used for fluorescent confocal microscopy.

6.3.4.2 Measurement of tumor volume

Six-μm-thick coronal sections obtained serially at 0.5 mm intervals from each of the blocks containing the tumor were stained with H&E for calculation of tumor size. Please refer to Chapter 5 for the detailed method of tumor volume calculation.

6.3.4.3 Immunohistochemistry

Ki67 (rabbit monoclonal, IgG antiboday, 1:300 dilution; Lab Vision, CA) immunostaining was performed. Ki67 antigen is the prototypic cell cycle related nuclear protein, expressed in proliferating cells. Six-μm-thick paraffin sections were incubated with a primary antibody followed by a biotinylated secondary antibody. 3'3'-diaminobenzidine-tetrahydrochloride (DAB; Sigma) was used to routinely detect reaction product, which can be visualized directly by bright-field light.

In situ apoptosis assay was conducted by examining fragmented DNA on paraffin embedded tissue sections with the TUNEL ApopTag kit (Chemicon) in conjunction with hematoxylin counterstaining.

6.3.4.4 Quantification

One hundred-μm-thick sections containing the U87 tumor, obtained from animals administered with FITC-dextran, were imaged using a confocal microscope, and analyzed with MCID program. For measurement of vascular density, five fields of view from the tumor area in each of the five coronal sections per animal were analyzed and the positive area was measured. Vascular density (% of positive pixel) was calculated by dividing the positive pixels by the field of view. With fluorescent confocal microscopy, aberrant vascular structures inside the tumor were identified as regions of high vessel density and/or the presence of abnormally large vessels. The volume of the regions containing

aberrant vasculature was calculated by multiplying the appropriate area by the section interval thickness.

For quantification of immunoreactivity of TUNEL and Ki67, images of corresponding immunostained 6-μm-thick coronal sections were scanned using either a X40 objective (0.074 mm^2 field of view, for Ki67) or a X20 objective (0.296 mm^2 field of view, for TUNEL) via the MCID computer imaging analysis system. For each immunostaining type, five fields of view per section and five sections per animal that contain the tumor were quantified. The numbers of TUNEL positive or Ki67 positive cells were counted in the tumor area within each section. The total number of positive cells was divided by the total tissue area to determine cell density (cell number/mm^2) and the value was averaged for each animal.

6.3.5 Behavioral testing (rearing)

Mice were placed in a Plexiglas cylinder, 15 cm in height with a diameter of 10 cm (Baskin et al., 2003; Starkey et al., 2005; Wells et al., 2005). An experimenter scored independent use of the left or right forepaw, or simultaneous use of both forepaws, for contacting the wall of the cylinder during a full rear, to initiate a weight-shifting movement or to regain center of gravity while moving laterally in a vertical posture along the wall. Twenty consecutive instances of limb use behavior were recorded and the asymmetry score was calculated as percent use of the ipsilateral (unaffected) forelimb minus that of the contralateral (affected) forelimb.

6.3.6 Statistical analysis

Histology data from two sampled groups were compared with Student's t-tests. Repeated measures ANOVA was used to evaluate functional performance across testing days and one-way ANOVA was used to examine differences among the means of several

different groups at each specific time point. When there was a significant overall effect, post-hoc tests were carried out to compare all groups of subjects with each other. All data are presented as mean ± standard error.

6.4 RESULTS

6.4.1 Delayed onset of significant functional deficits in U87 glioma-bearing mice treated with MF1 and DC101

Unlike the U87 tumor control group, in which only 2 out of 8 animals were still alive at day 29, all of the animals in the MF1+DC101-treated U87 tumor group were alive at day 29. In the rearing test (Fig. 6.1), U87 glioma-bearing mice without MF1+DC101 treatment exhibited significant behavioral deficits at day 27, compared with either tumor-bearing animals receiving MF1+DC101 treatment ($p < 0.05$) or sham-surgery animals ($p < 0.05$). By day 29, tumor-bearing animals subjected to MF1+DC101 treatment also displayed significant deficits compared with sham-surgery animals ($p < 0.01$). MF1+DC101-treated tumor-bearing animals did not show worse behavioral deficits in comparison with their untreated tumor controls at comparable time points before day 27.

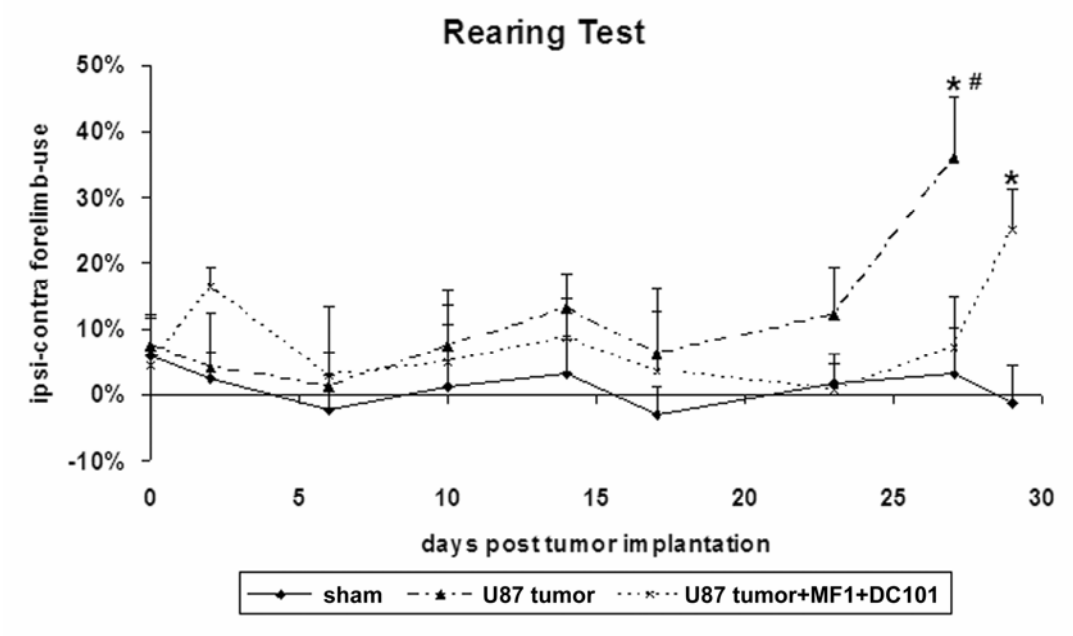

Figure 6.1: Retarded onset of significant behavioral deficits in U87 tumor-bearing mice after MF1 and DC101 treatment.

Animals' behaviors were measured by the rearing (forelimb-use asymmetry) test. * $p < 0.05$ compared to sham controls, # $p < 0.05$ compared to untreated tumor controls, at corresponding time points.

6.4.2 Reduced U87 glioma growth under treatment with MF1 and DC101

The mice were sacrificed after they had lost over 20% of their body weight, and all surviving animals were sacrificed at day 29. Tumor size was measured on H&E-stained slices. Fig. 6.2 A and B show representative slices from the U87 tumor control group (Fig. 6.2 A) and the MF1+DC101-treated U87 tumor group (Fig. 6.2 B), respectively. The tumor size of the tumor control group was significantly larger than that of its MF1+DC101-treated counterpart (Fig. 6.2 C, $p < 0.01$).

6.4.3 Increased tumor necrosis and apoptosis and reduced tumor cell proliferation after treatment with MF1 and DC101

Treatment-related pathological changes in tumor tissues were identified with H&E staining. A marked decrease in cellularity and patches of necrosis with disperse extravascular hemorrhage were observed in MF1+DC101-treated U87 tumors (Fig. 6.2 E), compared with U87 tumor controls (Fig. 6.2 D).

The TUNEL assay revealed that MF1+DC101-treated U87 tumor cells (Fig. 6.2 G) had a significantly higher rate of apoptosis (Fig. 6.2 H, $p < 0.01$) than untreated U87 tumor cells (Fig. 6.2 F).

A significant decrease in tumor cell proliferation, as measured by the number of Ki67 positive cells (Fig. 6.2 K, $p < 0.01$) was seen in MF1+DC101-treated U87 tumors (Fig. 6.2 J) compared with their untreated counterparts (Fig. 6.2 I).

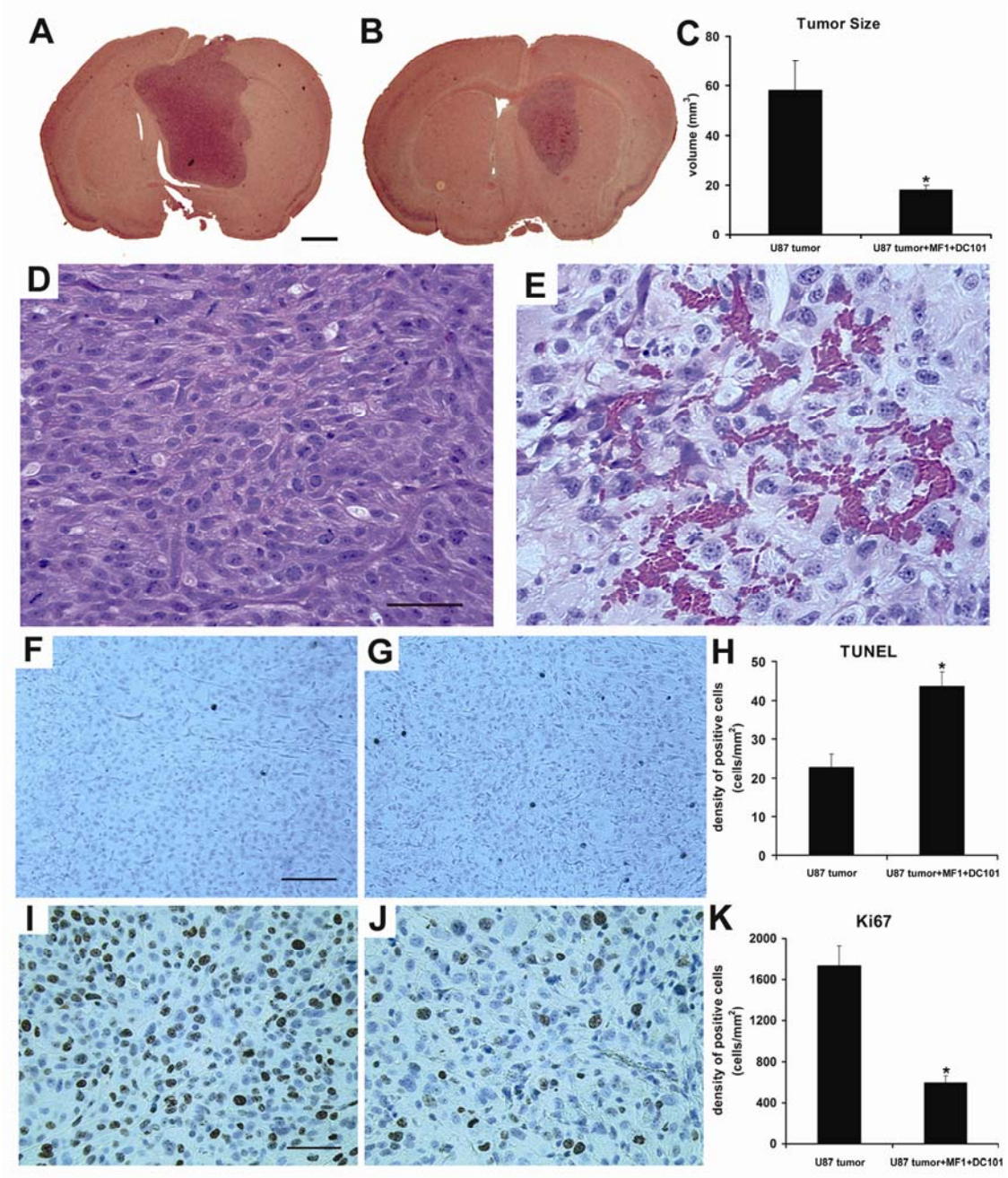

Figure 6.2: Reduced U87 tumor growth after MF1 and DC101 treatment.

A and B, Representative H&E-stained U87 tumor slices obtained from mice without treatment sacrificed sequentially between day 23 and day 29 (A) and from those treated with MF1+DC101 sacrificed at day 29 (B) after tumor implantation. C, The mean tumor

size decreased significantly after MF1+DC101 treatment. D and E, magnified H&E-stained images of the U87 tumors treated with (E) or without (D) MF1+DC101. Extravascular hemorrhage and patchy necrosis are present in MF1+DC101-treated U87 tumors (E). F and G, TUNEL-stained images of the U87 tumors treated with (G) or without (F) MF1+DC101. H, MF1+DC101 treatment resulted in a significant increase in tumor cell apoptosis, as measured by the density of the TUNEL-positive cells (dark brown). I and J, Ki67-stained images of the U87 tumors treated with (J) or without (I) MF1+DC101. K, MF1+DC101 treatment resulted in a significant decrease in tumor cell proliferation, as measured by the density of the Ki67-positive cells. * $p < 0.05$ compared to untreated U87 tumor controls in C, H and K. Scale bars, 1 mm in A, 100 μm in D and I, 200 μm in F.

The vessel density and the volume of the regions containing abnormally-high-density neovascularization were measured on fluorescence images obtained after administration of the fluorescent dextran. The volume of the regions containing aberrant neovascularization was slightly larger than the corresponding tumor volume (data not shown). The volume of the regions containing aberrant neovascularization was significantly reduced following MF1+DC101 treatment in parallel with the volume of the tumor. However, the vascular density inside the MF1+DC101 treated tumors was not significantly different from that of untreated control tumors (data not shown).

6.5 DISCUSSION

6.5.1 Importance of functional assessment in preclinical research of brain tumor therapy

In earlier research, the rationale for the safety of antiangiogenic agents lies in limited angiogenesis in the adult brain. Thus, therapies that target specific receptors, which are upregulated on proliferating endothelium, could potentially avoid widespread toxicity in the patient (Scappaticci, 2002). However, brain insults from tumor expansion and surgery may render the brain more vulnerable. There is evidence that inhibition of endogenous VEGF impedes revascularization and astroglial proliferation during the

repair of brain injury (Krum and Khaibullina, 2003). Therefore, functional evaluation is indispensable in brain tumor research and may lead to better decision-making when weighing the benefits and risks of a specific cancer treatment.

6.5.2 Behavioral changes in mouse models of brain tumors

Mouse tumor models are particularly useful because in contrast to rats, there are many genetically engineered mice, and various antibodies have been produced targeting mouse antigens. The present study showed, for the first time, behavioral changes in mouse models of brain tumors and introduced functional assessment into brain tumor treatment evaluation using mouse models. The rearing test primarily assesses forelimb motor asymmetry by producing quantitative scores, and has been shown to be sensitive and effective in various CNS lesion models in mice (Baskin et al., 2003; Starkey et al., 2005; Wells et al., 2005). There were no changes in the general activity of the tumor-implanted animals whose test results were collected. The behavioral deficits observed are mainly attributed to dysfunction or destruction of normal brain tissue in the SMC and underlying striatum due to tumor compression and invasion, whereas generalized increased intracerebral pressure (ICP) alone may not play an essential role because it should have produced bilateral deficits rather than asymmetries.

Significant behavioral asymmetry was found in the late tumor-bearing stage. Our results are consistent with previous reports by Whittle and Marston and our investigations in rat glioma models (Whittle and Marston, 1997; Yang et al., 2007b).

6.5.3 Rationale for using antiangiogenic therapy targeting both VEGFR-1 and -2 to treat gliomas

VEGF secreted by glioma cells is a pivotal mediator of tumor neoangiogenesis (Plate et al., 1992; Plate et al., 1993). Accumulating evidence indicates the central role of

the VEGF/VEGF-2 signal transduction system for tumor angiogenesis and tumor growth (Millauer et al., 1994; Millauer et al., 1996). Systemic treatment with a monoclonal antibody against VEGFR-2 (DC101) inhibits tumor angiogenesis and growth of several mouse and human tumors, including gliomas (Prewett et al., 1999; Kunkel et al., 2001; Davis et al., 2004). A newly recognized role of VEGFR-1 in mobilization and functional incorporation of bone-marrow-derived cells into rapidly expanding tumor vasculature makes VEGFR-1 an intriguing target for antiangiogenesis therapy (Carmeliet et al., 2001; Hattori et al., 2002; Rafii et al., 2002). Inhibition of VEGFR-1 with a monoclonal antibody (MF1) attenuates the growth and vascularization of VEGF-transduced rat C6 gliomas implanted in nude mice (Luttun et al., 2002). Recent data demonstrate enhanced tumor suppression by combination of the two antibodies targeting both VEGFR-1 (MF1) and VEGFR-2 (DC101) in intradermally inoculated mice with either B6RV2 lymphoma or Lewis lung carcinoma cells, compared with the effects of either single neutralizing antibody (Lyden et al., 2001). All these previous findings warrant further exploitation of combined antibodies against both VEGFR-1 and VEGFR-2 in glioma management.

The two neutralizing antibodies MF1 and DC101 were developed specifically for mice, and an in vivo brain cancer model with a human origin glioma cell line may better recapitulate the clinical situation. We employed the orthotopic nude mouse model of human U87 glioma to investigate the effect of the combination antibody therapy for malignant gliomas. The current study is the first, to our knowledge, to employ this novel antiangiogenic regimen to treat gliomas.

6.5.4 Functional effects of the novel antiangiogenic treatment targeting both VEGFR-1 and -2 on the tumor-bearing brain

It is important to use a model that, at some time points, yields very minor deficits, or no deficits, in untreated animals so that treatments that exaggerate dysfunction can be readily detected. In this study, we demonstrate that antiangiogenic treatment with MF1 and DC101 delayed the onset of significant behavioral deficits by inhibiting tumor growth. Our results bear out the presumption that brain tumor patients may benefit, with an enhanced quality of life, from a long-term cytostatic therapy like the antiangiogenic therapy, if it can continuously limit tumor progression within the dormant stages. However, because angiogenesis may play a role in functional plasticity during tumor growth (Yang et al., 2007b), as it does in cerebral ischemia (Wei et al., 2005a), and inhibition of angiogenesis was shown to impede brain repair in a rat model of stab-wound injury (Krum and Khaibullina, 2003), the behavioral deficits that occurred in the MF1 and DC101-treated glioma mice may be influenced overlappingly by tumor-related injury and inhibition of neuroplasticity by antiangiogenesis. Recently we found that certain anti-cancer therapies had an adverse effect on functional outcome in a rat model in which mass-related events were fixed (Yang et al., 2006b; Yang et al., 2006a). To address whether antiangiogenic therapy can interfere with the tumor-induced neuroplastic mechanisms which help keep the tumor "dormant" by not exhibiting noticeable functional deficits, we propose to compare behavioral performance of animals bearing a similar size tumor with or without antiangiogenic therapy. Furthermore, tumor therapy can be screened and optimized by analyzing and comparing behavioral performance of animals with similar-size tumor but receiving different kinds of anti-cancer treatments, and eventually, treatments that have comparable efficacy in limiting tumor progression but better efficacy in permitting neuroplasticity to take place optimally will be favored.

6.5.5 Suppression of glioma growth by the novel antiangiogenic treatment targeting both VEGFR-1 and -2

Our results demonstrate that systemic administration of combined MF1 and DC101 leads to a 69% reduction in mean tumor volume, a 66% decrease of proliferative activity and a 1.9-fold-increased apoptotic rate, compared with untreated tumor control. Based on a previous report that IgG may have a significant effect only when treatment is initiated immediately after tumor implantation, instead of against established tumors (Kunkel et al., 2001), we simply used untreated tumors as controls. Previous studies showed evidence of decreased tumor vascular density following continuous MF1, DC101, or MF1 + DC101 treatment (Kunkel et al., 2001). However, in this study, the vascular density inside the tumors was not significantly altered by MF1 + DC101 treatment, when it was examined two weeks after cessation of MF1 + DC101 administration. Furthermore, it was reported that withdrawal of DC101 treatment resulted in regrowth of tumors with similar kinetics to that of tumor controls in various tumor models (Prewett et al., 1999). Taken together, these results suggest that withdrawal of antiangiogenic therapy leads to vascular regrowth which provides a basis for progression of tumor growth. Therefore, it may be necessary to deliver antiangiogenic agents in sufficient quantities over a sustained period of time for the management of malignant gliomas. We sacrificed animals while they were still behaviorally testable to examine tumor size and its relationship to functional outcome. Our gross observations on survival rate indicate that systemic administration of combined MF1 and DC101 can prolong the survival time of glioma-bearing animals.

6.5.6 Summary

We demonstrated the capability of using behavioral measurement to assess brain tumor progression in mice. Evaluating functional outcome after anti-cancer treatment in mouse glioma models may be a valuable adjunct to brain imaging and survival analysis in the development of efficient screening methods for preclinical research. Future research should focus not only on maximizing the anti-cancer benefits of brain tumor treatments but also on limiting potential adverse effects on neuroplasticity and recovery of function.

Chapter 7: Systemic Administration of BCNU Suppresses Glioma Growth and Inhibits the Onset of Glioma-induced Sensorimotor Deficits

7.1 ABSTRACT

This study investigated the behavioral responses to systemic administration of a classic chemotherapy drug — 1,3-bis(2-chloroethyl)-1-nitrosourea (BCNU) in 9L glioma-bearing rats. MRI was used to dynamically evaluate tumor response to therapy. We found that a single bolus of BCNU dramatically inhibited tumor growth and the onset of glioma-induced somatosensory deficit. One rat exhibited delayed placing deficit after the use of BCNU, suggesting chemo-induced central neurotoxicity. Assessment of learning and memory function is warranted to further investigate BCNU-associated neurotoxicity.

7.2 INTRODUCTION

1,3-bis(2-chloroethyl)-1-nitrosourea (BCNU) kills tumor cells via its carbamoylating cytotoxicity, which irreversibly inhibits glutathione reductase with resultant accumulation of oxidized form of glutathione causing oxidative stress (Yang et al., 2005). Furthermore, BCNU significantly delays the tumor doubling time contributing to the delay of tumor repopulation (Ross et al., 1998). Experimental in vitro and in vivo studies have shown that BCNU is an effective treatment for malignant gliomas (Rosenblum et al., 1975; Rosenblum et al., 1976; Rosenblum et al., 1977; Rosenblum et al., 1980). The efficacy of BCNU and/or radiotherapy in the treatment of glioma patients who were operated on has been demonstrated in clinical trials (Walker et al., 1978). Currently, BCNU is the FDA approved mainstay in clinical chemotherapy for malignant

gliomas. However, the clinical outcome of patients treated solely with BCNU is not as efficacious as would be predicted by the responses observed in the experimental tumor model (Kornblith and Walker, 1988).

Fatal central neurotoxicity that commonly presents as leucoencephalopathy has been reported in clinical observations complicating the treatment of malignant gliomas with BCNU, especially through the intra-arterial and the intracarotid routes (Foo et al., 1986; Mahaley et al., 1986; Rosenblum et al., 1989). Previous study on neurotoxicity of chemotherapeutic agents after blood-brain barrier (BBB) modification suggests that the lack of neurotoxicity associated with the usual administration of most chemotherapeutic agents likely stems from limited entry of drug into the brain through an intact BBB (Neuwelt et al., 1983b).

9L tumor is induced by N-methylnitrosourea and classified as a gliosarcoma. The 9L rat brain tumor has been developed as both in vivo and in vitro models and used for more than forty years to investigate a variety of potential therapeutic agents, combinations, schedules, and approaches that might be applicable to the management of high-grade malignant brain tumors (Kimler, 1994). Animal survival, clonogenic cell survival, and tumor growth delay traditionally provide means to measure the effectiveness of treatment modalities in this tumor model (Weizsaecker et al., 1981).

The goal of the present study was to investigate the behavioral responses to systemic administration of BCNU using the classic 9L rat brain tumor model. MRI was used for dynamic assessment of tumor response to therapy.

7.3 MATERIALS AND METHODS

7.3.1 Animals

A total of 16 adult male Fischer rats (Charles River Breeding, Wilmington, MA) weighing 180-250 g were used in this study.

7.3.2 9L gliosarcoma cell culture and 9L cell implantation in Fischer rats

All 16 rats were subjected to intracerebral implantation of 9L glioma cells. Please see the related method in Chapter 5.

7.3.3 BCNU treatment regimen

Five days after the tumor implantation, 8 tumor-bearing rats received a single dose of 26.6 mg/kg BCNU therapy through i.p. injection. The BCNU dose was equivalent to double an LD10 dose, based on previous literature (Ross et al., 1998; Schepkin et al., 2005; Schepkin et al., 2006).

7.3.4 Behavioral testing

Behavioral tests, including forelimb-use asymmetry, somatosensory asymmetry, and vibrissae-evoked forelimb placing tests, were carried out before and after BCNU treatment. Please refer to the method details in Chapter 2.

7.3.5 MRI measurement

Please see Chapter 5 for details.

7.3.6 Statistical analysis

One-way ANOVA was used to determine differences in both functional performance and tumor growth between the tumor-bearing animals with or without BCNU treatment at each time point. Repeated-measures ANOVA was used to evaluate the within-subject effects before vs. after BCNU treatment.

7.4 RESULTS

Tumor-bearing animals without BCNU treatment started to die on day 14 after tumor implantation. One BCNU-treated rat died on the day of BCNU injection, and another died 10 days after BCNU injection, while the remaining BCNU-treated tumor-bearing rats were still alive on day 35 after tumor implantation. Nontreatment tumor-bearing animals displayed significant somatosensory asymmetry on day 14, while the average performance in forelimb-use did not change after tumor implantation. One untreated tumor-bearing rat showed both same-side and cross-midline placing deficits on its contralateral side 14 days following tumor implantation. One-way ANOVA revealed that tumor-burdened animals with BCNU treatment showed significantly less behavioral deficits than their untreated counterparts in the somatosensory asymmetry test on day 14 following tumor implantation ($p < 0.05$, Fig. 7.1). Repeated-measures ANOVA showed no significant within-subject effects before vs. after BCNU treatment in all three behavioral tests. However, one rat from the tumor+BCNU group displayed substantial cross-midline placing deficit on day 27, and the deficit persisted on day 35 after tumor implantation.

MRI measurement demonstrated that the tumors were significantly smaller in the BCNU-treated tumor group than those in the tumor control group, on days 12 ($p < 0.05$)

and 16 ($p < 0.01$) after tumor implantation (Fig. 7.2). The tumor size was still very small in the BCNU group 35 days post tumor implantation with an average only 0.10 mm^3.

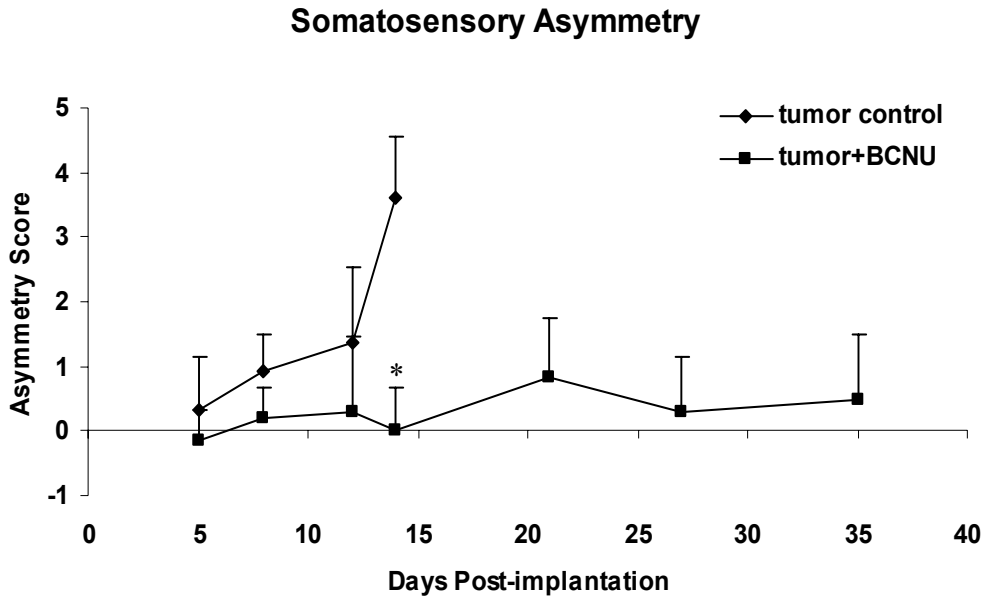

Figure 7.1: Systemic BCNU treatment inhibits the onset of glioma-induced somatosensory deficit.

The somatosensory asymmetry score in the tumor+BCNU group was significantly lower than that in the tumor control group on day 14 after tumor implantation. * $p < 0.05$.

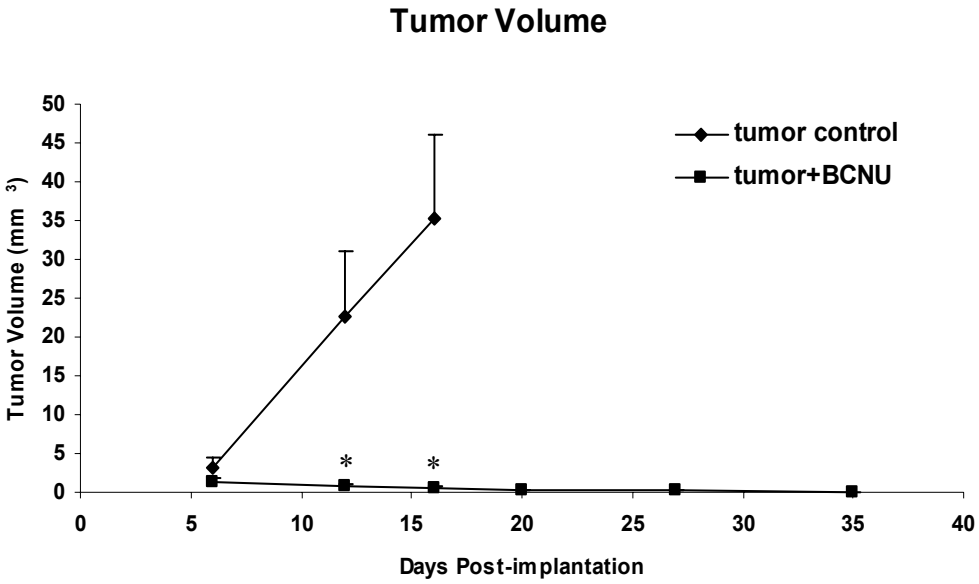

Figure 7.2: Systemic BCNU treatment inhibits tumor growth.

The tumor volume in the tumor+BCNU group was significantly smaller than that in the tumor control group measured on days 12 and 16 after tumor implantation. * $p < 0.05$.

7.5 DISCUSSION

Consistent with our previous study (Yang et al., 2007b), nontreatment glioma-bearing animals exhibited significant somatosensory deficit at the late stage of tumor growth, and a minority of them showed a placing deficit, while their average performance in forelimb-use was similar to that of normal ones.

Our results demonstrated that systemic administration of BCNU suppressed glioma growth and prolonged the survival of the glioma-bearing rats. These results are consistent with previous studies on the effectiveness of BCNU in treating gliomas (Rosenblum et al., 1975; Rosenblum et al., 1976; Rosenblum et al., 1977; Rosenblum et al., 1980). Even a single bolus of BCNU resulted in a dramatic tumor cell kill and a

significant increase in life span in the 9L gliosarcoma-burdened rats (Rosenblum et al., 1976).

Concurrent with the inhibition of tumor growth, BCNU inhibited the onset of glioma-induced somatosensory asymmetry. We have previously proved the highly significant correlation between magnitude of somatosensory asymmetry and tumor volume measured by MRI (Yang et al., 2007b). The somatosensory asymmetry test can detect tumor progression dynamically, non-invasively, and inexpensively, although not as accurately and sensitively as MRI. In addition to measuring tumor volume, proton and sodium MRI can reveal early changes in tumor sodium content and cellularity and therefore can be used as a biomarker to assess earliest response to cancer therapy (Schepkin et al., 2005; Schepkin et al., 2006).

Although the average performance in both forelimb-use and somatosensory asymmetry tests did not alter after BCNU treatment, there really were some signs of BCNU-induced neurotoxicity. One animal died on the same day of BCNU injection; another died ten days after; and still another one showed persistent placing deficit three weeks after BCNU treatment. Previous clinical observation documented that the BCNU-induced neurotoxicity was usually delayed, commencing several weeks following BCNU treatment (Mahaley et al., 1986). In this study, BCNU-treated animals were allowed to live for 5 weeks. Long-term follow-up study is warranted to investigate possible delayed placing deficit. Clinical pathological and neuroimaging studies demonstrated that the central neurotoxicity following BCNU chemotherapy, presenting as massive coagulative necrosis involving primarily though not exclusively the white matter, was mediated by vascular injury and direct neural damage (Foo et al., 1986; Mahaley et al., 1986; Rosenblum et al., 1989). A study in rats showed changes in BBB permeability and neurotoxicity after intracarotid BCNU administration, in which ipsilateral subcortical

structures such as the hypothalamus, amygdala, internal capsule, and caudate putamen had the highest incidence of neurotoxicity, closely related to the histopathological damage seen in human BCNU leucoencephalopathy (Nagahiro et al., 1991). The lack of change in forelimb-use and somatosensory performance after BCNU therapy may be because both sides of the brain were affected by systemic BCNU administration and the two asymmetry tests are not able to detect bilateral deficits. Furthermore, the sensorimotor asymmetry tests are usually used to examine damage to the sensorimotor cortex and the striatum (Schallert et al., 2000; Schallert et al., 2002; Schallert and Woodlee, 2005), and they may not be sensitive enough to detect the deficit produced by the BCNU-affected subcortical brain structures. Our previous study demonstrated that local fluorouracil chemotherapy exaggerated brain tissue loss and functional impairments after focal cortical compression, through inducing elevated necrosis and apoptosis in the compressed brain (Yang et al., 2006a). Local infusion of the chemotherapeutic agents into the brain areas where functional tests can detect damage may increase the positive-finding rate of chemo-induced central neurotoxicity. Nitrosourea-based chemotherapy can cause dementia (Vigliani et al., 1999; Plotkin and Wen, 2003; Aarsen et al., 2006). Hippocampus and amygdala are two pivotal brain structures associated with learning and memory and are also vulnerable to damage by BCNU therapy. Therefore, behavioral testing for learning and memory function is warranted to further investigate BCNU-induced neurotoxicity.

Chapter 8: Photofrin-mediated Photodynamic Therapy Induces Behavioral Deficits and Attempts at Using a Neurorestorative Agent for Functional Recovery

8.1 ABSTRACT

This study investigated the behavioral deficits following high-dose photodynamic therapy (PDT) applied to normal rat brain and the functional outcome of PDT-treated rats after neurorestorative treatment by atorvastatin. Photofrin™ at 2 mg/kg was injected intraperitoneally 24 hours before laser treatment as photosensitizer. The dose of laser energy was 280 J/cm^2. Atorvastatin at 3 mg/kg was administered orally every day for 14 days starting 24 hours after laser treatment. We found that PDT induced significant behavioral deficits, however, atorvastatin failed to promote functional recovery after PDT.

8.2 INTRODUCTION

Experimental photodynamic therapy (PDT) of cancer has a 100 year-history, and for more than 25 years, PDT has been established in the clinical environment as a useful adjuvant to standard cancer treatments (Stylli and Kaye, 2006a, b). PDT involves exposure to tissue-penetrating laser light following systemic administration of a photosensitizing drug, such as Photofrin, which is absorbed and accumulated by cancer cells with some selectivity. When exposed to light, the photosensitizing drug produces toxic oxygen species and kills the cancer cells (Goodell and Muller, 2001; Huang, 2005; Stylli and Kaye, 2006a, b). Clinical trials are currently in progress evaluating PDT as a treatment for a number of cancers including cancer of the prostate, oesophagus, head and

neck, and brain tumors. In February 2006, PDT has been approved by the national institute for health and clinical excellence (NICE) to treat some types of skin cancer.

Since 1980, over five hundred glioma patients have been treated globally with PDT. An intra-operative PDT procedure has been introduced to clinic, in which photoillumination is carried out to the tumor cavity produced by surgical resection, (Perria et al., 1980; Muller and Wilson, 1990). Several clinical studies showed that adjuvant PDT following surgical resection of the tumor significantly prolonged the median survival of patients with newly diagnosed or recurrent gliomas (Muller and Wilson, 1995, 1996; Stylli et al., 2005). Treatment responses appear to be related to adequate light delivery to the tumor (Muller and Wilson, 1990, 1996). Experimental studies of glioma response to PDT showed that increasing optical energy doses led to increased volume of tumor necrosis (Chopp et al., 1996a; Chopp et al., 1996b). However increasing the light dose delivered to the tumor increases the risks of inducing a permanent neurological deficit (Krishnamurthy et al., 2000).

The currently available photosensitizers have limited selectivity with regard to cancer cells and their retention in the normal tissue is unavoidable. Although Photofrin is retained in the tumor tissue to a higher degree than the normal brain tissue, the normal tissue is more sensitive to PDT than the tumor under identical treatment parameters (Dereski et al., 1991; Chopp et al., 1996a).

Increased tumor elimination requires an increase in PDT intensity. However, increased PDT intensity leads to increased damage to normal surrounding tissue and aggravated neurological deficits. The concern on functional impairment sets the dose limit of PDT in the clinic. Current PDT doses are inadequate for complete elimination of the established brain tumor. The remaining tumor cells give rise to recurrent tumors. Therefore, high-dose PDT is needed to treat gliomas, and concurrently, a neurorestorative

strategy is desperately needed to promote functional recovery after the aggressive anti-cancer treatment.

Atorvastatin, with the brand name Lipitor, is a drug clinically used for the treatment of high cholesterol and triglyceride levels, and its long-term safety has been proved (Newman et al., 2006). Atorvastatin has recently been found to have neurorestorative effects, independent of its antilipid effects. Atorvastatin can improve functional outcome after stroke (Chen et al., 2003a; Chen et al., 2005), intracerebral hemorrhage (Seyfried et al., 2004), and traumatic brain injury (Lu et al., 2004c; Lu et al., 2004b; Lu et al., 2004d; Lu et al., 2004a).

The objective of this study was to investigate the behavioral deficits following high-dose PDT applied to normal rat brain and the functional outcome of PDT-treated rats after administration of atorvastatin.

8.3 MATERIALS AND METHODS

8.3.1 Animals

A total of 32 adult male Fischer rats were used.

8.3.2 Experimental model

Light delivery: A semiconductor diode laser (University Health Network, Toronto, Canada) provided the light (635 ± 5 nm wavelength) for the PDT treatment. The light was coupled into a 200 μm diameter optical fiber with a distal microlens (PDT, Santa Barbara, CA, USA) for a 7 mm diameter, uniform spot for superficial irradiation. The power at the distal end of the fiber was adjusted to 100 mW and was measured before and after each treatment using a power meter (Photodyne, Westlake Village, CA,

USA) with a 1-inch integrating sphere detector head. The irradiation power was shown to be stable in all of the experiments.

PDT treatment: Photofrin™ (QuadraLogic Technologies, Vancouver, BC, Canada) was dissolved in 5% dextrose solution. Consistent with the clinical dose of Photofrin™ (Muller and Wilson, 1996), 2 mg/kg Photofrin™ was administered i.p. to 18 Fischer rats. Twenty-four hours after Photofrin™ administration, these animals were treated with laser. The surgery procedure was performed as described previously (Jiang et al., 1997; Jiang et al., 1998; Jiang et al., 2004). The rats were anesthetized by i.p. injections of ketamine (80 mg/kg) and xylazine (13 mg/kg). After the animals were fixed in a stereotaxic device, a 9-10 mm incision was carried directly down the midline, and the scalp was retracted to expose the cranium. Using a dental drill, a 5 x 5-mm-square craniectomy was made over the sensorimotor cortex. Laser light was delivered through the craniectomy. The optical dose employed in this study was 280 J/cm^2. The craniectomy was then covered with a piece of polyvinyl chloride glued to the surrounding intact bone and the incision was closed with 4-0 silk sutures. Six rats served as surgery controls, having scalp incision and skull removal, but without Photofrin™ administration and laser treatment.

Atorvastatin administration: Eighteen PDT-treated rats were equally divided into 2 groups based on their behavioral performance 24 hours after laser treatment. Nine of them received a continued daily oral administration of 3 mg/kg atorvastatin for 14 days starting 24 hours after laser treatment. Atorvastatin at this oral dose was shown to promote functional recovery after stroke in rats (Chen et al., 2003a). The other nine animals served as PDT-treated controls.

Histological studies were carried out on 8 additional animals that underwent PDT treatment, but these animals did not receive atorvastatin. Three of them were sacrificed

on day 3 and the other 5 were sacrificed on day 7 after laser treatment to examine for the PDT-induced lesion.

8.3.3 Behavioral testing

Behavioral tests, including forelimb-use asymmetry, somatosensory asymmetry, and vibrissae-evoked forelimb placing tests, were carried out before and after surgical procedures. Please refer to the method details in Chapter 2.

8.3.4 Histological assessment

Tissue preparation: Eight PDT-treated animals were sacrificed on days 3 and 7, respectively, after laser treatment, and the other 24 animals that underwent behavioral testing repeatedly were sacrificed two weeks after surgery. Under anesthesia, they were perfused and fixed with 4% paraformaldehyde. Brains were removed, processed, embedded in paraffin, and cut into seven 2-mm-thick coronal blocks.

Pathological examination: Six-μm-thick coronal sections containing the lesion were stained with hematoxylin and eosin (H&E) for microscopic examination.

8.3.5 Statistical analysis

Raw scores from the four behavioral tests, including forelimb-use asymmetry, magnitude of somatosensory asymmetry, same-side placing and cross-midline placing, were combined to produce a composite score for each animal at each time point, as described in Chapter 5. Repeated-measures ANOVA was applied to analyze behavioral data across time. One-way ANOVA was used to examine behavioral differences among the three groups at each time point. Data are presented as mean ± standard error.

8.4 RESULTS

Behavioral data are shown in Figure 8.1. Repeated-measures ANOVA showed that there were significant time effect ($F(6,126) = 26.559$; $p < 0.001$), significant group effect ($F(2,21) = 10.914$; $p < 0.01$), and significant time by group effect ($F(12,126) = 4.827$; $p < 0.001$) among the three groups. Post-hoc analyses revealed significant differences between the PDT-only group and the surgery control group ($p < 0.01$), and between the PDT + atorvastatin group and the surgery control group ($p < 0.01$); however, the PDT + atorvastatin group and the PDT-only group were not significantly different. One-way ANOVA showed that there were significant differences among the three groups at day 2 ($F(2,21) = 18.088$; $p < 0.001$), day 5 ($F(2,21) = 6.200$; $p < 0.01$), day 7 ($F(2,21) = 4.318$; $p < 0.05$), and day 9 ($F(2,21) = 6.462$; $p < 0.01$). Post-hoc analyses revealed that the PDT-only rats displayed significantly more behavioral deficits than the surgery controls at day 2 ($p < 0.001$), day 5 ($p < 0.01$), day 7 ($p < 0.05$), and day 9 ($p < 0.01$), and that the PDT-treated rats receiving atorvastatin exhibited significantly more behavioral deficits than the surgery controls at day 2 ($p < 0.001$), day 5 ($p < 0.05$), and day 9 ($p < 0.05$); however, the PDT + atorvastatin group did not significantly differ from the PDT-only group at any time point.

H&E staining revealed substantial necrosis, patchy hemorrhage, and vacuolization in the PDT lesion area 3 days after PDT (Fig. 8.2 A). Hemorrhage was absorbed 7 days after PDT (Fig. 8.2 B). The lesion shrank and became less manifest 14 days after PDT (Fig. 8.2 C).

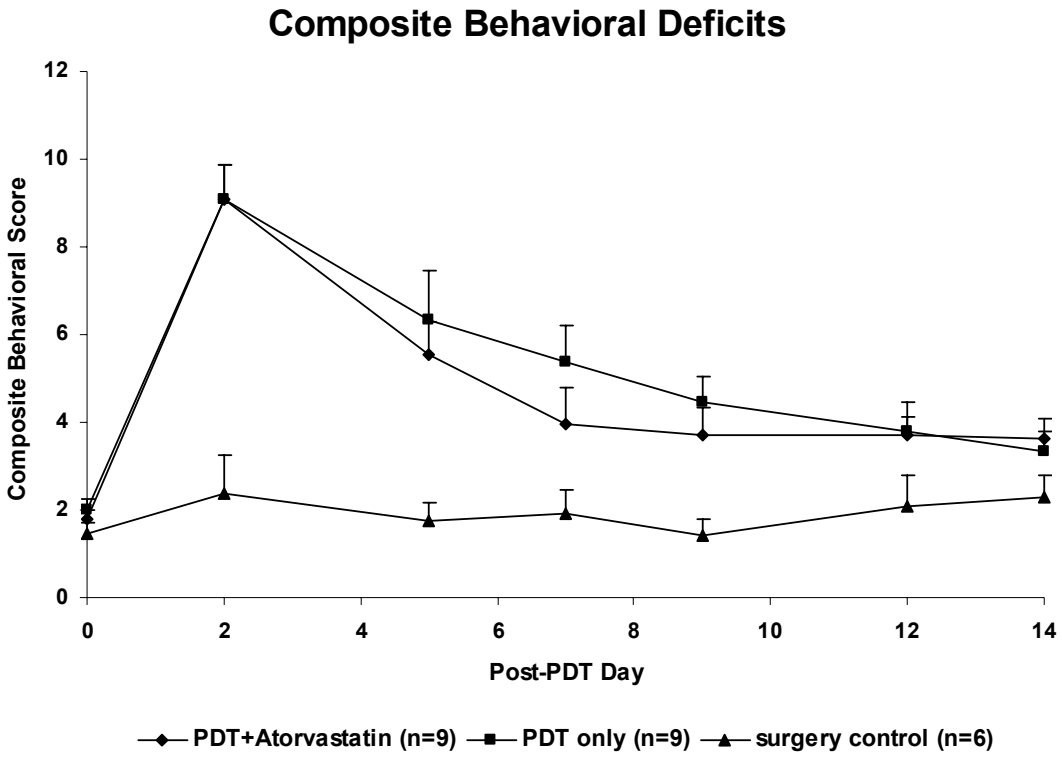

Figure 8.1: Behavioral response to high-dose PDT and functional outcome after atorvastatin administration to PDT-treated rats.

Composite behavioral results showed that PDT induced significant behavioral deficits, however, atorvastatin failed to promote functional recovery after PDT.

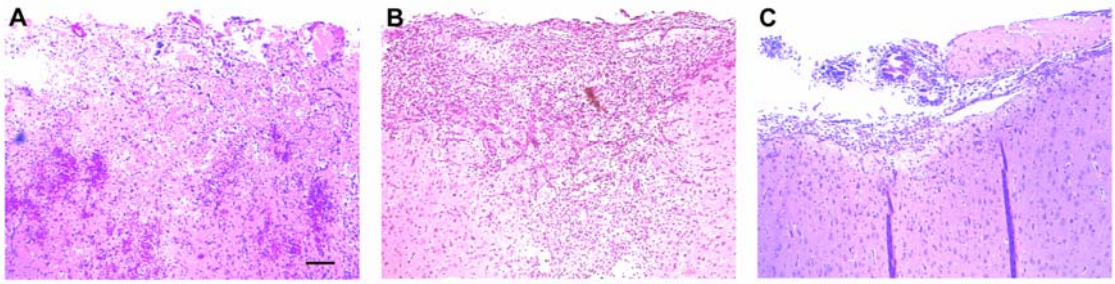

Figure 8.2: Histological images of PDT-induced brain damage.

H&E staining images (100 times magnification) collected from brains 3 days (A), 7 days (B), and 14 days (C), respectively, after PDT. PDT induced significant damage to the normal brain. Bar = 100 μm.

8.5 DISCUSSION

This study investigated the behavioral responses under PDT with a combination of the clinically relevant dose of 2 mg/kg Photofrin and a high optical dose of 280 J/cm^2 laser light. PDT-treated animals exhibited significant behavioral deficits. Concurrently, histological examination demonstrated substantial brain damage associated with PDT. Previous studies showed that normal brain is extremely vulnerable to PDT damage (Chen et al., 1996). PDT generated necrosis in normal brain was found to be a function of incident optical energy dose, with lesions histologically detectable at a dose as low as 3 J/cm^2 (Dereski et al., 1991; Chopp et al., 1996a; Chopp et al., 1996b).

We did not find any neurorestorative effect of atorvastatin after PDT. Atorvastatin has been shown to promote functional recovery after stroke (Chen et al., 2003a; Chen et al., 2005), intracerebral hemorrhage (Seyfried et al., 2004), and traumatic brain injury (Lu et al., 2004c; Lu et al., 2004b; Lu et al., 2004d; Lu et al., 2004a). Increased production of vascular endothelial growth factor (VEGF) and brain-derived neurotrophic factor (BDNF) (Chen et al., 2005), induction of neurogenesis, angiogenesis, and synaptogenesis (Chen et al., 2003a; Lu et al., 2004c; Seyfried et al., 2004), and reduction of intravascular thrombosis (Lu et al., 2004b; Lu et al., 2004d) and hematoma (Lu et al., 2004a), all likely contribute to the neurorestorative effects of atorvastatin. In this study, there was a dramatic spontaneous functional recovery after PDT, which may have masked the neurorestorative effect of atorvastatin. Furthermore, no close assessment was done to investigate whether atorvastatin showed the same stimulatory effects on neuroplasticity in

the PDT model as in other models. There is a possibility that atorvastatin may have no neurorestorative effects after PDT-induced cortical damage.

Chapter 9: General Discussion and Future Directions

Together, this set of studies focus on a relatively neglected, but potentially crucial area of preclinical brain tumor research: functional assessment and neuroplasticity. Optimal treatment strategies should limit or reduce tumor growth without compromising the integrity of the brain.

We characterized the behavioral responses of focal brain compression in a model of rapid displacement of brain tissue elicited by epidural implantation of a hemisphere-shaped plastic bead (Yang et al., 2006c). The rapid brain compression induced mild behavioral deficits which depended on the location, magnitude and duration of the focal compression, and which resolved spontaneously even while the compression remained (Yang et al., 2006c). We then examined the impact of some cancer interventions on the compressed brain. Long-term administration of the NMDA receptor antagonist MK801 did not change the recovery rate but caused a reinstatement of behavioral deficits after complete recovery from focal brain compression (Yang et al., 2006b). Local chemotherapy with fluorouracil exacerbated compression-induced functional deficits (Yang et al., 2006a). This controlled mass compression model does not have the growth and invasion properties of an actual tumor, but isolates the compression characteristics of a brain tumor, allowing investigation of the functional impact of anti-cancer treatments on the compressed brain, independent of their tumor-shrinking effects. The mild lesion pattern of this mass compression model makes it especially suitable to detect the adverse effects of anti-cancer treatments on functional integrity of the brain.

Further histological assessment is warranted to investigate whether mass compression can change the ventricle size and how different magnitudes of mass compression would affect the ventricle size. Furthermore, future improvements may

include a controlled-rate compression device that is able to inflate and deflate slowly over weeks or months. Such an advance in the technique would more closely model the slower-growing property of many tumors. Because the inert mass cannot secrete chemicals and invade the surrounding brain tissue, the focus would be on manipulation of tumor mass so that compression and plasticity effects can be examined specifically. Future study would benefit from a controlled-rate focal compression model to test anti-cancer drugs with similar tumor-shrinking effects, and to screen for the ones with reduced harm to the compressed brain and its plastic ability.

We investigated the behavioral responses as the brain tumor progresses and found a late-onset pattern of the behavioral deficits (Yang et al., 2007b). Tumor size typically increases faster and faster toward the late stage of its growth. The time when behavioral deficits occur is the time of the steep incline of the tumor growth. Rapid growth of the tumor strongly attacks the surrounding normal brain tissue, and finally reveals itself. A brain tumor shares important characteristics of a slow-degenerative brain lesion, inducing neuroplasticity continuously. Previous study characterized the neurogenic response of the subventricular zone (SVZ) to the growth of malignant brain tumors in the striatum (Duntsch et al., 2005; Glass et al., 2005; Bexell et al., 2007). We demonstrated astrocytic activation, angiogenesis, and synaptogenesis in the peritumoral area, which are all reactive neuroplastic responses to lesions (Yang et al., 2007b) that may or may not involve the SVZ directly. We further investigated the impact of some anti-cancer treatments on the tumor-bearing brain. Antiangiogenic treatment with a combination of antibodies against both the VEGF receptors 1 and 2 delayed the onset of brain tumor-induced behavioral deficits (Yang et al., 2007a). Systemic chemotherapy with BCNU inhibited the occurrence of behavioral deficits associated with tumor growth, but a minority of animals showed deficits possibly associated with delayed chemo-induced

neurotoxicity (Chapter 7). It is difficult to find the neurotoxicity and the adverse effects on neuroplasticity when the treatments are administered systemically in a tumor implantation model, because the tumor-slowing or shrinking effects can mask the adverse effects on the remaining brain function, unless the adverse effects are very severe and occur in the tumor-dormant stage before the tumor grows large. This tumor implantation model may not be sensitive enough to reveal suboptimal treatments, but it can well recapitulate the clinical situation, and can test the anti-cancer effects directly. Therefore, the advantage of this model is that it can show the integrative effects, and treatments can be compared and optimized. Use of both a tumor implantation model and a controlled-rate non-tumor compression/deflation model may improve investigation of optimal treatments.

Further behavioral assessment will be conducted in glioma-bearing rats using the water maze test because hippocampus is affected as well by the tumor in this model. Behavioral tests for bilateral functional assessment are needed because increased intracerebral pressure affects bilateral function, and the tumor can compress and invade the contralateral hemisphere. We will also use the water maze test to investigate whether systemic administration of BCNU to the glioma-bearing rat can induce learning and memory deficits, because BCNU can limit the tumor growth within a very small size, and BCNU has been reported to cause dementia (Vigliani et al., 1999; Plotkin and Wen, 2003; Aarsen et al., 2006). Further experiments are warranted to investigate the temporal pattern of peri-tumoral reactive neuroplastic responses. It will be interesting to block some neuroplastic events, for examples, anti-VEGF, anti-BFGF, or block their receptors, and then compare the behavioral responses of animals bearing the tumors of similar size and location with or without treatment. This experiment is aimed at investigating whether the tumor-induced neuroplastic mechanisms contribute to behavioral compensation.

Because the treatments that block neuroplasticity may also slow tumor growth, MRI is needed to monitor the tumor size and location, and the comparison will be made between treated and non-treated tumors of similar size while not considering time. It also would be intriguing to investigate whether life styles, for example, exercise, can affect glioma growth. Exercise can reduce the risk of breast cancer (Bernstein et al., 2005; Hewitt et al., 2005; Tehard et al., 2006), significantly improve the quality of life (QOL) outcomes and physiological capacity of breast cancer survivors (Hewitt et al., 2005), prolong their survival (Holmes et al., 2005), and is likely to prevent recurrence of breast cancer (Hann et al., 2005). Running alone or combined with caffeine guards against skin cancer in mice (Michna et al., 2006; Lu et al., 2007). Also, motor enrichment and exercise have been shown to promote neuroplasticity and to rescue brain tissue from progressive degeneration in animal models of Parkinson's, Alzheimer's and other brain diseases (Kleim et al., 2003; Woodlee and Schallert, 2006).

Furthermore, we need to test one same anti-cancer therapy administered at the same dosage, by the same route, and under the same schedule, in the non-tumor compression model and the tumor implantation model, respectively, to bridge these two treatment screening systems. An example of an anti-cancer treatment that can interfere with functional recovery in the non-tumor compression model but can slow tumor growth and concurrently delay the onset of significant functional deficits in the tumor implantation model, may better demonstrate the necessity of utilizing both models to screen for treatments with improved anti-cancer effects and reduced adverse effects on functional integrity of the brain.

We found that high-dose photodynamic therapy (PDT) induced significant behavioral deficits in normal rats (Chapter 8). We attempted to use a neurorestorative agent atorvastatin to promote the functional recovery after PDT, but failed (Chapter 8).

There was a marked spontaneous functional recovery after PDT, and atorvastatin did not accelerate the recovery (Chapter 8). The neural toxicity of many cancer therapies, such as local radiation (Kim et al., 2004), local chemotherapy (Yang et al., 2006a), as well as PDT (Chapter 8), can be revealed through direct administration to normal brain. The advantage of this model is simplicity. However, unlike the focal compression model, interruption of neuroplasticity cannot be investigated as easily in the normal brain.

Future research will be focused on establishment of a model with long-lasting behavioral deficits, and examination of whether neurorestorative strategies can promote functional recovery after cancer therapies. Such models may include aspiration lesion or stab wound lesions, designed to mimick as closely as possible certain aspects of tumor resection surgery, and focal delivery of radiation to the normal brain. Neurorestorative strategies may include physical therapy, gene therapy, other neurorestorative agents such as erythropoietin and sildenafil, and cell therapy (Zhang et al., 2002; Zhang et al., 2005; Chen and Chopp, 2006; Chopp and Li, 2006; Liu et al., 2006; Mahmood et al., 2006; McFarlin et al., 2006; Seyfried et al., 2006; Zhang et al., 2006; Mahmood et al., 2007a; Mahmood et al., 2007b; Shen et al., 2007a; Shen et al., 2007b; Wang et al., 2007a). Functional promotion effects should be established initially in the nontumor animal undergoing cancer therapies. The effects of the neurorestorative strategies on tumor growth and regrowth should also be examined in the tumor-bearing animal with and without cancer therapies. Our preliminary data showed that atorvastatin did not promote glioma growth in nude mice. Additional studies should explore potential integrative effects of combinations of cancer therapy and neurorestorative therapy in glioma-bearing animals. Functional outcome and survival time both should be included as outcome measures.

Note that animals can functionally recover by themselves from the bead compression, even when the bead remains implanted permanently (Yang et al., 2006c), from the 5FU intracerebral injection (Yang et al., 2006a), and from the photodynamic therapy (Chapter 8). This phenomenon occurs in other lesion types as well, such as stroke (Zhang et al., 2002; Zhang et al., 2005), and traumatic brain injury (Lu et al., 2004c; Lu et al., 2004d; Lu et al., 2005). The spontaneous functional recovery can be accounted for by the compensatory reorganization of the contiguous and remote brain areas (Weiller et al., 1992; Seitz et al., 1995; Nudo et al., 1996; Rossini et al., 1998; Cramer et al., 2000; Pineiro et al., 2001), and by the neuroplastic mechanisms, such as neurogenesis, angiogenesis, and synaptogenesis, to self-repair the brain damage to some extent (Gomez-Pinilla et al., 1992; Cramer and Chopp, 2000; Chao et al., 2002; Keyvani and Schallert, 2002; Mattson et al., 2002; Parent et al., 2002).

In summary, the studies conducted for this dissertation started to fill a critical behavioral void in the early phases of translational brain tumor research. Longer term goals are to continue to develop models to facilitate functional assessment, to screen for optimal cancer treatment strategies with reduced harm to brain function, and to search for novel neurorestorative strategies to promote functional outcome following standard brain tumor treatments, such as surgery, radiation and chemotherapy. An improved collaboration among scientists in the areas of behavioral neuroscience, experimental and clinical neuro-oncology, neurosurgery and neurology would be needed to find better ways to help patients have maximum functioning and quality of life.

Glossary

1,3-bis(2-chloroethyl)-1-nitrosourea (BCNU)

3'3'-diaminobenzidine-tetrahydrochloride (DAB)

4',6-diamidino-2-phenylindole (DAPI)

alpha-amino-3-hydroxy-5-methyl-4-isoxazolepropionic acid (AMPA)

analysis of variance (ANOVA)

angiopoietin (Ang)

angiotensin-converting enzyme (ACE)

basic fibroblast growth factor (FGF-2)

blood-brain barrier (BBB)

brain-derived neurotrophic factor (BDNF)

central brain tumor registry of the United States (CBTRUS)

central nervous system (CNS)

ethylenediaminetetraacetic acid (EDTA)

field of view (FOV)

fluorescein isothiocyanate (FITC)

fluorouracil (5FU)

gadolinium-diethylanetriamine pentaacetic acid (Gd-DTPA)

glial fibrillary acid protein (GFAP)

hematoxylin and eosin (H&E)

intracerebral pressure (ICP)

intraperitoneally (i.p.)

intravenously (i.v.)

magnetic resonance contrast agents (MRCA)

magnetic resonance imaging (MRI)

microtubule-associated protein 2 (MAP2)

minimum essential media (MEM)

monoclonal antibodies (mAbs)

national institute for health and clinical excellence (NICE)

nerve growth factor (NGF)

neurotrophin 3 (NT-3)

N-methyl-D-aspartate (NMDA)

phosphate buffered saline (PBS)

photodynamic therapy (PDT)

post-operative (post-op)

proton spin-lattice relaxation time (T1)

quality of life (QOL)

regions of interest (ROIs)

repetition time (TR)

sensorimotor cortex (SMC)

standard error of the mean (SEM)

subventricular zone (SVZ)

surveillance epidemiology and end results (SEER)

terminal deoxynucleotidyl transferase dUTP nick end labeling (TUNEL)

time to echo (TE)

vascular endothelial growth factor (VEGF)

vascular endothelial growth factor receptor (VEGFR)

von Willebrand factor (vWF)

References

Aarsen FK, Paquier PF, Reddingius RE, Streng IC, Arts WF, Evera-Preesman M, Catsman-Berrevoets CE (2006) Functional outcome after low-grade astrocytoma treatment in childhood. Cancer 106:396-402.

Abe T, Black PM, Foley L (1984) Changes in parenchymal and ventricular pressure with experimental epidural compression. Surg Neurol 22:477-480.

Abramovitch R, Marikovsky M, Meir G, Neeman M (1999) Stimulation of tumour growth by wound-derived growth factors. Br J Cancer 79:1392-1398.

Adams FS, Schwarting RK, Huston JP (1994) Behavioral and neurochemical asymmetries following unilateral trephination of the rat skull: is this control operation always appropriate? Physiol Behav 55:947-952.

Akiba T, Okeda R, Tajima T (1996) Metabolites of 5-fluorouracil, alpha-fluoro-beta-alanine and fluoroacetic acid, directly injure myelinated fibers in tissue culture. Acta Neuropathol (Berl) 92:8-13.

Aldskogius H, Liu L, Svensson M (1999) Glial responses to synaptic damage and plasticity. J Neurosci Res 58:33-41.

Allred RP, Jones TA (2004) Unilateral ischemic sensorimotor cortical damage in female rats: forelimb behavioral effects and dendritic structural plasticity in the contralateral homotopic cortex. Exp Neurol 190:433-445.

Arrieta O, Guevara P, Escobar E, Garcia-Navarrete R, Pineda B, Sotelo J (2005) Blockage of angiotensin II type I receptor decreases the synthesis of growth factors and induces apoptosis in C6 cultured cells and C6 rat glioma. Br J Cancer 92:1247-1252.

Audero E, Cascone I, Zanon I, Previtali SC, Piva R, Schiffer D, Bussolino F (2001) Expression of angiopoietin-1 in human glioblastomas regulates tumor-induced angiogenesis: in vivo and in vitro studies. Arterioscler Thromb Vasc Biol 21:536-541.

Auguste P, Gursel DB, Lemiere S, Reimers D, Cuevas P, Carceller F, Di Santo JP, Bikfalvi A (2001) Inhibition of fibroblast growth factor/fibroblast growth factor receptor activity in glioma cells impedes tumor growth by both angiogenesis-dependent and -independent mechanisms. Cancer Res 61:1717-1726.

Baba A (1998) Role of endothelin B receptor signals in reactive astrocytes. Life Sci 62:1711-1715.

Barbieux C, Patri B, Cerf I, de Parades V (1996) [Acute cerebellar syndrome after treatment with 5-fluorouracil]. Bull Cancer 83:77-80.

Barth TM, Grant ML, Schallert T (1990a) Effects of MK-801 on recovery from sensorimotor cortex lesions. Stroke 21:III153-157.

Barth TM, Jones TA, Schallert T (1990b) Functional subdivisions of the rat somatic sensorimotor cortex. Behav Brain Res 39:73-95.

Barth TM, Hoane MR, Barbay S (1998) Effects of glutamate antagonists on the recovery and maintenance of behavioral functions after brain injury. In: Restorative

Neurology Advances in Pharmacotherapy for Recovery after Stroke (Goldstein LB, ed), pp 121-140. Armonk, NY: Futura Publishing Co Inc.

Baskin YK, Dietrich WD, Green EJ (2003) Two effective behavioral tasks for evaluating sensorimotor dysfunction following traumatic brain injury in mice. J Neurosci Methods 129:87-93.

Bechmann I, Nitsch R (1997) Astrocytes and microglial cells incorporate degenerating fibers following entorhinal lesion: a light, confocal, and electron microscopical study using a phagocytosis-dependent labeling technique. Glia 20:145-154.

Benveniste H, Drejer J, Schousboe A, Diemer NH (1984) Elevation of the extracellular concentrations of glutamate and aspartate in rat hippocampus during transient cerebral ischemia monitored by intracerebral microdialysis. J Neurochem 43:1369-1374.

Bergstrom BP, Schertz KE, Weirick T, Nafziger B, Takacs SA, Lopes KO, Massa KJ, Walker QD, Garris PA (2001) Partial, graded losses of dopamine terminals in the rat caudate-putamen: an animal model for the study of compensatory adaptation in preclinical parkinsonism. J Neurosci Methods 106:15-28.

Bernstein L, Patel AV, Ursin G, Sullivan-Halley J, Press MF, Deapen D, Berlin JA, Daling JR, McDonald JA, Norman SA, Malone KE, Strom BL, Liff J, Folger SG, Simon MS, Burkman RT, Marchbanks PA, Weiss LK, Spirtas R (2005) Lifetime recreational exercise activity and breast cancer risk among black women and white women. J Natl Cancer Inst 97:1671-1679.

Bexell D, Gunnarsson S, Nordquist J, Bengzon J (2007) Characterization of the subventricular zone neurogenic response to rat malignant brain tumors. Neuroscience 147:824-832.

Biegon A, Fry PA, Paden CM, Alexandrovich A, Tsenter J, Shohami E (2004) Dynamic changes in N-methyl-D-aspartate receptors after closed head injury in mice: Implications for treatment of neurological and cognitive deficits. Proc Natl Acad Sci U S A 101:5117-5122.

Bofill JS, Chaves M, Moreno JA (2000) Fluorouracil-induced aphasia. Ann Pharmacother 34:955.

Burger PC, Kleihues P (1989) Cytologic composition of the untreated glioblastoma with implications for evaluation of needle biopsies. Cancer 63:2014-2023.

Butcher SP, Bullock R, Graham DI, McCulloch J (1990) Correlation between amino acid release and neuropathologic outcome in rat brain following middle cerebral artery occlusion. Stroke 21:1727-1733.

Bygrave HA, Geh JI, Jani Y, Glynne-Jones R (1998) Neurological complications of 5-fluorouracil chemotherapy: case report and review of the literature. Clin Oncol (R Coll Radiol) 10:334-336.

Caceres A, Mautino J, Kosik KS (1992) Suppression of MAP2 in cultured cerebellar macroneurons inhibits minor neurite formation. Neuron 9:607-618.

Carmeliet P, Jain RK (2000) Angiogenesis in cancer and other diseases. Nature 407:249-257.

Carmeliet P, Moons L, Luttun A, Vincenti V, Compernolle V, De Mol M, Wu Y, Bono F, Devy L, Beck H, Scholz D, Acker T, DiPalma T, Dewerchin M, Noel A, Stalmans I, Barra A, Blacher S, Vandendriessche T, Ponten A, Eriksson U, Plate KH, Foidart JM, Schaper W, Charnock-Jones DS, Hicklin DJ, Herbert JM, Collen D, Persico MG (2001) Synergism between vascular endothelial growth factor and placental growth factor contributes to angiogenesis and plasma extravasation in pathological conditions. Nat Med 7:575-583.

Chao JY, Wei L, Yin K, Lin TN, Hsu CY (2002) Angiogenesis after experimental cerebral ischemia-reperfusion. In: Pharmacology of Cerebral Ischemia (Krieglstein J, Klumpp S, eds), pp 131-140. Stuttgart: Medpharm Scientific Publishers.

Chen J, Chopp M (2006) Neurorestorative treatment of stroke: cell and pharmacological approaches. NeuroRx 3:466-473.

Chen J, Zhang C, Jiang H, Li Y, Zhang L, Robin A, Katakowski M, Lu M, Chopp M (2005) Atorvastatin induction of VEGF and BDNF promotes brain plasticity after stroke in mice. J Cereb Blood Flow Metab 25:281-290.

Chen J, Zhang ZG, Li Y, Wang Y, Wang L, Jiang H, Zhang C, Lu M, Katakowski M, Feldkamp CS, Chopp M (2003a) Statins induce angiogenesis, neurogenesis, and synaptogenesis after stroke. Ann Neurol 53:743-751.

Chen JR, Wang YJ, Tseng GF (2003b) The effect of epidural compression on cerebral cortex: a rat model. J Neurotrauma 20:767-780.

Chen JR, Wang YJ, Tseng GF (2004) The effects of decompression and exogenous NGF on compressed cerebral cortex. J Neurotrauma 21:1640-1651.

Chen Q, Chopp M, Madigan L, Dereski MO, Hetzel FW (1996) Damage threshold of normal rat brain in photodynamic therapy. Photochem Photobiol 64:163-167.

Cheng SY, Huang HJ, Nagane M, Ji XD, Wang D, Shih CC, Arap W, Huang CM, Cavenee WK (1996) Suppression of glioblastoma angiogenicity and tumorigenicity by inhibition of endogenous expression of vascular endothelial growth factor. Proc Natl Acad Sci U S A 93:8502-8507.

Chopp M, Li Y (2006) Transplantation of bone marrow stromal cells for treatment of central nervous system diseases. Adv Exp Med Biol 585:49-64.

Chopp M, Dereski MO, Madigan L, Jiang F, Logie B (1996a) Sensitivity of 9L gliosarcomas to photodynamic therapy. Radiat Res 146:461-465.

Chopp M, Madigan L, Dereski M, Jiang F, Li Y (1996b) Photodynamic therapy of human glioma (U87) in the nude rat. Photochem Photobiol 64:707-711.

Chou TT, Trojanowski JQ, Lee VM (1997) Neurotrophin signal transduction in medulloblastoma. J Neurosci Res 49:522-527.

Chung WJ, Lyons SA, Nelson GM, Hamza H, Gladson CL, Gillespie GY, Sontheimer H (2005) Inhibition of cystine uptake disrupts the growth of primary brain tumors. J Neurosci 25:7101-7110.

Cramer SC, Chopp M (2000) Recovery recapitulates ontogeny. Trends Neurosci 23:265-271.

Cramer SC, Moore CI, Finklestein SP, Rosen BR (2000) A pilot study of somatotopic mapping after cortical infarct. Stroke 31:668-671.

Davis DW, Inoue K, Dinney CP, Hicklin DJ, Abbruzzese JL, McConkey DJ (2004) Regional effects of an antivascular endothelial growth factor receptor monoclonal antibody on receptor phosphorylation and apoptosis in human 253J B-V bladder cancer xenografts. Cancer Res 64:4601-4610.

DeAngelis LM, Loeffler JS, Mamelak AN (2004) Primary brain tumors. In: Cancer Management: A Multidisciplinary Approach: Medical, Surgical and Radiation Oncology (8th ed) (Pazdur R, Coia LR, Hoskins WJ, Wagman LD, eds), pp 591-606. Manhasset, NY: CMP Healthcare Media, Oncology Publishing Group.

Dereski MO, Chopp M, Garcia JH, Hetzel FW (1991) Depth measurements and histopathological characterization of photodynamic therapy generated normal brain necrosis as a function of incident optical energy dose. Photochem Photobiol 54:109-112.

Dietrich J, Han R, Yang Y, Mayer-Proschel M, Noble M (2006) CNS progenitor cells and oligodendrocytes are targets of chemotherapeutic agents in vitro and in vivo. J Biol 5:22.

Ding H, Roncari L, Wu X, Lau N, Shannon P, Nagy A, Guha A (2001) Expression and hypoxic regulation of angiopoietins in human astrocytomas. Neuro Oncol 3:1-10.

Dinsmore JH, Solomon F (1991) Inhibition of MAP2 expression affects both morphological and cell division phenotypes of neuronal differentiation. Cell 64:817-826.

Doble A (1999) The role of excitotoxicity in neurodegenerative disease: implications for therapy. Pharmacol Ther 81:163-221.

Dong Y, Benveniste EN (2001) Immune function of astrocytes. Glia 36:180-190.

Douzinas EE, Kostopoulos V, Kypriades E, Pappas YZ, Lymberis A, Karmpaliotis DI, Katsouyanni K, Andrianakis I, Papalois A, Roussos C (1999) Brain eigenfrequency shifting as a sensitive index of cerebral compliance in an experimental model of epidural hematoma in the rabbit: preliminary study. Crit Care Med 27:978-984.

Duntsch C, Zhou Q, Weimar JD, Frankel B, Robertson JH, Pourmotabbed T (2005) Up-regulation of neuropoiesis generating glial progenitors that infiltrate rat intracranial glioma. J Neurooncol 71:245-255.

Eberhart CG, Kaufman WE, Tihan T, Burger PC (2001) Apoptosis, neuronal maturation, and neurotrophin expression within medulloblastoma nodules. J Neuropathol Exp Neurol 60:462-469.

Elkiran ET, Altundag K, Beyazit Y, Guler N, Kars A (2004) Fluorouracil-induced neurotoxicity presenting with generalized tonic-clonic seizure. Ann Pharmacother 38:2171.

Ewing JR, Brown SL, Lu M, Panda S, Ding G, Knight RA, Cao Y, Jiang Q, Nagaraja TN, Churchman JL, Fenstermacher JD (2006) Model selection in magnetic resonance imaging measurements of vascular permeability: Gadomer in a 9L model of rat cerebral tumor. J Cereb Blood Flow Metab 26:310-320.

Faden AI, Demediuk P, Panter SS, Vink R (1989) The role of excitatory amino acids and NMDA receptors in traumatic brain injury. Science 244:798-800.

Felt BT, Schallert T, Shao J, Liu Y, Li X, Barks JD (2002) Early appearance of functional deficits after neonatal excitotoxic and hypoxic-ischemic injury: fragile recovery after development and role of the NMDA receptor. Dev Neurosci 24:418-425.

Figueredo AT, Fawcet SE, Molloy DW, Dobranowski J, Paulseth JE (1995) Disabling encephalopathy during 5-fluorouracil and levamisole adjuvant therapy for resected colorectal cancer: a report of two cases. Cancer Invest 13:608-611.

Fleming SM, Delville Y, Schallert T (2005) An intermittent, controlled-rate, slow progressive degeneration model of Parkinson's disease: antiparkinson effects of Sinemet and protective effects of methylphenidate. Behav Brain Res 156:201-213.

Foo SH, Choi IS, Berenstein A, Wise A, Ransohoff J, Koslow M, George A, Lin J, Feigin I, Budzilovich G, et al. (1986) Supraophthalmic intracarotid infusion of BCNU for malignant glioma. Neurology 36:1437-1444.

Fournier E, Passirani C, Montero-Menei C, Colin N, Breton P, Sagodira S, Menei P, Benoit JP (2003) Therapeutic effectiveness of novel 5-fluorouracil-loaded poly(methylidene malonate 2.1.2)-based microspheres on F98 glioma-bearing rats. Cancer 97:2822-2829.

Glass R, Synowitz M, Kronenberg G, Walzlein JH, Markovic DS, Wang LP, Gast D, Kiwit J, Kempermann G, Kettenmann H (2005) Glioblastoma-induced attraction

of endogenous neural precursor cells is associated with improved survival. J Neurosci 25:2637-2646.

Goel S, Wharton SB, Brett LP, Whittle IR (2003) Morphological changes and stress responses in neurons in cerebral cortex infiltrated by diffuse astrocytoma. Neuropathology 23:262-270.

Gomez-Pinilla F, Lee JW, Cotman CW (1992) Basic FGF in adult rat brain: cellular distribution and response to entorhinal lesion and fimbria-fornix transection. J Neurosci 12:345-355.

Goodell TT, Muller PJ (2001) Photodynamic therapy: a novel treatment for primary brain malignancy. J Neurosci Nurs 33:296-300.

Hamel W, Westphal M, Szonyi E, Escandon E, Nikolics K (1993) Neurotrophin gene expression by cell lines derived from human gliomas. J Neurosci Res 34:147-157.

Hann D, Baker F, Denniston M, Entrekin N (2005) Long-term breast cancer survivors' use of complementary therapies: perceived impact on recovery and prevention of recurrence. Integr Cancer Ther 4:14-20.

Hattori K, Heissig B, Wu Y, Dias S, Tejada R, Ferris B, Hicklin DJ, Zhu Z, Bohlen P, Witte L, Hendrikx J, Hackett NR, Crystal RG, Moore MA, Werb Z, Lyden D, Rafii S (2002) Placental growth factor reconstitutes hematopoiesis by recruiting VEGFR1(+) stem cells from bone-marrow microenvironment. Nat Med 8:841-849.

Hewitt JA, Mokbel K, van Someren KA, Jewell AP, Garrod R (2005) Exercise for breast cancer survival: the effect on cancer risk and cancer-related fatigue (CRF). Int J Fertil Womens Med 50:231-239.

Holash J, Maisonpierre PC, Compton D, Boland P, Alexander CR, Zagzag D, Yancopoulos GD, Wiegand SJ (1999) Vessel cooption, regression, and growth in tumors mediated by angiopoietins and VEGF. Science 284:1994-1998.

Holmes MD, Chen WY, Feskanich D, Kroenke CH, Colditz GA (2005) Physical activity and survival after breast cancer diagnosis. Jama 293:2479-2486.

Hook CC, Kimmel DW, Kvols LK, Scheithauer BW, Forsyth PA, Rubin J, Moertel CG, Rodriguez M (1992) Multifocal inflammatory leukoencephalopathy with 5-fluorouracil and levamisole. Ann Neurol 31:262-267.

Hua Y, Tang L, Keep RF, Schallert T, Fewel ME, Muraszko KM, Hoff JT, Xi G (2005a) The role of thrombin in gliomas. J Thromb Haemost 3:1917-1923.

Hua Y, Tang LL, Fewel ME, Keep RF, Schallert T, Muraszko KM, Hoff JT, Xi GH (2005b) Systemic use of argatroban reduces tumor mass, attenuates neurological deficits and prolongs survival time in rat glioma models. Acta Neurochir Suppl 95:403-406.

Huang Z (2005) A review of progress in clinical photodynamic therapy. Technol Cancer Res Treat 4:283-293.

Ibanez CF, Hokfelt T, Olson L, Fuxe K, Jornvall H, Ottoson D, eds (1995) Life and Death in the Nervous System: Role of Neurotrophic Factors and their Receptors. New York: Elsevier Science Pub Co.

Ikonomidou C, Stefovska V, Turski L (2000) Neuronal death enhanced by N-methyl-D-aspartate antagonists. Proc Natl Acad Sci U S A 97:12885-12890.

Ikonomidou C, Bosch F, Miksa M, Bittigau P, Vockler J, Dikranian K, Tenkova TI, Stefovska V, Turski L, Olney JW (1999) Blockade of NMDA receptors and apoptotic neurodegeneration in the developing brain. Science 283:70-74.

Im JJ, Park BR (2002) Does oxygen deficit to the cerebral blood flow caused by subdural hematoma and/or increased intracranial pressure affect the variations in auditory evoked potentials in white New Zealand rabbits? Neurosci Lett 317:139-142.

Ishiuchi S, Tsuzuki K, Yoshida Y, Yamada N, Hagimura N, Okado H, Miwa A, Kurihara H, Nakazato Y, Tamura M, Sasaki T, Ozawa S (2002) Blockage of Ca(2+)-permeable AMPA receptors suppresses migration and induces apoptosis in human glioblastoma cells. Nat Med 8:971-978.

Jain RK (2005) Normalization of tumor vasculature: an emerging concept in antiangiogenic therapy. Science 307:58-62.

Jiang F, Lilge L, Logie B, Li Y, Chopp M (1997) Photodynamic therapy of 9L gliosarcoma with liposome-delivered photofrin. Photochem Photobiol 65:701-706.

Jiang F, Lilge L, Belcuig M, Singh G, Grenier J, Li Y, Chopp M (1998) Photodynamic therapy using Photofrin in combination with buthionine sulfoximine (BSO) to treat 9L gliosarcoma in rat brain. Lasers Surg Med 23:161-166.

Jiang F, Zhang ZG, Katakowski M, Robin AM, Faber M, Zhang F, Chopp M (2004) Angiogenesis induced by photodynamic therapy in normal rat brains. Photochem Photobiol 79:494-498.

Jiang F, Zhang Z, Kalkanis S, Katakowksi M, Robin AM, Zhang X, Gotlib A, Chelst I, Mikkelsen T, Chopp M (2005) A quantitative model of tumor-induced angiogenesis in the nude mouse. Neurosurgery 57:320-324.

Johnson DA, Zhang J, Frase S, Wilson M, Rodriguez-Galindo C, Dyer MA (2007) Neuronal differentiation and synaptogenesis in retinoblastoma. Cancer Res 67:2701-2711.

Johnson GV, Jope RS (1992) The role of microtubule-associated protein 2 (MAP-2) in neuronal growth, plasticity, and degeneration. J Neurosci Res 33:505-512.

Jones TA, Schallert T (1992) Subcortical deterioration after cortical damage: effects of diazepam and relation to recovery of function. Behav Brain Res 51:1-13.

Jones TA, Schallert T (1994) Use-dependent growth of pyramidal neurons after neocortical damage. J Neurosci 14:2140-2152.

Kadish I, Van Groen T (2003) Differences in lesion-induced hippocampal plasticity between mice and rats. Neuroscience 116:499-509.

Kargiotis O, Rao JS, Kyritsis AP (2006) Mechanisms of angiogenesis in gliomas. J Neurooncol 78:281-293.

Kaur B, Khwaja FW, Severson EA, Matheny SL, Brat DJ, Van Meir EG (2005) Hypoxia and the hypoxia-inducible-factor pathway in glioma growth and angiogenesis. Neuro Oncol 7:134-153.

Ke LD, Shi YX, Im SA, Chen X, Yung WK (2000) The relevance of cell proliferation, vascular endothelial growth factor, and basic fibroblast growth factor production to angiogenesis and tumorigenicity in human glioma cell lines. Clin Cancer Res 6:2562-2572.

Kevil CG, Payne DK, Mire E, Alexander JS (1998) Vascular permeability factor/vascular endothelial cell growth factor-mediated permeability occurs through disorganization of endothelial junctional proteins. J Biol Chem 273:15099-15103.

Keyvani K, Schallert T (2002) Plasticity-associated molecular and structural events in the injured brain. J Neuropathol Exp Neurol 61:831-840.

Kim JH, Brown SL, Kolozsvary A, Jenrow KA, Ryu S, Rosenblum ML, Carretero OA (2004) Modification of radiation injury by ramipril, inhibitor of angiotensin-converting enzyme, on optic neuropathy in the rat. Radiat Res 161:137-142.

Kim KJ, Li B, Winer J, Armanini M, Gillett N, Phillips HS, Ferrara N (1993) Inhibition of vascular endothelial growth factor-induced angiogenesis suppresses tumour growth in vivo. Nature 362:841-844.

Kim MW, Bang MS, Han TR, Ko YJ, Yoon BW, Kim JH, Kang LM, Lee KM, Kim MH (2005) Exercise increased BDNF and trkB in the contralateral hemisphere of the ischemic rat brain. Brain Res 1052:16-21.

Kimler BF (1994) The 9L rat brain tumor model for pre-clinical investigation of radiation-chemotherapy interactions. J Neurooncol 20:103-109.

Kleihues P, Louis DN, Scheithauer BW, Rorke LB, Reifenberger G, Burger PC, Cavenee WK (2002) The WHO classification of tumors of the nervous system. J Neuropathol Exp Neurol 61:215-225; discussion 226-219.

Kleim JA, Jones TA, Schallert T (2003) Motor enrichment and the induction of plasticity before or after brain injury. Neurochem Res 28:1757-1769.

Kleim JA, Chan S, Pringle E, Schallert K, Procaccio V, Jimenez R, Cramer SC (2006) BDNF val66met polymorphism is associated with modified experience-dependent plasticity in human motor cortex. Nat Neurosci 9:735-737.

Kohn EC, Liotta LA (1995) Molecular insights into cancer invasion: strategies for prevention and intervention. Cancer Res 55:1856-1862.

Kornblith PL, Walker M (1988) Chemotherapy for malignant gliomas. J Neurosurg 68:1-17.

Kozlowski DA, Schallert T (1998) Relationship between dendritic pruning and behavioral recovery following sensorimotor cortex lesions. Behav Brain Res 97:89-98.

Kozlowski DA, Jones TA, Schallert T (1994) Pruning of dendrites and restoration of function after brain damage: role of the NMDA receptor. Rest Neurol Neurosci 7:119-126.

Kozlowski DA, Hilliard S, Schallert T (1997) Ethanol consumption following recovery from unilateral damage to the forelimb area of the sensorimotor cortex: reinstatement of deficits and prevention of dendritic pruning. Brain Res 763:159-166.

Krishnamurthy S, Powers SK, Witmer P, Brown T (2000) Optimal light dose for interstitial photodynamic therapy in treatment for malignant brain tumors. Lasers Surg Med 27:224-234.

Krum JM, Khaibullina A (2003) Inhibition of endogenous VEGF impedes revascularization and astroglial proliferation: roles for VEGF in brain repair. Exp Neurol 181:241-257.

Kundrotiene J, Wagner A, Liljequist S (2002) Extradural compression of sensorimotor cortex: a useful model for studies on ischemic brain damage and neuroprotection. J Neurotrauma 19:69-84.

Kundrotiene J, Wagner A, Liljequist S (2004a) Fluoro-Jade and TUNEL staining as useful tools to identify ischemic brain damage following moderate extradural compression of sensorimotor cortex. Acta Neurobiol Exp (Wars) 64:153-162.

Kundrotiene J, Cebers G, Wagner A, Liljequist S (2004b) The NMDA NR2B subunit-selective receptor antagonist, CP-101,606, enhances the functional recovery the NMDA NR2B subunit-selective receptor and reduces brain damage after cortical compression-induced brain ischemia. J Neurotrauma 21:83-93.

Kunkel P, Ulbricht U, Bohlen P, Brockmann MA, Fillbrandt R, Stavrou D, Westphal M, Lamszus K (2001) Inhibition of glioma angiogenesis and growth in vivo by

systemic treatment with a monoclonal antibody against vascular endothelial growth factor receptor-2. Cancer Res 61:6624-6628.

Landis SH, Murray T, Bolden S, Wingo PA (1998) Cancer statistics, 1998. CA Cancer J Clin 48:6-29.

Leclerc N, Beesley PW, Brown I, Colonnier M, Gurd JW, Paladino T, Hawkes R (1989) Synaptophysin expression during synaptogenesis in the rat cerebellar cortex. J Comp Neurol 280:197-212.

Lemaire L, Roullin VG, Franconi F, Venier-Julienne MC, Menei P, Jallet P, Le Jeune JJ, Benoit JP (2001) Therapeutic efficacy of 5-fluorouracil-loaded microspheres on rat glioma: a magnetic resonance imaging study. NMR Biomed 14:360-366.

Levin VA, Chadwick M, Little AD (1972) Distribution of 5-fluorouracil-2- 14 C and its metabolites in a murine glioma. J Natl Cancer Inst 49:1577-1584.

Levin VA, Edwards MS, Wara WM, Allen J, Ortega J, Vestnys P (1984) 5-Fluorouracil and 1-(2-chloroethyl)-3-cyclohexyl-1-nitrosourea (CCNU) followed by hydroxyurea, misonidazole, and irradiation for brain stem gliomas: a pilot study of the Brain Tumor Research Center and the Childrens Cancer Group. Neurosurgery 14:679-681.

Lindner MD, Gribkoff VK, Donlan NA, Jones TA (2003) Long-lasting functional disabilities in middle-aged rats with small cerebral infarcts. J Neurosci 23:10913-10922.

Liu Y, Dulchavsky DS, Gao X, Kwon D, Chopp M, Dulchavsky S, Gautam SC (2006) Wound repair by bone marrow stromal cells through growth factor production. J Surg Res 136:336-341.

Lu D, Mahmood A, Qu C, Goussev A, Lu M, Chopp M (2004a) Atorvastatin reduction of intracranial hematoma volume in rats subjected to controlled cortical impact. J Neurosurg 101:822-825.

Lu D, Mahmood A, Goussev A, Qu C, Zhang ZG, Chopp M (2004b) Delayed thrombosis after traumatic brain injury in rats. J Neurotrauma 21:1756-1766.

Lu D, Mahmood A, Qu C, Goussev A, Schallert T, Chopp M (2005) Erythropoietin enhances neurogenesis and restores spatial memory in rats after traumatic brain injury. J Neurotrauma 22:1011-1017.

Lu D, Goussev A, Chen J, Pannu P, Li Y, Mahmood A, Chopp M (2004c) Atorvastatin reduces neurological deficit and increases synaptogenesis, angiogenesis, and neuronal survival in rats subjected to traumatic brain injury. J Neurotrauma 21:21-32.

Lu D, Mahmood A, Goussev A, Schallert T, Qu C, Zhang ZG, Li Y, Lu M, Chopp M (2004d) Atorvastatin reduction of intravascular thrombosis, increase in cerebral microvascular patency and integrity, and enhancement of spatial learning in rats subjected to traumatic brain injury. J Neurosurg 101:813-821.

Lu M, Chen J, Lu D, Yi L, Mahmood A, Chopp M (2003) Global test statistics for treatment effect of stroke and traumatic brain injury in rats with administration of bone marrow stromal cells. J Neurosci Methods 128:183-190.

Lu YP, Nolan B, Lou YR, Peng QY, Wagner GC, Conney AH (2007) Voluntary exercise together with oral caffeine markedly stimulates UVB light-induced apoptosis and decreases tissue fat in SKH-1 mice. Proc Natl Acad Sci U S A 104:12936-12941.

Luttun A, Tjwa M, Moons L, Wu Y, Angelillo-Scherrer A, Liao F, Nagy JA, Hooper A, Priller J, De Klerck B, Compernolle V, Daci E, Bohlen P, Dewerchin M, Herbert JM, Fava R, Matthys P, Carmeliet G, Collen D, Dvorak HF, Hicklin DJ, Carmeliet P (2002) Revascularization of ischemic tissues by PlGF treatment, and inhibition of tumor angiogenesis, arthritis and atherosclerosis by anti-Flt1. Nat Med 8:831-840.

Lyden D, Hattori K, Dias S, Costa C, Blaikie P, Butros L, Chadburn A, Heissig B, Marks W, Witte L, Wu Y, Hicklin D, Zhu Z, Hackett NR, Crystal RG, Moore MA, Hajjar KA, Manova K, Benezra R, Rafii S (2001) Impaired recruitment of bone-marrow-derived endothelial and hematopoietic precursor cells blocks tumor angiogenesis and growth. Nat Med 7:1194-1201.

Macdonald DR (1991) Neurologic complications of chemotherapy. Neurol Clin 9:955-967.

Magda D, Lepp C, Gerasimchuk N, Lee I, Sessler JL, Lin A, Biaglow JE, Miller RA (2001) Redox cycling by motexafin gadolinium enhances cellular response to ionizing radiation by forming reactive oxygen species. Int J Radiat Oncol Biol Phys 51:1025-1036.

Mahaley MS, Jr., Whaley RA, Blue M, Bertsch L (1986) Central neurotoxicity following intracarotid BCNU chemotherapy for malignant gliomas. J Neurooncol 3:297-314.

Mahmood A, Lu D, Qu C, Goussev A, Chopp M (2006) Long-term recovery after bone marrow stromal cell treatment of traumatic brain injury in rats. J Neurosurg 104:272-277.

Mahmood A, Lu D, Qu C, Goussev A, Chopp M (2007a) Treatment of traumatic brain injury with a combination therapy of marrow stromal cells and atorvastatin in rats. Neurosurgery 60:546-553; discussion 553-544.

Mahmood A, Lu D, Qu C, Goussev A, Zhang ZG, Lu C, Chopp M (2007b) Treatment of traumatic brain injury in rats with erythropoietin and carbamylated erythropoietin. J Neurosurg 107:392-397.

Masliah E, Terry RD, Alford M, DeTeresa R (1990) Quantitative immunohistochemistry of synaptophysin in human neocortex: an alternative method to estimate density of presynaptic terminals in paraffin sections. J Histochem Cytochem 38:837-844.

Masliah E, Fagan AM, Terry RD, DeTeresa R, Mallory M, Gage FH (1991) Reactive synaptogenesis assessed by synaptophysin immunoreactivity is associated with GAP-43 in the dentate gyrus of the adult rat. Exp Neurol 113:131-142.

Mattson MP, Culmsee C, Slevin JR, Liu D (2002) Synaptic apoptosis and neuroprotective strategies. In: Pharmacology of Cerebral Ischemia (Krieglstein J, Klumpp S, eds), pp 419-429. Stuttgart: Medpharm Scientific Publishers.

McFarlin K, Gao X, Liu YB, Dulchavsky DS, Kwon D, Arbab AS, Bansal M, Li Y, Chopp M, Dulchavsky SA, Gautam SC (2006) Bone marrow-derived mesenchymal stromal cells accelerate wound healing in the rat. Wound Repair Regen 14:471-478.

Menei P, Boisdron-Celle M, Croue A, Guy G, Benoit JP (1996) Effect of stereotactic implantation of biodegradable 5-fluorouracil-loaded microspheres in healthy and C6 glioma-bearing rats. Neurosurgery 39:117-123; discussion 123-114.

Menei P, Jadaud E, Faisant N, Boisdron-Celle M, Michalak S, Fournier D, Delhaye M, Benoit JP (2004) Stereotaxic implantation of 5-fluorouracil-releasing microspheres in malignant glioma. Cancer 100:405-410.

Michna L, Wagner GC, Lou YR, Xie JG, Peng QY, Lin Y, Carlson K, Shih WJ, Conney AH, Lu YP (2006) Inhibitory effects of voluntary running wheel exercise on UVB-induced skin carcinogenesis in SKH-1 mice. Carcinogenesis 27:2108-2115.

Miguel-Hidalgo JJ, Alvarez XA, Cacabelos R, Quack G (2002) Neuroprotection by memantine against neurodegeneration induced by beta-amyloid(1-40). Brain Res 958:210-221.

Mikkelsen T (1998) Cytostatic Agents in the Management of Malignant Gliomas. Cancer Control 5:150-162.

Mikkelsen T, Edvardsen K (1996) Invasiveness in nervous system tumors. In: Cancer of the Nervous System (Black PM, Loeffler JS, eds), pp 346-363. Cambridge, MA: Blackwell Scientific Publications.

Millauer B, Shawver LK, Plate KH, Risau W, Ullrich A (1994) Glioblastoma growth inhibited in vivo by a dominant-negative Flk-1 mutant. Nature 367:576-579.

Millauer B, Longhi MP, Plate KH, Shawver LK, Risau W, Ullrich A, Strawn LM (1996) Dominant-negative inhibition of Flk-1 suppresses the growth of many tumor types in vivo. Cancer Res 56:1615-1620.

Moreira T, Cebers G, Cebere A, Wagner A, Liljequist S (2005) Extradural compression of the sensorimotor cortex delays the acquisition but not the recalling of a lever-pressing task in Wistar rats. Behav Brain Res 164:250-265.

Moreira T, Cebers G, Salehi M, Wagner A, Liljequist S (2006) Impaired long-term habituation is dissociated from increased locomotor activity after sensorimotor cortex compression. Behav Brain Res 167:9-22.

Moreira T, Cebers G, Pickering C, Ostenson CG, Efendic S, Liljequist S (2007) Diabetic Goto-Kakizaki rats display pronounced hyperglycemia and longer-lasting cognitive impairments following ischemia induced by cortical compression. Neuroscience 144:1169-1185.

Muller PJ, Wilson BC (1990) Photodynamic therapy of malignant brain tumours. Can J Neurol Sci 17:193-198.

Muller PJ, Wilson BC (1995) Photodynamic therapy for recurrent supratentorial gliomas. Semin Surg Oncol 11:346-354.

Muller PJ, Wilson BC (1996) Photodynamic therapy for malignant newly diagnosed supratentorial gliomas. J Clin Laser Med Surg 14:263-270.

Nagahiro S, Yamamoto YL, Diksic M, Mitsuka S, Sugimoto S, Feindel W (1991) Neurotoxicity after intracarotid 1,3-bis(2-chloroethyl)-1-nitrosourea administration in the rat: hemodynamic changes studied by double-tracer autoradiography. Neurosurgery 29:19-25; discussion 26.

Naumovski L, Ramos J, Sirisawad M, Chen J, Thiemann P, Lecane P, Magda D, Wang Z, Cortez C, Boswell G, Gyu Cho D, Sessler J, Miller R (2005) Sapphyrins

induce apoptosis in hematopoietic tumor-derived cell lines and show in vivo antitumor activity. Mol Cancer Ther 4:968-976.

Naumovski L, Sirisawad M, Lecane P, Chen J, Ramos J, Wang Z, Cortez C, Magda D, Thiemann P, Boswell G, Miles D, Cho DG, Sessler JL, Miller R (2006) Tumor localization and antitumor efficacy of novel sapphyrin compounds. Mol Cancer Ther 5:2798-2805.

Neuwelt EA, Barnett PA, Frenkel EP (1984) Chemotherapeutic agent permeability to normal brain and delivery to avian sarcoma virus-induced brain tumors in the rodent: observations on problems of drug delivery. Neurosurgery 14:154-160.

Neuwelt EA, Barnett PA, Glasberg M, Frenkel EP (1983a) Pharmacology and neurotoxicity of cis-diamminedichloroplatinum, bleomycin, 5-fluorouracil, and cyclophosphamide administration following osmotic blood-brain barrier modification. Cancer Res 43:5278-5285.

Neuwelt EA, Glasberg M, Frenkel E, Barnett P (1983b) Neurotoxicity of chemotherapeutic agents after blood-brain barrier modification: neuropathological studies. Ann Neurol 14:316-324.

Newman C, Tsai J, Szarek M, Luo D, Gibson E (2006) Comparative safety of atorvastatin 80 mg versus 10 mg derived from analysis of 49 completed trials in 14,236 patients. Am J Cardiol 97:61-67.

Nicholas MK, Prados MD, Larson DA (1997) Malignant astrocytomas. In: Cancer of the Nervous System (Black PM, Loeffler JS, eds), pp 464-491. London: Blackwell Publishers.

Noordhuis P, Holwerda U, Van der Wilt CL, Van Groeningen CJ, Smid K, Meijer S, Pinedo HM, Peters GJ (2004) 5-Fluorouracil incorporation into RNA and DNA in relation to thymidylate synthase inhibition of human colorectal cancers. Ann Oncol 15:1025-1032.

Nudo RJ, Wise BM, SiFuentes F, Milliken GW (1996) Neural substrates for the effects of rehabilitative training on motor recovery after ischemic infarct. Science 272:1791-1794.

Ohab JJ, Fleming S, Blesch A, Carmichael ST (2006) A neurovascular niche for neurogenesis after stroke. J Neurosci 26:13007-13016.

Okeda R, Shibutani M, Matsuo T, Kuroiwa T (1988) Subacute neurotoxicity of 5-fluorouracil and its derivative, carmofur, in cats. Acta Pathol Jpn 38:1255-1266.

Okeda R, Karakama T, Kimura S, Toizumi S, Mitsushima T, Yokoyama Y (1984) Neuropathologic study on chronic neurotoxicity of 5-fluorouracil and its masked compounds in dogs. Acta Neuropathol (Berl) 63:334-343.

Okeda R, Shibutani M, Matsuo T, Kuroiwa T, Shimokawa R, Tajima T (1990) Experimental neurotoxicity of 5-fluorouracil and its derivatives is due to poisoning by the monofluorinated organic metabolites, monofluoroacetic acid and alpha-fluoro-beta-alanine. Acta Neuropathol (Berl) 81:66-73.

Olney JW, Zorumski CF, Stewart GR, Price MT, Wang GJ, Labruyere J (1990) Excitotoxicity of L-dopa and 6-OH-dopa: implications for Parkinson's and Huntington's diseases. Exp Neurol 108:269-272.

Olney JW, Tenkova T, Dikranian K, Qin YQ, Labruyere J, Ikonomidou C (2002) Ethanol-induced apoptotic neurodegeneration in the developing C57BL/6 mouse brain. Brain Res Dev Brain Res 133:115-126.

Osoba D, Aaronson NK, Muller M, Sneeuw K, Hsu MA, Yung WK, Brada M, Newlands E (1997) Effect of neurological dysfunction on health-related quality of life in patients with high-grade glioma. J Neurooncol 34:263-278.

Papetti M, Herman IM (2002) Mechanisms of normal and tumor-derived angiogenesis. Am J Physiol Cell Physiol 282:C947-970.

Parent JM, Vexler ZS, Gong C, Derugin N, Ferriero DM (2002) Rat forebrain neurogenesis and striatal neuron replacement after focal stroke. Ann Neurol 52:802-813.

Parsons CG, Danysz W, Quack G (1999) Memantine is a clinically well tolerated N-methyl-D-aspartate (NMDA) receptor antagonist--a review of preclinical data. Neuropharmacology 38:735-767.

Peck DJ, Windham JP, Soltanian-Zadeh H, Roebuck JR (1992) A fast and accurate algorithm for volume determination in MRI. Med Phys 19:599-605.

Peck DJ, Windham JP, Emery LL, Soltanian-Zadeh H, Hearshen DO, Mikkelsen T (1996) Cerebral tumor volume calculations using planimetric and eigenimage analysis. Med Phys 23:2035-2042.

Perria C, Capuzzo T, Cavagnaro G, Datti R, Francaviglia N, Rivano C, Tercero VE (1980) Fast attempts at the photodynamic treatment of human gliomas. J Neurosurg Sci 24:119-129.

Pineiro R, Pendlebury S, Johansen-Berg H, Matthews PM (2001) Functional MRI detects posterior shifts in primary sensorimotor cortex activation after stroke: evidence of local adaptive reorganization? Stroke 32:1134-1139.

Pirzada NA, Ali, II, Dafer RM (2000) Fluorouracil-induced neurotoxicity. Ann Pharmacother 34:35-38.

Planells-Cases R, Montoliu C, Humet M, Fernandez AM, Garcia-Martinez C, Valera E, Merino JM, Perez-Paya E, Messeguer A, Felipo V, Ferrer-Montiel A (2002) A novel N-methyl-D-aspartate receptor open channel blocker with in vivo neuroprotectant activity. J Pharmacol Exp Ther 302:163-173.

Plate KH, Risau W (1995) Angiogenesis in malignant gliomas. Glia 15:339-347.

Plate KH, Breier G, Weich HA, Risau W (1992) Vascular endothelial growth factor is a potential tumour angiogenesis factor in human gliomas in vivo. Nature 359:845-848.

Plate KH, Breier G, Millauer B, Ullrich A, Risau W (1993) Up-regulation of vascular endothelial growth factor and its cognate receptors in a rat glioma model of tumor angiogenesis. Cancer Res 53:5822-5827.

Plate KH, Breier G, Weich HA, Mennel HD, Risau W (1994) Vascular endothelial growth factor and glioma angiogenesis: coordinate induction of VEGF receptors, distribution of VEGF protein and possible in vivo regulatory mechanisms. Int J Cancer 59:520-529.

Plotkin SR, Wen PY (2003) Neurologic complications of cancer therapy. Neurol Clin 21:279-318, x.

Pollard H, Khrestchatisky M, Moreau J, Ben-Ari Y, Represa A (1994) Correlation between reactive sprouting and microtubule protein expression in epileptic hippocampus. Neuroscience 61:773-787.

Prewett M, Huber J, Li Y, Santiago A, O'Connor W, King K, Overholser J, Hooper A, Pytowski B, Witte L, Bohlen P, Hicklin DJ (1999) Antivascular endothelial growth factor receptor (fetal liver kinase 1) monoclonal antibody inhibits tumor angiogenesis and growth of several mouse and human tumors. Cancer Res 59:5209-5218.

Raber J, Fan Y, Matsumori Y, Liu Z, Weinstein PR, Fike JR, Liu J (2004) Irradiation attenuates neurogenesis and exacerbates ischemia-induced deficits. Ann Neurol 55:381-389.

Rafii S, Lyden D, Benezra R, Hattori K, Heissig B (2002) Vascular and haematopoietic stem cells: novel targets for anti-angiogenesis therapy? Nat Rev Cancer 2:826-835.

Rege TA, Fears CY, Gladson CL (2005) Endogenous inhibitors of angiogenesis in malignant gliomas: nature's antiangiogenic therapy. Neuro Oncol 7:106-121.

Ries LAG, Hankey BF, Miller BA, Hartman AM, Edwards BK (1991) Cancer statistics review 1973-88: National Cancer Institute Publication NIH 91-2789. I.31 VI.44.

Rosenblum MK, Knebel KD, Vasquez DA, Wilson CB (1977) Brain-tumor therapy. Quantitative analysis using a model system. J Neurosurg 46:145-154.

Rosenblum MK, Delattre JY, Walker RW, Shapiro WR (1989) Fatal necrotizing encephalopathy complicating treatment of malignant gliomas with intra-arterial BCNU and irradiation: a pathological study. J Neurooncol 7:269-281.

Rosenblum ML, Knebel KD, Vasquez DA, Wilson CB (1976) In vivo clonogenic tumor cell kinetics following 1,3-bis(2-chloroethyl)-1-nitrosourea brain tumor therapy. Cancer Res 36:3718-3725.

Rosenblum ML, Wheeler KT, Wilson CB, Barker M, Knebel KD (1975) In vitro evaluation of in vivo brain tumor chemotherapy with 1,3-bis(2-chloroethyl)-1-nitrosourea. Cancer Res 35:1387-1391.

Rosenblum ML, Dougherty DA, Deen DF, Hoshino T, Wilson CB (1980) Analysis of clonogenic human brain tumour cells: preliminary results of tumour sensitivity testing with BCNU. Br J Cancer Suppl 4:181-185.

Ross BD, Zhao YJ, Neal ER, Stegman LD, Ercolani M, Ben-Yoseph O, Chenevert TL (1998) Contributions of cell kill and posttreatment tumor growth rates to the repopulation of intracerebral 9L tumors after chemotherapy: an MRI study. Proc Natl Acad Sci U S A 95:7012-7017.

Rossini PM, Caltagirone C, Castriota-Scanderbeg A, Cicinelli P, Del Gratta C, Demartin M, Pizzella V, Traversa R, Romani GL (1998) Hand motor cortical area reorganization in stroke: a study with fMRI, MEG and TCS maps. Neuroreport 9:2141-2146.

Rowntree S, Kolb B (1997) Blockade of basic fibroblast growth factor retards recovery from motor cortex injury in rats. Eur J Neurosci 9:2432-2441.

Rzeski W, Turski L, Ikonomidou C (2001) Glutamate antagonists limit tumor growth. Proc Natl Acad Sci U S A 98:6372-6377.

Scappaticci FA (2002) Mechanisms and future directions for angiogenesis-based cancer therapies. J Clin Oncol 20:3906-3927.

Schallert T, Whishaw IQ (1984) Bilateral cutaneous stimulation of the somatosensory system in hemidecorticate rats. Behav Neurosci 98:518-540.

Schallert T, Lindner MD (1990) Rescuing neurons from trans-synaptic degeneration after brain damage: helpful, harmful, or neutral in recovery of function? Can J Psychol 44:276-292.

Schallert T, Tillerson JL (2000) Intervention strategies for degeneration of dopamine neurons in parkinsonism: optimizing behavioral assessment of outcome. In: Central Nervous System Diseases: Innovative Animal Models from Lab to Clinic (Emerich DF, Dean III RL, Sanberg PR, eds), pp 131-151. Totowa, NJ: Humana Press.

Schallert T, Woodlee MT (2005) Motor systems: orienting and placing. In: The Behavior of the Laboratory Rat: A Hand Book with Tests (Whishaw IQ, Kolb B, eds), pp 129-140. New York: Oxford University Press.

Schallert T, Woodlee MT, Fleming SM (2002) Disentangling multiple types of recovery from brain injury. In: Pharmacology of Cerebral Ischemia 2002 (Krieglstein J, Klumpp S, eds), pp 201-216. Stuttgart: Medpharm Scientific Publishers.

Schallert T, Fleming SM, Leasure JL, Tillerson JL, Bland ST (2000) CNS plasticity and assessment of forelimb sensorimotor outcome in unilateral rat models of stroke,

cortical ablation, parkinsonism and spinal cord injury. Neuropharmacology 39:777-787.

Schallert T, Upchurch M, Lobaugh N, Farrar SB, Spirduso WW, Gilliam P, Vaughn D, Wilcox RE (1982) Tactile extinction: distinguishing between sensorimotor and motor asymmetries in rats with unilateral nigrostriatal damage. Pharmacol Biochem Behav 16:455-462.

Schepkin VD, Ross BD, Chenevert TL, Rehemtulla A, Sharma S, Kumar M, Stojanovska J (2005) Sodium magnetic resonance imaging of chemotherapeutic response in a rat glioma. Magn Reson Med 53:85-92.

Schepkin VD, Lee KC, Kuszpit K, Muthuswami M, Johnson TD, Chenevert TL, Rehemtulla A, Ross BD (2006) Proton and sodium MRI assessment of emerging tumor chemotherapeutic resistance. NMR Biomed 19:1035-1042.

Segal DH, Germano IM, Bederson JB (1997) Effects of basic fibroblast growth factor on in vivo cerebral tumorigenesis in rats. Neurosurgery 40:1027-1033.

Seitz RJ, Huang Y, Knorr U, Tellmann L, Herzog H, Freund HJ (1995) Large-scale plasticity of the human motor cortex. Neuroreport 6:742-744.

Senger DR, Galli SJ, Dvorak AM, Perruzzi CA, Harvey VS, Dvorak HF (1983) Tumor cells secrete a vascular permeability factor that promotes accumulation of ascites fluid. Science 219:983-985.

Sessler JL, Miller RA (2000) Texaphyrins: new drugs with diverse clinical applications in radiation and photodynamic therapy. Biochem Pharmacol 59:733-739.

Seyfried D, Han Y, Lu D, Chen J, Bydon A, Chopp M (2004) Improvement in neurological outcome after administration of atorvastatin following experimental intracerebral hemorrhage in rats. J Neurosurg 101:104-107.

Seyfried D, Ding J, Han Y, Li Y, Chen J, Chopp M (2006) Effects of intravenous administration of human bone marrow stromal cells after intracerebral hemorrhage in rats. J Neurosurg 104:313-318.

Shao Y, McCarthy KD (1994) Plasticity of astrocytes. Glia 11:147-155.

Shapiro WR (1971) Studies on the chemotherapy of experimental brain tumors: evaluation of 1-(2-chloroethyl)-3-cyclohexyl-1-nitrosourea, vincristine, and 5-fluorouracil. J Natl Cancer Inst 46:359-368.

Shapiro WR, Young DF (1984) Neurological complications of antineoplastic therapy. Acta Neurol Scand Suppl 100:125-132.

Shapiro WR, Green SB, Burger PC, Selker RG, VanGilder JC, Robertson JT, Mealey J, Jr., Ransohff J, Mahaley MS, Jr. (1992) A randomized comparison of intra-arterial versus intravenous BCNU, with or without intravenous 5-fluorouracil, for newly diagnosed patients with malignant glioma. J Neurosurg 76:772-781.

Shen LH, Li Y, Chen J, Cui Y, Zhang C, Kapke A, Lu M, Savant-Bhonsale S, Chopp M (2007a) One-year follow-up after bone marrow stromal cell treatment in middle-aged female rats with stroke. Stroke 38:2150-2156.

Shen LH, Li Y, Chen J, Zacharek A, Gao Q, Kapke A, Lu M, Raginski K, Vanguri P, Smith A, Chopp M (2007b) Therapeutic benefit of bone marrow stromal cells administered 1 month after stroke. J Cereb Blood Flow Metab 27:6-13.

Sherer M, Meyers CA, Bergloff P (1997) Efficacy of postacute brain injury rehabilitation for patients with primary malignant brain tumors. Cancer 80:250-257.

Singh SK, Clarke ID, Hide T, Dirks PB (2004) Cancer stem cells in nervous system tumors. Oncogene 23:7267-7273.

Sontheimer H (2003) Malignant gliomas: perverting glutamate and ion homeostasis for selective advantage. Trends Neurosci 26:543-549.

Soo EW, Galindo EG, Levin VA (1995) Brain tumors. In: Medical Oncology: A Comprehensive Review (2nd ed) (Pazdur R, ed), pp 469-481. Huntington, NY: PRR.

Stan AC, Nemati MN, Pietsch T, Walter GF, Dietz H (1995) In vivo inhibition of angiogenesis and growth of the human U-87 malignant glial tumor by treatment with an antibody against basic fibroblast growth factor. J Neurosurg 82:1044-1052.

Starkey ML, Barritt AW, Yip PK, Davies M, Hamers FP, McMahon SB, Bradbury EJ (2005) Assessing behavioural function following a pyramidotomy lesion of the corticospinal tract in adult mice. Exp Neurol 195:524-539.

Stratmann A, Risau W, Plate KH (1998) Cell type-specific expression of angiopoietin-1 and angiopoietin-2 suggests a role in glioblastoma angiogenesis. Am J Pathol 153:1459-1466.

Stroemer RP, Kent TA, Hulsebosch CE (1992) Increase in synaptophysin immunoreactivity following cortical infarction. Neurosci Lett 147:21-24.

Stroemer RP, Kent TA, Hulsebosch CE (1993) Acute increase in expression of growth associated protein GAP-43 following cortical ischemia in rat. Neurosci Lett 162:51-54.

Stylli SS, Kaye AH (2006a) Photodynamic therapy of cerebral glioma - a review. Part II - clinical studies. J Clin Neurosci 13:709-717.

Stylli SS, Kaye AH (2006b) Photodynamic therapy of cerebral glioma--a review Part I--a biological basis. J Clin Neurosci 13:615-625.

Stylli SS, Kaye AH, MacGregor L, Howes M, Rajendra P (2005) Photodynamic therapy of high grade glioma - long term survival. J Clin Neurosci 12:389-398.

Sun FY, Faden AI (1995) Pretreatment with antisense oligodeoxynucleotides directed against the NMDA-R1 receptor enhances survival and behavioral recovery following traumatic brain injury in rats. Brain Res 693:163-168.

Suri C, Jones PF, Patan S, Bartunkova S, Maisonpierre PC, Davis S, Sato TN, Yancopoulos GD (1996) Requisite role of angiopoietin-1, a ligand for the TIE2 receptor, during embryonic angiogenesis. Cell 87:1171-1180.

Suri C, McClain J, Thurston G, McDonald DM, Zhou H, Oldmixon EH, Sato TN, Yancopoulos GD (1998) Increased vascularization in mice overexpressing angiopoietin-1. Science 282:468-471.

Takahashi Y, Kitadai Y, Bucana CD, Cleary KR, Ellis LM (1995) Expression of vascular endothelial growth factor and its receptor, KDR, correlates with vascularity, metastasis, and proliferation of human colon cancer. Cancer Res 55:3964-3968.

Takano T, Lin JH, Arcuino G, Gao Q, Yang J, Nedergaard M (2001) Glutamate release promotes growth of malignant gliomas. Nat Med 7:1010-1015.

Tehard B, Friedenreich CM, Oppert JM, Clavel-Chapelon F (2006) Effect of physical activity on women at increased risk of breast cancer: results from the E3N cohort study. Cancer Epidemiol Biomarkers Prev 15:57-64.

Teng J, Takei Y, Harada A, Nakata T, Chen J, Hirokawa N (2001) Synergistic effects of MAP2 and MAP1B knockout in neuronal migration, dendritic outgrowth, and microtubule organization. J Cell Biol 155:65-76.

Tse V, Xu L, Yung YC, Santarelli JG, Juan D, Fabel K, Silverberg G, Harsh Gt (2003) The temporal-spatial expression of VEGF, angiopoietins-1 and 2, and Tie-2 during tumor angiogenesis and their functional correlation with tumor neovascular architecture. Neurol Res 25:729-738.

Vaynman S, Ying Z, Gomez-Pinilla F (2004) Hippocampal BDNF mediates the efficacy of exercise on synaptic plasticity and cognition. Eur J Neurosci 20:2580-2590.

Vigliani MC, Duyckaerts C, Hauw JJ, Poisson M, Magdelenat H, Delattre JY (1999) Dementia following treatment of brain tumors with radiotherapy administered alone or in combination with nitrosourea-based chemotherapy: a clinical and pathological study. J Neurooncol 41:137-149.

Walker MD, Alexander E, Jr., Hunt WE, MacCarty CS, Mahaley MS, Jr., Mealey J, Jr., Norrell HA, Owens G, Ransohoff J, Wilson CB, Gehan EA, Strike TA (1978) Evaluation of BCNU and/or radiotherapy in the treatment of anaplastic gliomas. A cooperative clinical trial. J Neurosurg 49:333-343.

Wang Y, Zhang ZG, Rhodes K, Renzi M, Zhang RL, Kapke A, Lu M, Pool C, Heavner G, Chopp M (2007a) Post-ischemic treatment with erythropoietin or carbamylated erythropoietin reduces infarction and improves neurological outcome in a rat model of focal cerebral ischemia. Br J Pharmacol 151:1377-1384.

Wang Z, Lecane PS, Thiemann P, Fan Q, Cortez C, Ma X, Tonev D, Miles D, Naumovski L, Miller RA, Magda D, Cho DG, Sessler JL, Pike BL, Yeligar SM, Karaman MW, Hacia JG (2007b) Synthesis and biologic properties of hydrophilic sapphyrins, a new class of tumor-selective inhibitors of gene expression. Mol Cancer 6:9.

Wei L, Keogh CL, Whitaker VR, Theus MH, Yu SP (2005a) Angiogenesis and stem cell transplantation as potential treatments of cerebral ischemic stroke. Pathophysiology 12:47-62.

Wei WH, Fountain M, Magda D, Wang Z, Lecane P, Mesfin M, Miles D, Sessler JL (2005b) Gadolinium texaphyrin-methotrexate conjugates. Towards improved cancer chemotherapeutic agents. Org Biomol Chem 3:3290-3296.

Weiller C, Chollet F, Friston KJ, Wise RJ, Frackowiak RS (1992) Functional reorganization of the brain in recovery from striatocapsular infarction in man. Ann Neurol 31:463-472.

Weizsaecker M, Deen DF, Rosenblum ML, Hoshino T, Gutin PH, Barker M (1981) The 9L rat brain tumor: description and application of an animal model. J Neurol 224:183-192.

Wells JE, Biernaskie J, Szymanska A, Larsen PH, Yong VW, Corbett D (2005) Matrix metalloproteinase (MMP)-12 expression has a negative impact on sensorimotor function following intracerebral haemorrhage in mice. Eur J Neurosci 21:187-196.

Whittle IR, Marston HM (1997) Progressive focal neurological dysfunction following experimental implantation glioma. Neuroreport 8:1149-1153.

Whittle IR, Kelly PA (2001) Mechanisms of peritumoural brain dysfunction: metabolic and neuroreceptor findings in striatal C6 glioma. J Clin Neurosci 8:430-434.

Wingo PA, Tong T, Bolden S (1995) Cancer statistics, 1995. CA Cancer J Clin 45:8-30.

Woodlee MT, Schallert T (2006) The impact of motor activity and inactivity on the brain: implications for the prevention and treatment of nervous system disorders. Curr Direct Psychol Sci 15:203-206.

Woodlee MT, Asseo-Garcia AM, Zhao X, Liu SJ, Jones TA, Schallert T (2005) Testing forelimb placing "across the midline" reveals distinct, lesion-dependent patterns of recovery in rats. Exp Neurol 191:310-317.

Yang DI, Chen SD, Yin JH, Hsu CY (2005) S-nitrosoglutathione and hypoxia-inducible factor-1 confer chemoresistance against carbamoylating cytotoxicity of BCNU in rat C6 glioma cells. Ann N Y Acad Sci 1042:229-234.

Yang H, Zhang X, Chopp M, Jiang F, Schallert T (2006a) Local fluorouracil chemotherapy interferes with neural and behavioral recovery after brain tumor-like mass compression. Behav Brain Res 172:80-89.

Yang H, Chopp M, Jiang F, Zhang X, Schallert T (2006b) Interruption of functional recovery by the NMDA glutamate antagonist MK801 after compression of the sensorimotor cortex: implications for treatment of tumors or other mass-related brain injuries. Exp Neurol 200:262-266.

Yang H, Preston M, Chopp M, Jiang F, Zhang X, Schallert T (2006c) Mass-related traumatic tissue displacement and behavior: a screen for treatments that reduce [corrected] harm to bystander cells and recovery of function. J Neurotrauma 23:721-732.

Yang H, Chopp M, Zhang X, Jiang F, Zhang Z, Kalkanis S, Schallert T (2007a) Using behavioral measurement to assess tumor progression and functional outcome after antiangiogenic treatment in mouse glioma models. Behav Brain Res 182:42-50.

Yang H, Chopp M, Weiland B, Zhang X, Tepley N, Jiang F, Schallert T (2007b) Sensorimotor deficits associated with brain tumor progression and tumor-induced brain plasticity mechanisms. Exp Neurol 207:357-367.

Ye ZC, Sontheimer H (1999) Glioma cells release excitotoxic concentrations of glutamate. Cancer Res 59:4383-4391.

Zagzag D, Hooper A, Friedlander DR, Chan W, Holash J, Wiegand SJ, Yancopoulos GD, Grumet M (1999) In situ expression of angiopoietins in astrocytomas identifies angiopoietin-2 as an early marker of tumor angiogenesis. Exp Neurol 159:391-400.

Zhang L, Zhang RL, Wang Y, Zhang C, Zhang ZG, Meng H, Chopp M (2005) Functional recovery in aged and young rats after embolic stroke: treatment with a phosphodiesterase type 5 inhibitor. Stroke 36:847-852.

Zhang R, Wang Y, Zhang L, Zhang Z, Tsang W, Lu M, Zhang L, Chopp M (2002) Sildenafil (Viagra) induces neurogenesis and promotes functional recovery after stroke in rats. Stroke 33:2675-2680.

Zhang R, Zhang Z, Zhang C, Zhang L, Robin A, Wang Y, Lu M, Chopp M (2004a) Stroke transiently increases subventricular zone cell division from asymmetric to symmetric and increases neuronal differentiation in the adult rat. J Neurosci 24:5810-5815.

Zhang R, Zhang Z, Wang L, Wang Y, Gousev A, Zhang L, Ho KL, Morshead C, Chopp M (2004b) Activated neural stem cells contribute to stroke-induced neurogenesis and neuroblast migration toward the infarct boundary in adult rats. J Cereb Blood Flow Metab 24:441-448.

Zhang RL, Zhang Z, Zhang L, Wang Y, Zhang C, Chopp M (2006) Delayed treatment with sildenafil enhances neurogenesis and improves functional recovery in aged rats after focal cerebral ischemia. J Neurosci Res 83:1213-1219.

Zhang RL, LeTourneau Y, Gregg SR, Wang Y, Toh Y, Robin AM, Zhang ZG, Chopp M (2007a) Neuroblast division during migration toward the ischemic striatum: a study of dynamic migratory and proliferative characteristics of neuroblasts from the subventricular zone. J Neurosci 27:3157-3162.

Zhang RL, Zhang ZG, Wang Y, Letourneau Y, Liu XS, Zhang X, Gregg SR, Wang L, Chopp M (2007b) Stroke induces ependymal cell transformation into radial glia in the subventricular zone of the adult rodent brain. J Cereb Blood Flow Metab.

Zhang RW, Soong SJ, Liu TP, Barnes S, Diasio SB (1992) Pharmacokinetics and tissue distribution of 2-fluoro-beta-alanine in rats. Potential relevance to toxicity pattern of 5-fluorouracil. Drug Metab Dispos 20:113-119.

Copyright Statement

This statement is to clarify issues of intellectual property, responsibility and credit. The ideas of this dissertation are primarily mine with critical inputs from both Dr. Schallert, my supervisor at the University of Texas at Austin, and Dr. Chopp, an important collaborator of Dr. Schallert, from the Department of Neurology at Henry Ford Hospital, Detroit, MI. I designed all of the experiments myself. I prepared all of the graphs and wrote the entire dissertation by myself. I did most of the behavioral testing and histological image analysis work by myself with some help from undergraduate students and high school summer volunteers. I did most of the surgeries by myself with some help from Dr. Xuepeng Zhang, a postdoctoral fellow in Dr. Chopp's lab. I received significant assistance from technicians in Dr. Chopp's lab in brain tissue processing, slicing and staining. In one of my projects investigating the relationship between the behavior of rats bearing gliomas and the tumor volume, I did the regression analysis using my behavioral data and the corresponding MRI tumor volume data obtained from Dr. Weiland, who used to be a graduate student of Dr. Tepley from the Neuromagnetism Laboratory at Henry Ford Hospital. The MRI procedure was performed in the Department of Radiation at Henry Ford Hospital with the MRI pulse sequences designed by staffs there.

Papers with me as the first author were all written by myself. Dr. Schallert and Dr. Chopp helped me revise and edit them. Besides Dr. Schallert and Dr. Chopp, the following people appear as co-authors in my papers. Dr. Feng Jiang is the leader of the subgroup that I have been working with in Dr. Chopp's lab. He provided me resources to do my experiments there. Dr. Xuepeng Zhang helped me make some animal models.

Marnie Preston used to be an undergraduate student working with me in Dr. Schallert's lab and helped me with some behavioral testing and histology work. Dr. Zhenggang Zhang is the leader of another subgroup in Dr. Chopp's lab. He provided me with the antibodies against VEGFR-1 and 2 and gave me valuable advice to part of my research. Dr. Barbara Weiland and Dr. Norman Tepley from the Neuromagnetism Laboratory at Henry Ford Hospital were my collaborators in the rat glioma project. Dr. Tepley provided the fund to do MRI. Dr. Weiland did the tumor volume measurement using the MRI images produced by the Department of Radiation at Henry Ford Hospital. Dr. Steve Kalkanis from the Department of Neurosurgery at Henry Ford Hospital is a collaborator of Dr. Jiang and Dr. Chopp, and he provided part of the funding to perform my research.

Vita

Hongyan Yang was born in Tianjin, China, on December 31, 1979. She is the only child of Xinnan Wang and Wenkui Yang. She graduated with an MD from Peking University Health Science Center in 2001. She began working with Dr. Timothy Schallert at the University of Texas at Austin as a graduate student in 2003. During her PhD study, she has five first-author and five co-author papers published in peer-reviewed journals.

Permanent address: 930 W Forest Apt 12, Detroit, MI 48201

This dissertation was typed by the author, Hongyan Yang.